Millimeter-wave Contactless Waveguide Joints and Compact OMT Based on Gap Waveguide Technology

Turfa Sarah Amin

A Thesis
in
The Department
of
Electrical and Computer Engineering

Presented in Partial Fulfillment of the Requirements
For the Degree of
Master of Applied Science (Electrical and Computer Engineering) at
Concordia University
Montreal, Quebec, Canada

November 2020

CONCORDIA UNIVERSITY
SCHOOL OF GRADUATE STUDIES

This is to certify that the thesis prepared

By: Turfa Sarah Amin

Entitled: Millimeter-wave Contactless Waveguide Joints and Compact OMT Based on Gap Waveguide Technology

and submitted in partial fulfillment of the requirements for the degree of

Master of Applied Science (Electrical and Computer Engineering)

complies with the regulations of this University and meets the accepted standards with respect to originality and quality.

Signed by the final examining committee:

_____ Chair
Dr. R. Paknys

_____ External Examiner
Dr. A. Youssef (CIISE)

_____ Internal Examiner
Dr. R. Paknys

_____ Internal Examiner
Dr. C.W. Trueman

_____ Supervisor
Dr. A.A. Kishk

Approved by: _____
Dr. Y.R. Shayan, Chair
Department of Electrical and Computer Engineering

_____, 2020

_____
Dr. Mourad Debbabi, Interim Dean
Gina Cody School of Engineering and
Computer Science

Abstract

Millimeter-wave Contactless Waveguide Joints and Compact OMT Based on Gap Waveguide Technology

Turfa Sarah Amin

Concordia University, 2020

Amongst the contemporary gap waveguide structures, both ridge gap waveguide (RGW) and groove gap waveguide (GGWG) display low losses and are resistant to signal leakage without the requirement of electrical contacts. In both scenarios, the concept is to allow the wave propagation through the guiding part and eliminating signal leakage in all other directions. Since, at present, millimeter-wave (mm-wave) has gained attention due to its versatile usability at high-frequency applications, it is quite obligatory to develop components with superior electrical features, like high stability, wider bandwidth, as well as high power handling capability at that frequency range. Considering the stated advantages, the proposed devices in this research work emphases on the mm-wave application that are mainly accountable for connecting standard waveguides and feeding antenna systems.

The research work can be summarized in three segments. The first segment aims at designing waveguide adaptors based on the gap waveguide technology that do not necessarily require perfect electrical contact. The contact-free adaptor has been designed for both standard rectangular and circular waveguides covering multiple mm-wave frequency bands within 50- 110 GHz. Additionally, while designing the adaptor, surface roughness has been considered to achieve the response of the structure close enough to the practical case. The same adapter can also be used

with different standard waveguide dimensions operating within 50-110 GHz by changing the adapter's waveguide parameters. The proposed contact-free adaptor exhibits an excellent return loss and insertion loss of better than 20 dB and 0.3 dB, respectively, for both standard circular and rectangular waveguides, regardless of a smooth or uneven surface.

The second segment focuses on a contact-free flangeless pipe connection for both circular and rectangular standard waveguides, covering multiple frequency bands amid 50 and 110 GHz. The contactless, low-loss, flange-free, and pluggable contact aims at joining two slightly modified standard waveguides, along with a 60% downscaling of the recommended structure compared to the traditional UG-387/U waveguide flange, hence demonstrating a reflection coefficient better than -20 dB in each scenario.

In addition, the third segment is introducing microwave devices that can combine and separate two propagating polarizations, such as orthomode transducers (OMT). Aiming for high power applications with compact structure, the proposed configuration introduces a new design procedure of combining the ridge gap and groove gap waveguides for the OMTs, validating an acceptable matching level of better than -18 dB along with isolation higher than 70 dB.

Finally, some valuable recommendations as an extension of this research work are suggested in the final chapter.

Acknowledgments

I would like to express my sincere gratitude to Professor Ahmed A. Kishk, supervisor of the thesis, for his constant support and motivation. It would never have been possible for me to complete this research without his guidance and advice. I am also thankful to my committee members for reviewing my thesis and for providing constructive feedback.

I would also like to thank Dr. Shokry Shamseldin and my amazing colleagues from our research group. I am grateful to my friends Abdelmoniem Hassan, Riddhi Goswami, Elham Baghernia, and Babak Molaei for their encouragement.

Finally, I offer my love, blessings, and regards to my parents, and my beloved husband, for their unlimited support and inspiration.

Contents

List of Figures

List of Tables

List of Acronyms

1G	First Generation
3D	Three-Dimensional
5G	Fifth Generation
AMC	Artificial Magnetic Conductor
BW	Bandwidth
CST MWS	Computer Simulation Technology Microwave Studio
CWA	Contactless Waveguide Adaptor
CWC	Contactless Waveguide Connector
EBG	Electromagnetic Band Gap
EM	Electromagnetic
FD	Frequency Domain
FDTD	Finite Difference Time Domain
FIM	Finite Integral Method
FIT	Finite Integration Technique
FSS	Frequency Selective Structure
GGWG	Groove Gap Waveguide
GW	Gap Waveguide
HIS	High Impedance Surface
mm-wave	Millimeter-wave
OMT	Orthomode Transducer
PEC	Perfect Electric Conductor
PIM	Passive Intermodulation
PMC	Perfect Magnetic Conductor
RF	Radio Frequency
RGW	Ridge Gap Waveguide
RMS	Root-Mean-Square
SIW	Substrate Integrated Waveguide
TD	Time Domain
TE	Transverse Electric Wave
TEM	Transverse Electromagnetic Wave
TM	Transverse Magnetic Wave
VBA	Visual Basic for Applications
VHF	Very High Frequency

Chapter 1

Introduction

From the first generation (1G) to the recent fifth-generation (5G), the wireless communication system has experienced an outstanding revolution. The technological progression in the communication field has directed us to a new phase through high-performance antennas, signal integrity, and secure wireless network. To satisfy the rapid growth of consumer demands such as improved data transmission rate, increasing capacity, lower latency, and better quality of service, milliliter and sub-millimeter frequency bands, as well as ultra-wideband technology, have appealed to academic as well as industrial societies [1-3].

The augmented usage of high-frequency devices has been observed for the last few decades due to the inordinate progress of the wireless communication system [4]. Modern communication structures and radar applications are currently focusing on wider bandwidths due to its capability of allocating the increasing number of services to minimize the cost and dimension of the system as well as its ability of minimum power consumption. Information and communication technology has advanced enough to have significant impacts on all aspects of life. Wireless data transmission is not limited to communication purposes, but it has a significant impact on radio astronomy, remote sensing, automotive radars, military and space applications, imaging, and security screening [5]. For higher data transmission, the wide bandwidth is mandatory, which can be realized by the utilization of upper-frequency bands.

The implementation of passive components and interconnected transmission lines on these modules is sometimes tricky at millimeter-wave frequencies using classical technologies, such as

microstrip transmission lines and conventional waveguides. Thus, new technologies are needed in order to face the challenges of the next generation systems [6-7].

1.1 Characteristics of Millimeter-wave Frequency Band

The millimeter-wave (mm-wave) frequencies are allocated from 30 to 300 GHz, with wavelengths ranging from 10 to 1 mm. This wide range of a spectrum has drawn an immense interest in developing mm-wave communication systems for commercial applications. The mm-wave frequency band has many advantages, for instance, re-usage of high-level frequency, smaller dimensions of RF components, optimum usage for short-distance communication, and unrestricted operation with low interference [8]. In the following section, various waveguide structures are discussed, where the performance of the structures is emphasized, especially in the mm-wave frequency band.

1.2 Overview of Guiding Structures

One of the most critical and challenging areas in the microwave and millimeter-wave research area is the guiding structure through which the signal propagates. The core principles of the wave propagation within guided structures were well recognized after Hertz proved the predictions of Maxwell experimentally [9, 10]. Moreover, solutions of many guiding structures are based on the wave equations established by Hertz from the modified version of Maxwell's equations. These solutions are found useful in the design and analysis of all guiding structures like parallel-plate waveguides, rectangular waveguides, and circular waveguides [11].

1.2.1 Conventional Guiding Structures

Microwave signals ranging from 300 MHz to 300 GHz prefer to propagate as TEM waves due to its advantage of being non-dispersive with zero cutoff frequency over other TE and TM waves by

the guiding structure at a lower frequency range. Strip lines and microstrip lines are suitable for applications operating below the millimeter-wave range. Since they are printed on a dielectric substrate, with the growing frequency, these transmission lines suffer from high dielectric losses [11]. Moreover, at higher frequencies, the microstrip transmission line undergoes high cavity modes and surface waves that cause unwanted radiation. These limitations considerably affect the suitability of microstrip lines for mm-wave frequency bands. The co-planar waveguide is another type of planar waveguide which constructs on a dielectric substrate. Hence, it is preferred for low-frequency applications as well.

The above-mentioned drawbacks at higher frequencies direct towards diverse guiding structures, for example, waveguides. Even though waveguides do not support TEM mode (apart from coaxial lines), they demonstrate much lower losses due to their higher Q factor. This leads to utilizing these guiding structures at higher frequencies. However, waveguides have limited operating bandwidth for a single-mode operation with higher dispersion characteristics compared to the guiding structures supporting TEM mode. The dominant mode (mostly TE) of the waveguide can have a practically wideband that can reach 2:1, but the usable frequency range is typically lower. Nevertheless, other waveguide structures such as the ridge gap waveguide can have considerably wider bandwidth.

1.2.2 Modern Guiding Structures

In recent times, many guiding structures based on innovative technologies are introduced along with the traditional ones. These structures mostly emphasize the high-frequency range, such as millimeter wave bands. These new technologies have multiple examples such as Ridge Gap Waveguide (RGW), Groove Gap Waveguide (GGWG) as well as Substrate Integrated Waveguide

(SIW), as shown in Figure 1.1. However, these types are not well-established standards compared to the traditional category of guiding structures.

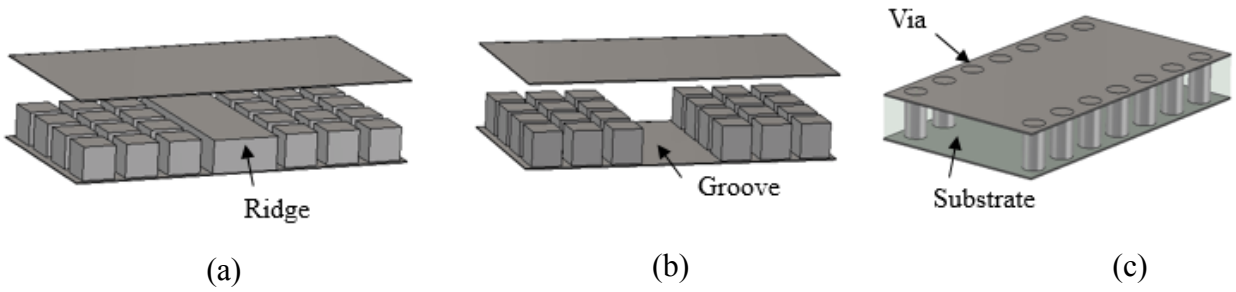

Fig.-1.1: Various modern guiding structures (a) RGW, (b) GGWG, and (c) SIW

The main concern of this thesis is about the interconnection between traditional rectangular and circular waveguides at mm-wave frequency bands along with passive component design based on periodic structures, such as RGW and GGWG. The RGW carries TEM mode, while the propagating mode for GGWG is the TE mode, resulting in more dispersion. The RGW and GGWG have no dielectric loss since the signal propagates inside an air gap. In terms of size, the width of the RGW with two rows is smaller than the width of the GGWG for the same frequency band. Moreover, the mechanical durability for both RGW and GGWG components is quite impressive [12].

Later in Chapter 2, more explanations regarding these periodic structures and the reasons behind the parameters selection are discussed. The motivations and objectives of this thesis are summarized in the upcoming sections. At the end of this chapter, the outlines of the thesis are presented as well.

1.3 Research Motivation

The demand for high performance microwave devices is increasing rapidly due to the requirement of massive advancement in the communication field. Furthermore, the necessity of better quality service and high data rates to meet consumer demand for the next generation communication system is inevitable nowadays. Another challenge for wireless communication, especially at the mm-wave band, is to realize an overall system ensuring low loss with integration between passive and active components while being cost-effective and compact size simultaneously. The gap waveguide was introduced a decade ago by Kildal [13] as a promising candidate for these applications since it can overcome the problems experienced with the traditional methods. In Gap waveguide technology, the PEC-PMC parallel plate structure was used to control the electromagnetic wave propagation between the two parallel surfaces. As long as the air gap between the two PEC-PMC plates is less than a quarter wavelength, the waves are not propagating. Thus, the electromagnetic bandgap of the structure is controlled. If the bottom surface includes a ridge, then the waves are propagating within the gap above the ridge only. However, the corrugated AMC surface must also include guiding structures in the form of a ridge, groove, or strip to form a complete waveguide configuration.

Another aspect to consider is the interconnection between waveguide components, which is generally accomplished by waveguide flanges. A typical waveguide flange is aligned by pins and screw holes. However, due to the machining error on the pins and screw holes, the misconnection of flanges is possible while connecting waveguides. Additionally, wave leakage between the two waveguides is another possibility while connecting them through the flanges. These errors can degrade measurements significantly at high frequencies, where waveguide dimensions are small, and the connection error, such as bad electrical contact, presents a substantial

element of the waveguide opening. In other words, as the flange misconnection becomes comparable with waveguide dimensions, its effects are not insignificant for precision measurements in the mm-wave frequency range.

1.4 Thesis Objectives

This work presents various microwave devices based on the gap waveguide theory that implements the corrugated surfaces, such as the Ridge Gape Waveguide (RGW) and Groove Gap Waveguide (GGWG). Such structures are suitable for mm-wave applications operating at high frequencies. They should provide a wide operating bandwidth that fulfills the requirements of such devices.

The first section of this thesis aims at designing waveguide adaptors that do not necessarily require perfect electrical contact that we could call contactless, covering multiple frequency bands based on the gap waveguide technology. This contact-free adaptor has been designed for both standard rectangular and circular waveguides. Moreover, while designing the structure, surface roughness has been considered to achieve the response of the structure close enough to the practical case. The primary objective of this design is to ensure a leakage-free low-loss contactless connection between two waveguide flanges while not modifying the original waveguide flange structure.

Waveguide flange definitely has a larger dimension compared to the waveguide that necessitates perfect alignment and contacts. For satellite and space application systems with strict limitations of weight and volume, this oversize might have some contrary outcome. For this reason, the second section of the thesis report focuses on a contact-free flangeless pipe connection for both circular and rectangular standard waveguides.

The third part of the thesis is introducing microwave devices that can combine and separate two propagating polarizations, such as orthomode transducers (OMT). The objective of this section is to develop the performance of OMTs by integrating gap waveguide technology. Aiming at high power applications with compact structure, this structure introduces a new design procedure of combining the ridge gap and groove gap waveguides for the OMTs. This integration facilitates the connection between the OMT and the other microwave components, thus reducing the complexity of the overall structure. According to the authors' knowledge, no OMTs combining RGW and GGWG technology have been proposed earlier in the literature.

1.5 Outline of the Thesis

Chapter 2 provides a literature review on gap waveguide technology, hard and soft surfaces, in conjunction with structures like Ridge Gape Waveguide (RGW) and Groove Gap Waveguide (GGWG) technologies along with their basic ideas. Later, a discussion on specific essential microwave components and devices, including waveguide interconnects and orthomode transducer, has been presented.

Chapter 3 exhibits a contact-free waveguide adaptor for standard circular and rectangular waveguides that cover multiple frequency ranges of V-band and W-band. The novelty of this adaptor is that it does not demand the original waveguide flange structure to be altered.

Chapter 4 focuses on connecting two standard waveguides without the implementation of waveguide flanges. The comparison between the standard waveguide flange and the proposed structure attests to the percentage of size reduction of the waveguide connector compared to the flanges.

Chapter 5 demonstrates orthomode transducers as a form of polarization separator of propagating EM wave uniting RGW and GGWG along with E-bend and H-bend to ensure compressed structure.

In conclusion, *Chapter 6* summarizes the thesis proposals as well as recommends valuable extensions in the form of future work.

Chapter 2

Literature Review

The progression of information and communication technology in the last decades resulted in a wide-ranging impact on society. Globalization has formed more independent and flexible organizations, hence generating communication technology as one of the competitive tools. At the present time, coordination, awareness, and network among people are facilitated by the rapid advancement of wireless communications compared to the past. The necessity to opt for millimeter-wave frequencies has also driven research and development to create powerful active and passive components, occupying lesser volume. However, the implementation of these components and interconnected transmission lines is difficult at millimeter waves with conventional technologies. The traditional guiding structures, for instance, microstrip lines, undergo high radiation loss, in addition to the dielectric loss at high frequencies. Therefore, the microstrip technology is not recommended for the millimeter-wave bands, even though they support the non-dispersive quasi-TEM mode. Therefore, a requirement for developing new technologies with multiple functionalities is considered nowadays [14].

This chapter consists of a literature review of some recently introduced technologies based on periodic structures to overcome the problems of the traditional guiding structures at the millimeter-wave frequency band. Followed by this, a brief review of some selected microwave components that are essential in any communication system is reviewed.

2.1 Periodic Structures

Gap waveguide technology has been under the spotlight for the last few years. These mechanisms are based on a periodic structure composed of metal pins that are covered by two-conductor surfaces on top and ground planes. This bed of pins generates a high impedance surface (HIS); in other words, an artificial magnetic conductor (AMC) prevents electromagnetic wave propagation in a specific frequency band. The key idea behind this technology is based on the procedure to direct the electromagnetic wave along with desired directions within the gap between metal plates and to avoid any propagation along with undesired ways. Thus, any leakage occurring in between the divided blocks of a circuit with poor metal connections as well as unwanted radiations can be avoided [15- 18]. In the next subsections, two main categories of periodic structures are briefly discussed.

2.1.1 Soft and Hard Surfaces

The concept of soft and hard surfaces was introduced by Kildal that describes the electromagnetic wave propagation along the corrugated surface [19]. “Soft and hard surfaces” are based on the terms from acoustics, which are related to materials type. Soft surfaces absorb acoustic signals and hard surfaces that reflect the acoustic signal. Basically, soft and hard surfaces are metamaterials, which are apparently artificial surfaces that demonstrate EM properties not found in nature. In general, the soft surface halts the wave propagation, whereas the hard surface supports the wave to transmit. The reason behind this feature is that the transversely placed corrugation for soft surface eliminates both the transverse electric field and the transverse magnetic field. Thus, abolishing both transverse field components discontinue wave propagation. On the contrary, the hard surfaces suspend only the longitudinal electric and magnetic field components and thus supporting only TEM mode propagation.

Preferably, a soft-hard surface can be understood by Perfect Electric Conductor (PEC) and Perfect Magnetic Conductor (PMC) strips, signifying the hard surface when the strips are longitudinal, i.e., oriented in the same direction as the wave propagates. In addition, the soft surface when they are at right angles, i.e., orthogonal to the direction of propagation, as illustrated in Figure 2.1 [20]. The PEC and PMC strips can be represented with a dielectric substrate along with transverse (soft) or longitudinal (hard) metal strips [21].

The quasi- TEM mode can propagate through the edges of corrugation when a metal plate is placed above, at a distance smaller than a quarter wavelength. The operation principle is the same as the PEC-PMC strips with a conducting sheet at the same distance above them, in which the waves are propagating only along the longitudinal direction whereas stop after placing the PEC-PMC strips along the crosswise direction [22].

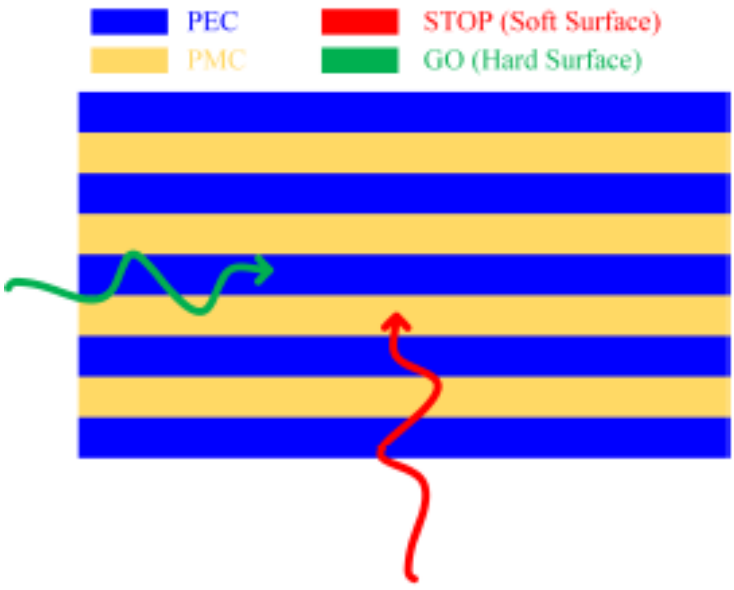

Fig.-2.1: Soft and hard surface representation with respect to the wave propagation direction [20]

2.1.2 Unit Cell Analysis

As previously mentioned, a PMC does not exist in nature, though it is possible to generate artificial magnetic conducting surfaces by utilizing periodic structures in two-dimensional space. The unit cell of the periodic structure controls the electromagnetic bandgap and the operating bandwidth of the gap waveguide through the AMC surface. The operating bandgap of the unit cell is achieved from the Eigenmode solver of CST Microwave Studio. Few parameters factors play an essential role in determining the bandgap, as mentioned below:

- Airgap between the AMC and upper PEC surface
- Height of the pins
- Dimension of the pins (shape)
- Gap between two consecutive pins

The proposed design structure of a unit cell, along with the dispersion diagram, is demonstrated in Figure 2.2. Depending on the requirement, it is possible to modify the bandgap by changing these four parameters [23].

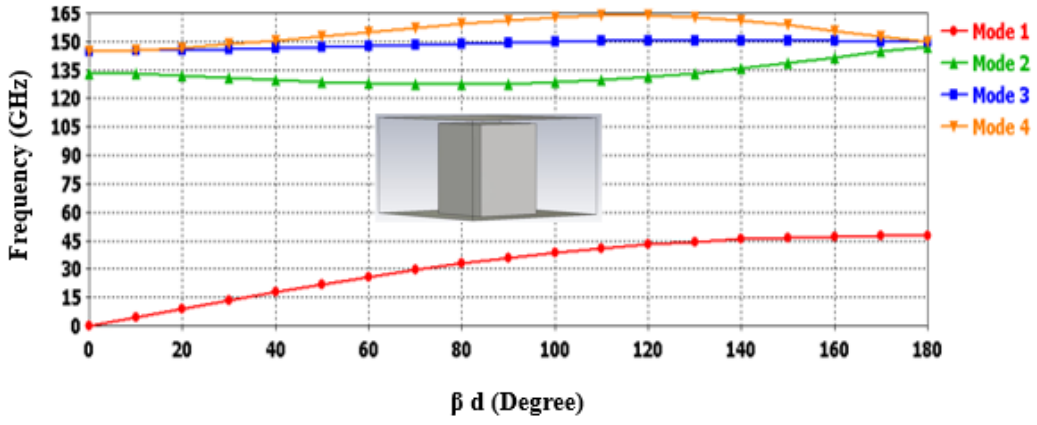

Fig 2.2: Dispersion diagram with a unit cell of a periodic structure

2.1.3 Ridge Gap Waveguide (RGW)

The Ridge Gap Waveguide (RGW) was published and patented by Kildal [13] in the last decade. This structure can be considered as an extension of the soft surfaces but in 2D periodicity. This structure is very promising for mm-wave applications due to low radiation loss, no dielectric loss, and wideband operation. There are no dielectric losses since the RGW is an air-filled guiding structure. The RGW utilizes periodic unit cells to stop the signal leakage, thus plummeting the radiation losses. PEC's ridge is embedded between these periodic pins to form a guiding structure of the propagating quasi-TEM wave. RGW consists of two parallel conducting plates, one plate with a texture of the periodic pins to prevent the wave propagation in all directions except through the ridge. The bandgap of the unit cell controls the operating frequency range of the RGW guiding structure. Numerous research work has been done to acquaint with various unit cells of multiple forms to expand the operating bandwidth [23- 25]. The geometry of RGW utilizing the previously mentioned unit cell is shown in Figure 2.3.

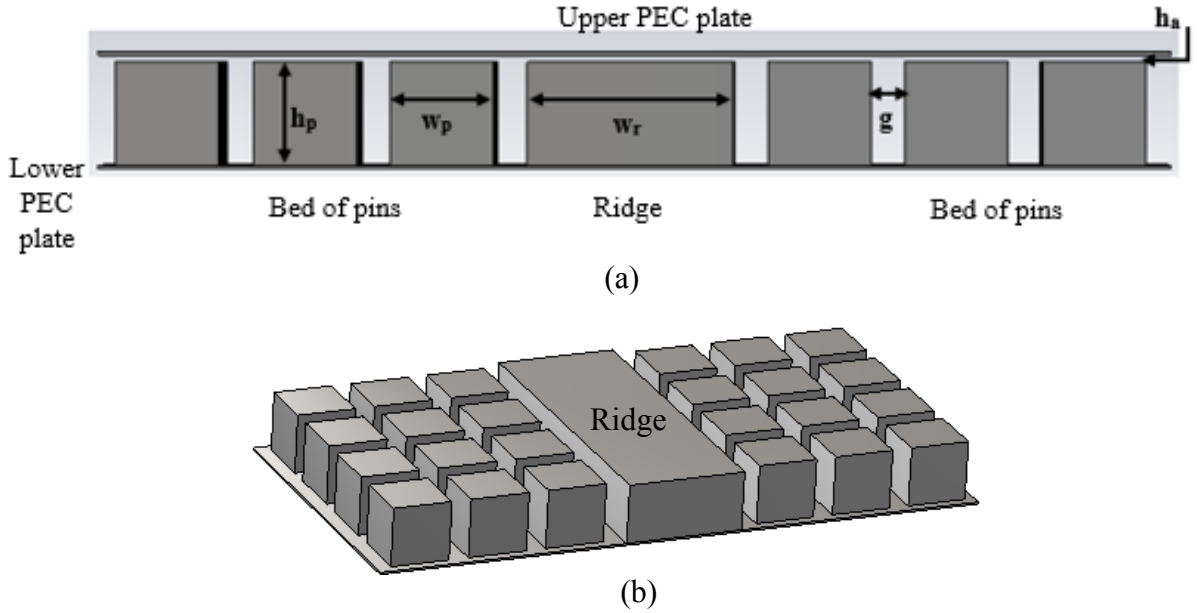

Fig 2.3: Ridge gap waveguide (a) One-row geometry and (b) 3D structure (upper PEC hidden)

2.1.4 Groove Gap Waveguide (GGWG)

The Groove Gap Waveguide (GGWG) is another extension of the RGW technology. In terms of geometry, the ridge is replaced by a groove embedded by the pins on both sides in a groove gap waveguide. The difference with the ridge gap waveguide is that the groove gap waveguide allows propagating TE/ TM modes as a substitute of quasi-TEM mode in the RGW. The dominant mode of groove gap waveguide is the same as the one of a rectangular waveguide that is TE_{10}. Thus the operation of GGWG is similar to the rectangular waveguides along with an additional advantage of not requiring electrical contact between the top and lower conductor layer of the guiding structure [26- 28]. Besides, the groove gap waveguide has fewer losses compared to the ridge gap waveguide since the ridge is removed from the bottom plate. Thus more space for signal propagation compared to RGW. In Fig 2.4, the structure of the groove gap waveguide is illustrated.

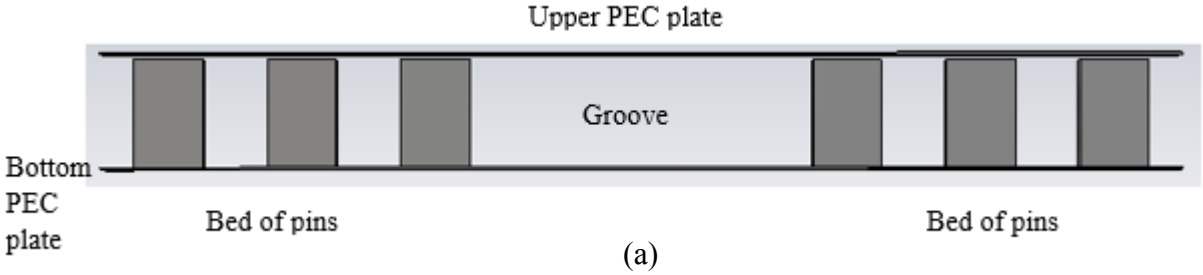

(a)

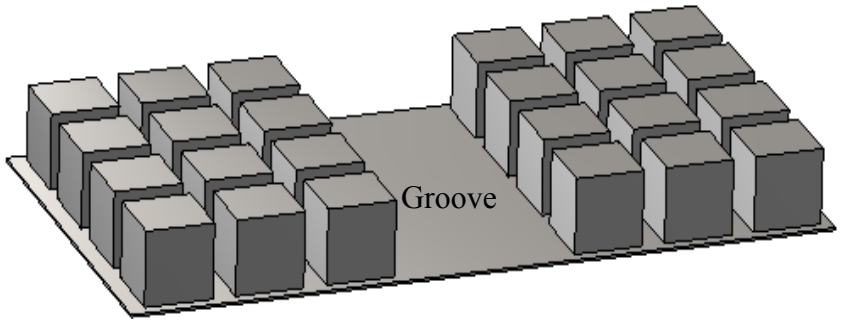

(b)

Fig 2.4: Groove gap waveguide (a) One-row geometry and (b) 3D structure (upper PEC hidden)

2.2 Some Essential Microwave Components and Devices

Some of the essential microwave components and devices are mentioned in the upcoming subsections to explain their progress nowadays.

2.2.1 Flange Adaptors for Standard Waveguides

Standard air-filled waveguide structures need to be connected, usually through waveguide flanges, in order to measure circuits and devices at high frequency. In these circumstances, standard waveguide flanges act as transitions in those interconnects. The connection between the waveguide flanges is very crucial since the flanges need to be firmly and steadily connected to each other, typically by metal screws. Additionally, an exceptionally high precision machining is essential for the purpose of assuring a proper alignment between the flanges. This task can become very time-consuming as well as challenging, particularly during the time of calibration performed by multiple known standards. This might cause leakage into free space followed by higher reflection at the connection, as a consequence of erroneous and unreliable results [29]. Figure 2.5 [31] illustrates the simulated return loss of two connected WR-3 waveguides. When a gap of 20 μm is applied at the joint of the waveguide flanges, the matching level declines significantly compared to the preferred no-gap scenario. Furthermore, when the gap between the flanges is increased to 40 μm, the return loss deteriorates to 10 dB [31]. It can be stated that the return loss performance is inversely proportional to the gap between two standard smooth waveguide flanges; thus, confirming the requirement of efficient, leakage-free waveguide connections at high frequencies even with no proper contact between the standard flanges. Gap waveguides with periodic structures are able to transmit signals amid two parallel placed conducting plates. In this case, the lower plate is a high-impedance surface due to a periodic bed of pins, which, if positioned at a distance smaller than a quarter wavelength from the upper plate, create a frequency bandgap

blocking all wave propagation. Under this bandgap condition, any periodic structure, such as a ridge or a groove, can be used to direct signals between the two parallel plates [30].

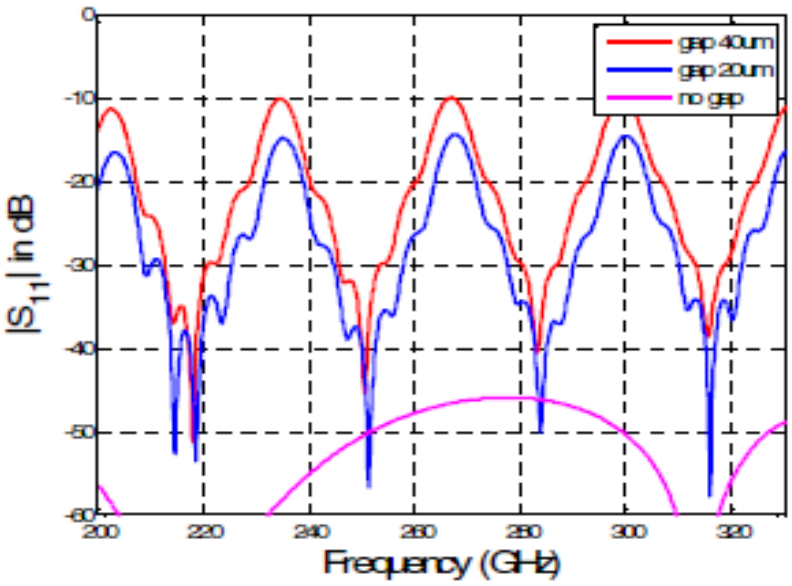

Fig 2.5: Simulated return loss of WR-3 waveguide connection when a gap of 20 µm and 40 µm is applied between the waveguide flanges compared to no-gap scenario [31]

Based on the gap waveguide technology, a contactless leakage-free waveguide flange implemented by a periodic bed of pins was first published in 2012 [31]. When the poor electrical contact between the waveguide flanges was found, that raised the need for contactless waveguide flange interconnection at high frequencies with excellent performance. In the proposed structure in [31], a circular region around the waveguide opening acting as an impedance transformer, with the same height of the pins was proposed. In the radial direction, the circular rim was about quarter wavelength to create a short circuit at the waveguide wall, thus ensuring better return loss from the waveguide interconnects. However, at lower frequencies, the dimensions of the pins and the rim around the waveguide opening, which depends on wavelength, becomes substantially larger, thus resulting in not fitting into the standard waveguide flange.

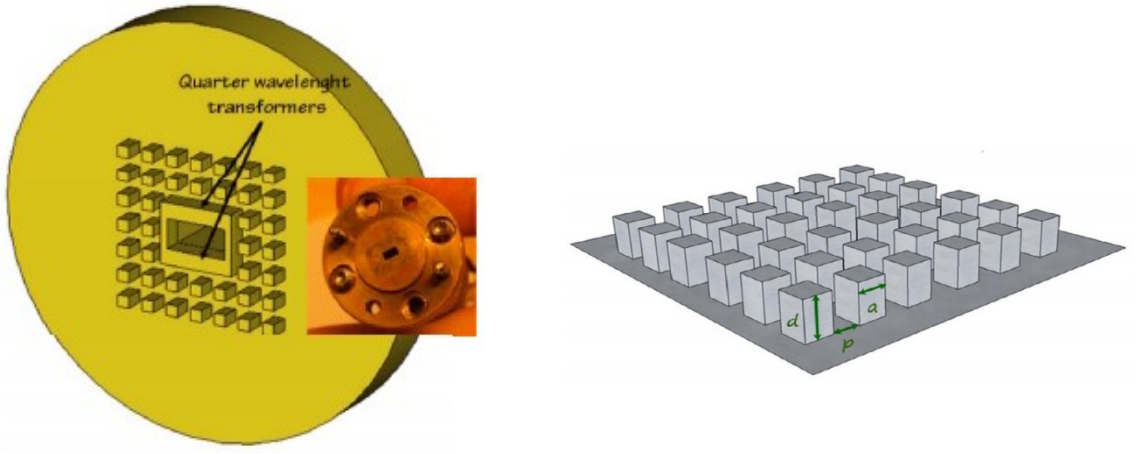

(a) (b)

Fig 2.6: Contactless waveguide flange proposed in [31] (a) Waveguide flange with pins and quarter wavelength transformer beside a photo of standard WR3 flange and (b) Bed of pins with dimensions of- a = 167 μm, d = 277.7 μm, p = 194 μm designed for a frequency range of 190-320 GHz

Another contactless adapter consisting of glide-symmetric holes around the waveguide aperture on the flanges is proposed in the literature for leakage-free wave propagation within two connecting waveguides [32- 37]. Because of the glide symmetry properties, a duplicate pattern of the holes is possible to design on both sides, thus resulting in a glide-symmetric structure when they are connected together. Though this glide-symmetric structure is convenient to fabricate, it has some drawbacks at lower frequencies since the periodicity of the holes is almost twice as much as the previously mentioned bed of pins. Moreover, the diameter of the holes is larger compared to the dimension of pins, which makes it challenging to accommodate around the waveguide opening at a lower frequency range.

(a) (b)

Fig 2.7: Glide-symmetric structure mentioned in [37] (a) Unit cell of a holey glide-symmetric method with dimensions of h = 2 mm and r = 1.4 mm designed for a frequency range of 40-60 GHz and (b) Rectangular waveguide joined to flanges with glide-symmetric holes on both sides

All of the aforementioned contactless waveguide flange adaptors have one common shortcoming that is to modify the structure of the original waveguide flange. Moreover, the periodic structures are either designed for standard rectangular waveguides or implement a choker-shaped impedance transformer around the waveguide opening to make the fabrication process complicated.

Another major concern in microwave communication systems is Passive Intermodulation (PIM), which is a significant nonlinear distortion when two or more high power tones are mixed in passive microwave components or systems [70, 85, 94- 96]. PIM can occur in various microwave passive components and thus severely affecting the communication systems. PIM's key mechanism is metal contact nonlinearity [96] that exists in most of the microwave connection structures, including waveguide flange connection. The typical solution to the PIM issue of waveguide flange is to improve the flange surface contact condition, for instance, rigorous surface machining process and high-pressure connection resulting in expensive manufacturing techniques [70]. However, several solutions for the PIM issue have been suggested in the literature, one of which is contactless waveguide flange based on gap waveguide technology [70, 85, 94]. In contrast

with the traditional waveguide smooth flange connection, physical contact does not exist in the contactless waveguide flange connection. Eliminating the metallic contact nonlinearity suppresses PIM.

Moreover, PIM is mostly noticeable in low-frequency applications, such as Ku-band or S-band, since the transmission power in these bands is generally higher than high-frequency ones [85]. Some PIM result analysis achieved at high-performance PIM measurement setup for contactless waveguide adapter published in literature is illustrated in Figure 2.8 [70, 85]. It is visible that for different PIM level, the experimental results of contactless waveguide adapter is quite impressive compared to typical standard waveguide smooth flange connection.

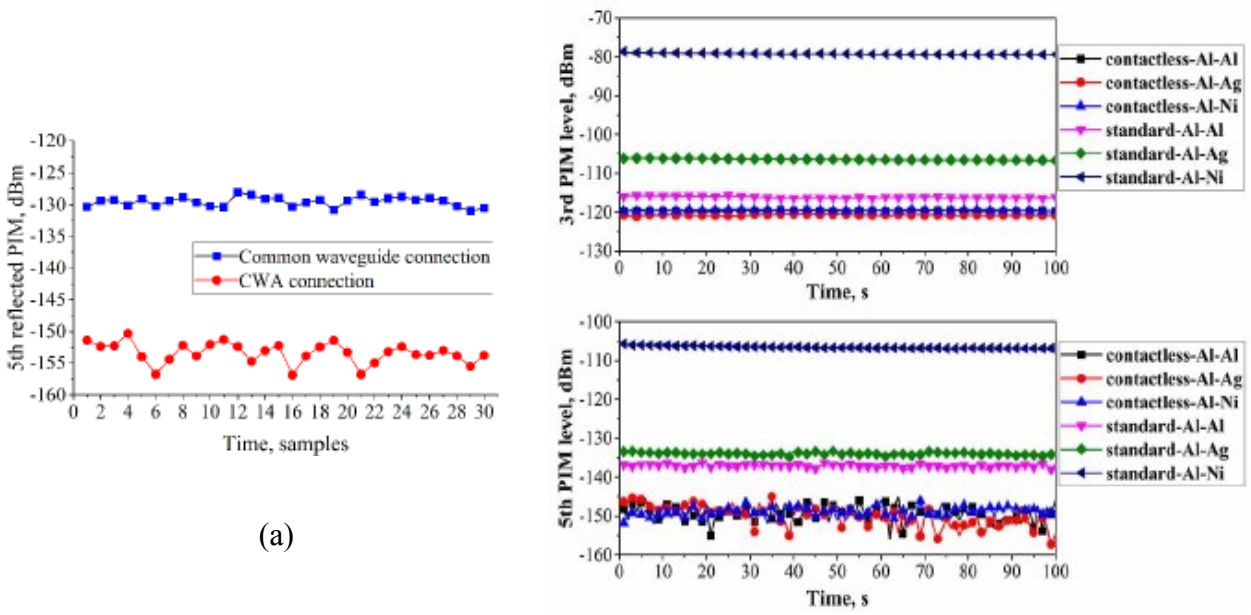

Fig 2.8: Experimental results collected at PIM measurement setup for contactless waveguide connection compared to standard waveguide flange connection for (a) Ku-band for WR-75 waveguide [70] and (b) S-band for WR-430 waveguide for different flange materials [85] for time samples

2.2.2 Flangeless Connector for Standard Waveguides

Waveguides are the extensively used microwave transmission lines because of their benefit of high power handling capacity and fewer losses, which possess an obvious downside due to its oversized flange. The waveguide flange is the most common joining structure used in numerous waveguide mechanisms. In space applications or satellite communications, this larger flange than the waveguide might hinder miniaturization, eventually limiting lighter weight and lesser volume. To ensure faster and reliable operation of waveguide connections, a contactless waveguide flange is first proposed for a millimeter-wave system [82]. Later a cylindrical contact-free waveguide flange is proposed for a bendable waveguide connection [83]. A concurrent rotatable rectangular waveguide connector is also designed based on a piled air-gapped waveguide structure [84]. Recently, another waveguide connector based on gap waveguide technology has been proposed to reduce the volume of the conventional waveguide flange [85]. Nevertheless, all the mentioned waveguide connectors yet possess greater dimensions than standard flange and the requirement of connecting screws. Moreover, all the structures are proposed for standard rectangular waveguides only.

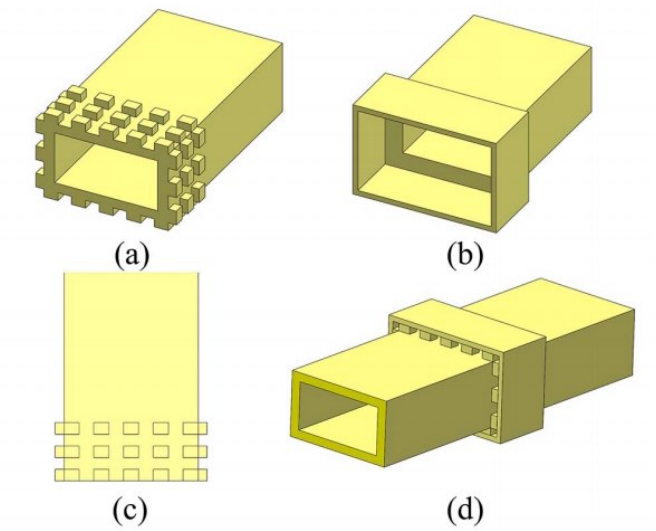

Fig 2.9: 3D view of the compact waveguide connection proposed in [82] (a) 3D view of the AMC structure, (b) 3D view of the hollow end structure (PEC), (c) Top view of the AMC structure, and (d) Complete structure

2.2.3 Orthomode Transducer

To double the channel capacities in wireless communication, one of the frequently used resolutions is twofold orthogonal polarizations [38], which consequentially cause the orthomode transducer (OMT) to be utilized. In general, an orthomode transducer is a vital element in feed systems where frequency recycling is implemented, for instance, in satellite communications. An OMT is a polarization separator that splits two orthogonal polarizations within the same frequency band. Thus, dual-frequency channels can then be simultaneously used, therefore enhancing system capacity. It is accountable for transmitting and /or receiving two orthogonal polarizations using an orthodox physical structure.

Generally, a conventional OMT is electrically a four-port structure, even though only three physical ports are exhibited. The common port is generally a circular or square cross-section (interfacing the feed horn), provides two electrical ports that are assigned to the independent

orthogonal dominant modes (TE_{10} and TE_{01}) for square waveguide and (TE_{11} and TE_{11}) for circular waveguide, respectively. The other two ports are designed using a standard waveguide or coaxial ports, allocating the individual fundamental signal mode. OMT has been stated for the first time in 1956 by Tompkins [39]. The single polarization ports can be applied by any apparatus such as microstrip lines [40], rectangular waveguides [41], or coaxial lines [42].

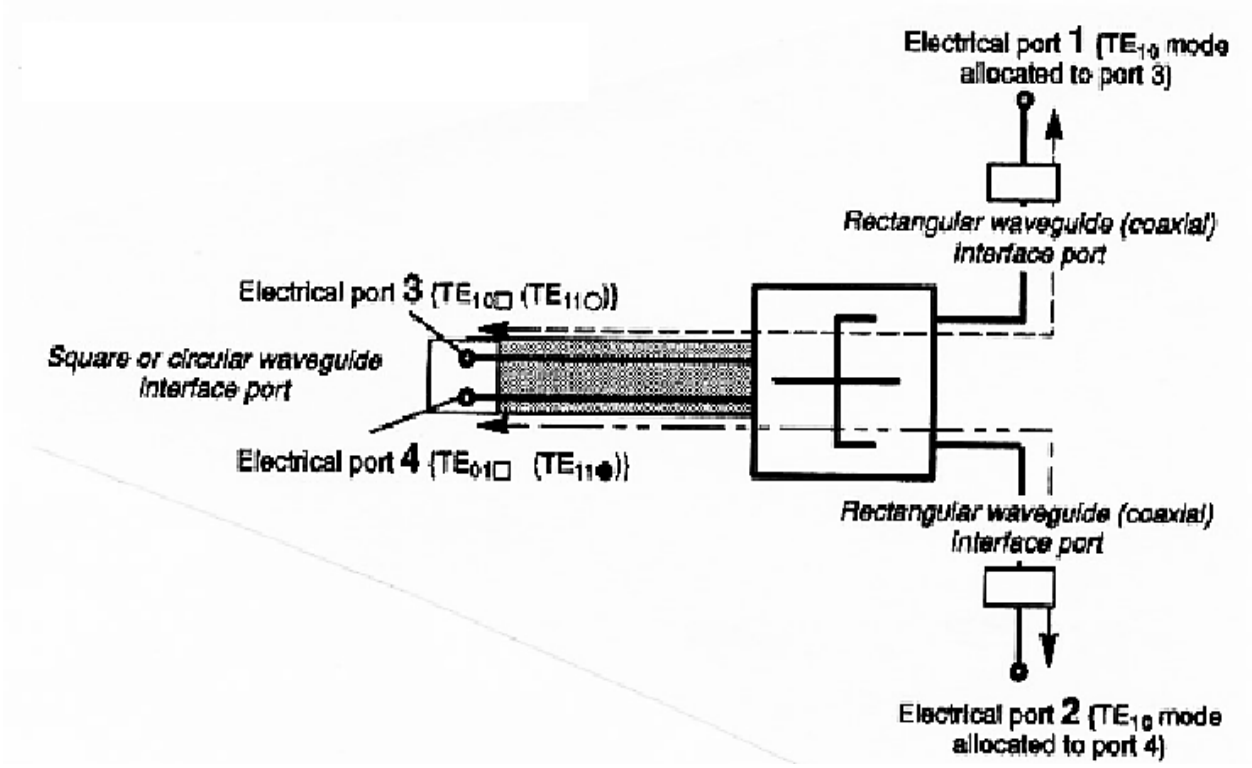

Fig 2.10: Principle equivalent circuit of an OMT [43]

The OMTs are necessary to differentiate two orthogonal polarized dominant modes delivered through the common port, generally interfaced with the feed horn and thus providing them the single signal interface ports while preserving a good matching at all electrical ports and high cross-polarization discrimination between the orthogonal modes. Figure 2.10 [43]

demonstrates an equivalent circuit of typical OMT. Ports 1 and 2 in Figure 2.10 [43] embodies the single fundamental mode ports, while the common port is formed by the electrical ports 3 and 4. Ports 1 and 3, as well as ports 2 and 4, are connected internally.

OMTs decrease the volume and mass of the feeding systems, which is very crucial in satellite communications and radio astronomy systems [44, 45]. OMTs comprising waveguide junctions are categorized into three divisions: one-fold symmetry, two-fold symmetry, and asymmetric [46- 49]. The one-fold symmetry OMT structures are primarily established on the T-junctions, where the horizontal polarization is propagated through the transverse port, whereas the vertical polarization is directed towards the other port implementing a differential feeding technique [50- 54]. The second design is the two-fold symmetrical OMT that splits two orthogonal modes as well as solves the higher-order mode excitation [49]. Symmetrical OMT configurations, for example, the Boifot OMT [49] and the turnstile junction OMT [55- 61], naturally demonstrate high isolation between orthogonal ports together with wider operating bandwidth. These benefits are gained at the cost of the mechanical complexity and oversized structure. Symmetric OMTs are usually applied by n-lines [62], ridge waveguides [42], and quad-ridged waveguides [63]. Finally, the third category is the asymmetric OMT that usually operates by dividing orthogonal modes in a compact size. Conversely, the asymmetric OMTs can only function at narrow operating bandwidth, thus avoiding the unnecessary coupling of the in-band higher-order modes [64]. Besides, in comparison with the symmetric OMT structures, the asymmetric OMTs generally possess a poor isolation level.

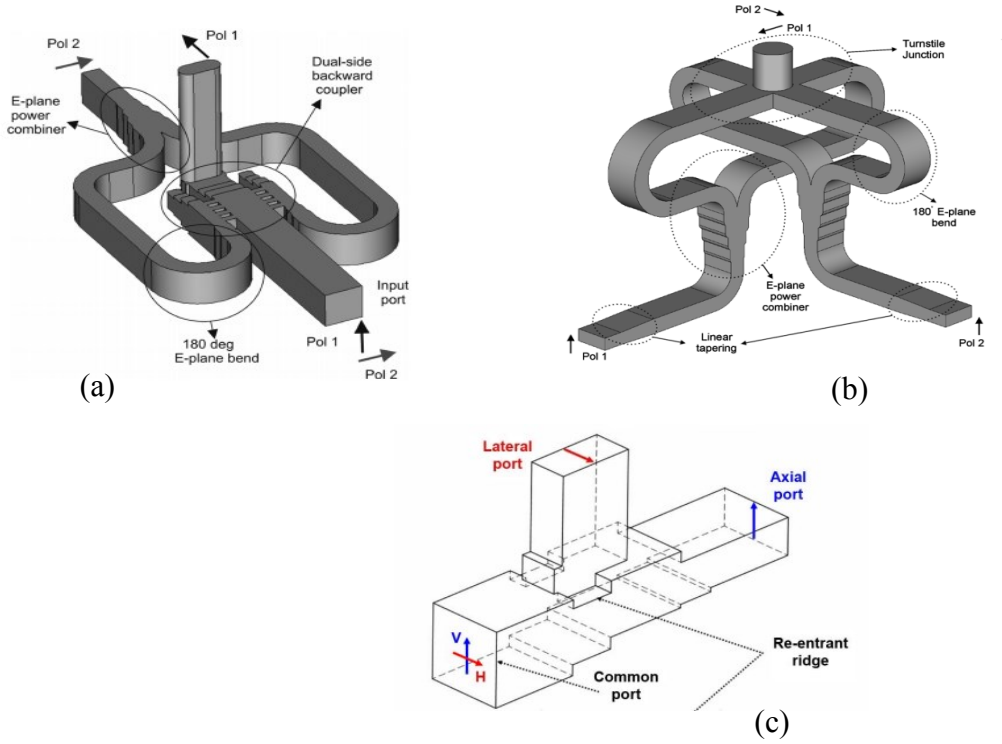

Fig 2.11: Different categories of OMTs in literature (a) One-fold symmetry [50], (b) Two-fold symmetry [55], and (c) Asymmetric [64] OMT

In this chapter, the elementary concepts of gap waveguide technology, for instance, unit cell analysis, are described, followed by certain guiding structures that fall under the periodic configurations, such as the ridge gap waveguide and groove gap waveguide. Afterward, few important microwave components, e.g., contactless adaptors, are designed considering standard waveguide flanges, contact-free, and flange-free pluggable waveguide connectors. Finally, a compact orthomode transducer, i.e., in-band polarization separators, is designed.

In the upcoming chapters, we discuss the design methodology of contactless waveguide adaptors, flangeless and contactless pipe contact, and compact OMT configuration. All these

structures are based on gap waveguide technology. The response of the structures is validated by two different simulation techniques.

Chapter 3

Contactless Waveguide Adaptor for Multiple Frequency Bands

The requirements for an improved connection between waveguides are very crucial to ensure leakage-free wave propagation. Lately, several rectangular waveguide connectors have been presented based on gap waveguide technology focusing on millimeter-wave applications [65-70]. However, most of the contactless waveguide adaptors propose to modify the original structure of the waveguide flange. However, our proposed structure does not need to modify the original structure of the waveguide flange while ensuring compact design, contact-free seamless transition, less manufacturing complexity and fabrication cost, minimal electromagnetic wave propagation loss, and of course, wider bandwidth covering multiple frequency bands: V-band and W-band in our case. This chapter discusses the contact-free waveguide adaptor for two different frequency bands for both circular and rectangular waveguides.

The principle of gap waveguide theory states that an artificial magnetic conductor structure usually consists of periodic pins mounted on one surface, whereas the other flat surface acts as perfect electric conductors [71].

3.1 Contactless Waveguide Adaptor (CWA) for Circular Waveguide

3.1.1 Design Methodology

Following the gap-waveguide technology, a consecutive dual-faced AMC structure is designed to ensure contact-free seamless transition like a gasket for circular waveguide within a wide frequency bandwidth. The 3D geometry of the proposed solution is illustrated in Figure 3.1. The

rudimentary structure consists of a metal plate along with a circular waveguide opening of standard diameter as well as screw holes for fixture and alignment.

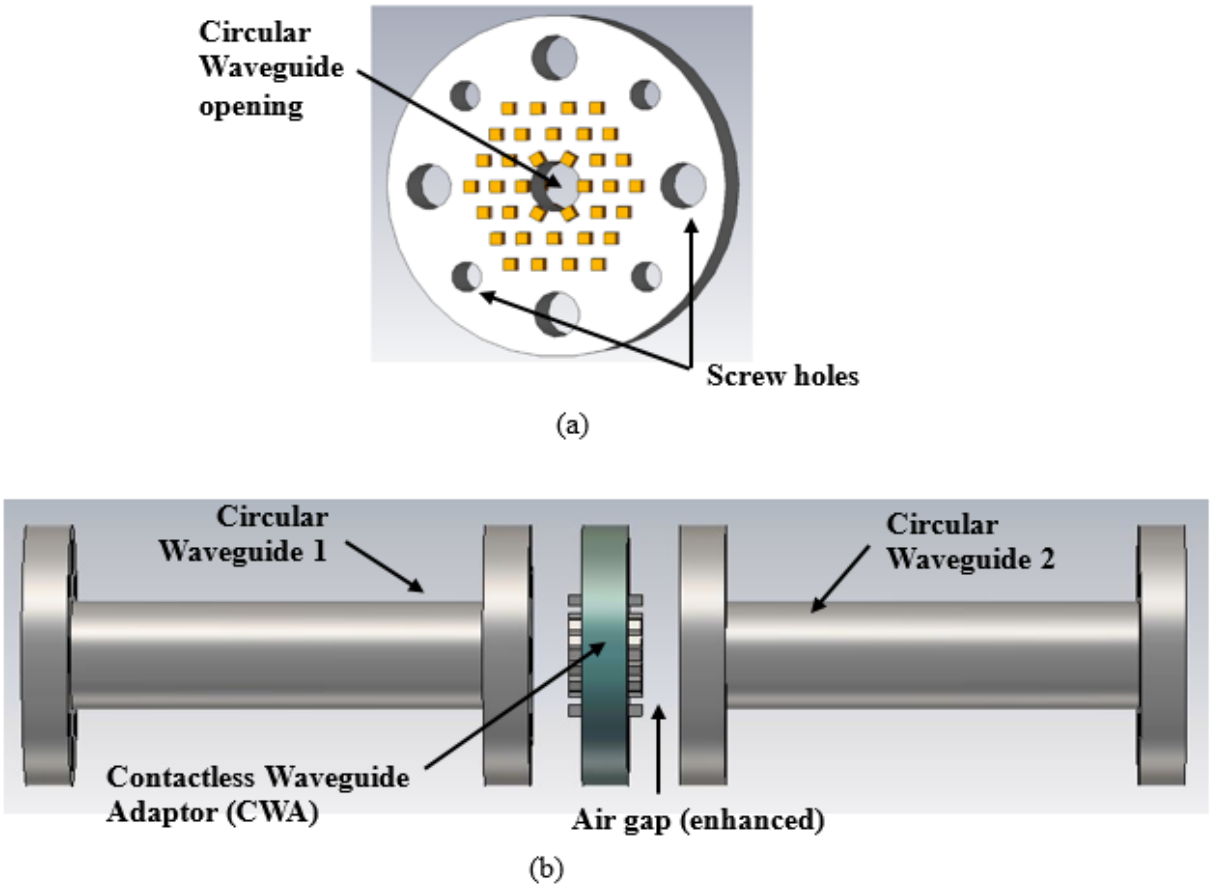

Fig.-3.1: (a) Contactless waveguide adaptor (CWA) for a circular waveguide with pin orientation using a triangular lattice and (b) Full view of the CWA while connecting two standard circular waveguides (airgap between adaptor and waveguide has been enhanced)

A standard UG-387/U round waveguide flange is modified by placing multiple rings of pins in a hexagonal arrangement, starting precisely from the circular waveguide opening. Thus, the dimensions of the adaptor are precisely equal to a standard waveguide flange. Additionally, pins' bed exists on both sides of the adaptor, forming a consecutive AMC structure. A triangular lattice [67] orientation method is followed to mount the pins uniformly around the circular

waveguide. Since electrical contact is not mandatory for the adaptor, magnets can also be used instead of screws for waveguide connection to ensure faster and reliable measurements [66].

Between the smooth flange of the standard waveguide and the adaptor's textured flange, a parallel-plate cut-off region within the airgap is created by the pins. Hence, the wave propagation is occurring only along the waveguides without much leakage amid the flanges.

3.1.2 Unit Cell and EBG Analysis

The pins' dimensions are designed appropriately to form a proper electromagnetic bandgap (EBG). The operating frequency is chosen to cover the multiband frequency range of 50- 110 GHz. Thus, the EBG should also be the same.

A unit cell with infinite periodic boundaries is simulated for accurate calculation of the EBG of the periodic contactless structure using CST Microwave Studio Eigenmode Solver, as shown in Figure 3.2. The unit cell's periodic structure results in a high surface impedance at the bottom surface, which does not allow wave propagation. The Eigenmode Solver of CST Microwave Studio resolves the problem from Maxwell's curl equations for electric and magnetic fields. Taking each of these equations' curl gives the wave equation of both electric and magnetic fields [72, 73]. The propagation constant calculated from the wave equation provides the stopband that depends mostly on the air gap between the ridge and upper PEC plate. Several parameters are modified to achieve the desired electromagnetic bandgap; for instance, the height of the pins (h_p) must be approximately $\lambda/4$ to transform a short circuit (PEC) to an open circuit (PMC). The lower cut-off frequency is defined by the height of the pins, h_p. The air gap must be smaller than $\lambda/4$ for signal propagation. After obtaining the bandgap, the following step is to design the contactless adaptor. For developing the adaptor, Transient Solver is used, which follows the Finite Integration

Technique (FIT) to solve the problem. The periodic nails act like an Artificial Magnetic Conductor (AMC), where the normal electric field is non-existed. The bandgap of the unit cell is considered as the operating bandwidth of the ridge gap waveguide.

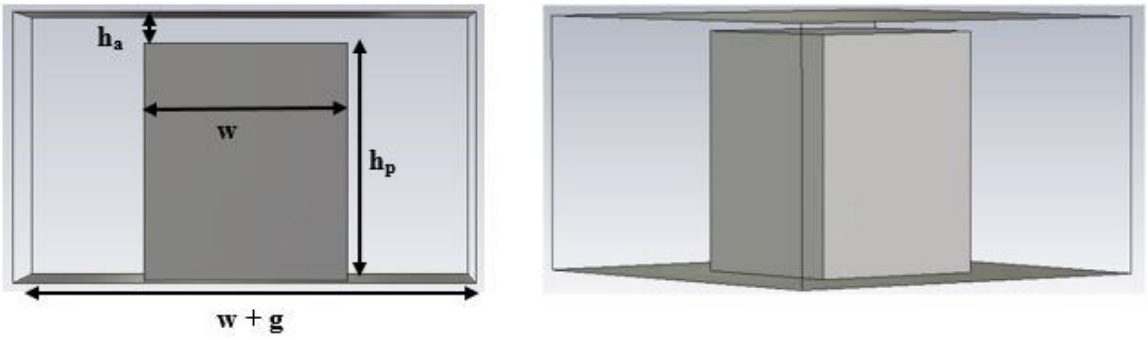

(a) (b)

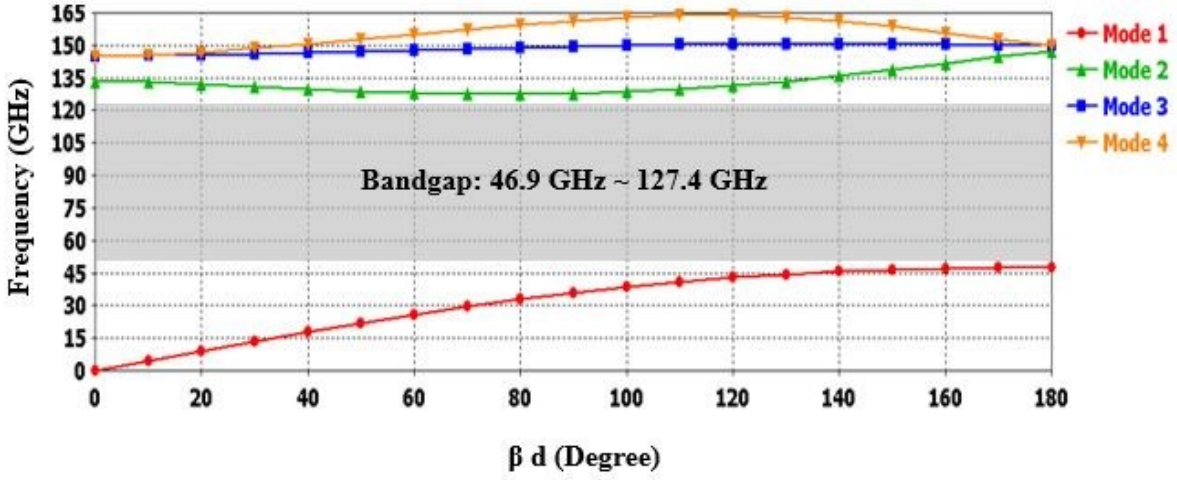

(c)

Fig-3.2: The Unit element (a) Front view, (b) Perspective view, and (c) Dispersion diagram

The unit element's dimensions are tabulated in Table 3.1, where w is the nail width, w+g is the cell width, g is the gap between two consecutive nails, h_p is the nail height, and h_a is the airgap between the nail and upper PEC layer.

Table 3.1: Dimensions of the Unit Element

Parametric Symbols	**Value (mm)**
h_p	0.84
h_a	0.1
w	0.65
g	0.8

According to the dispersion diagram in Figure 3.2, the EBG is from 46.9 to 127.4 GHz, which covers the entire operating frequency range. The width of the bandgap depends on the airgap h_a. The larger the airgap between the nail and the upper PEC plate, the narrower the bandgap, provided the airgap is less than quarter-wavelength [74]. This is shown in Figure 3.3, where a parametric study of the bandgap is represented with respect to airgap, h_a (mm) between the nails and the top PEC plate. From Figure 3.3, it is evident that the bandgap is getting narrower with increased airgap, h_a. When h_a = 0.0001mm (apparently no airgap), the bandgap is from 2.37 GHz to 142.58 GHz, which is quite extensive in terms of the frequency range. But considering the practical scenario, for instance, surface roughness, machining error, or misalignment, the airgap, h_a is suggested as 0.1mm. However, a smaller airgap can be considered for better performance. It should be mentioned that the gap is an accidental gap, and it is possible to be zero.

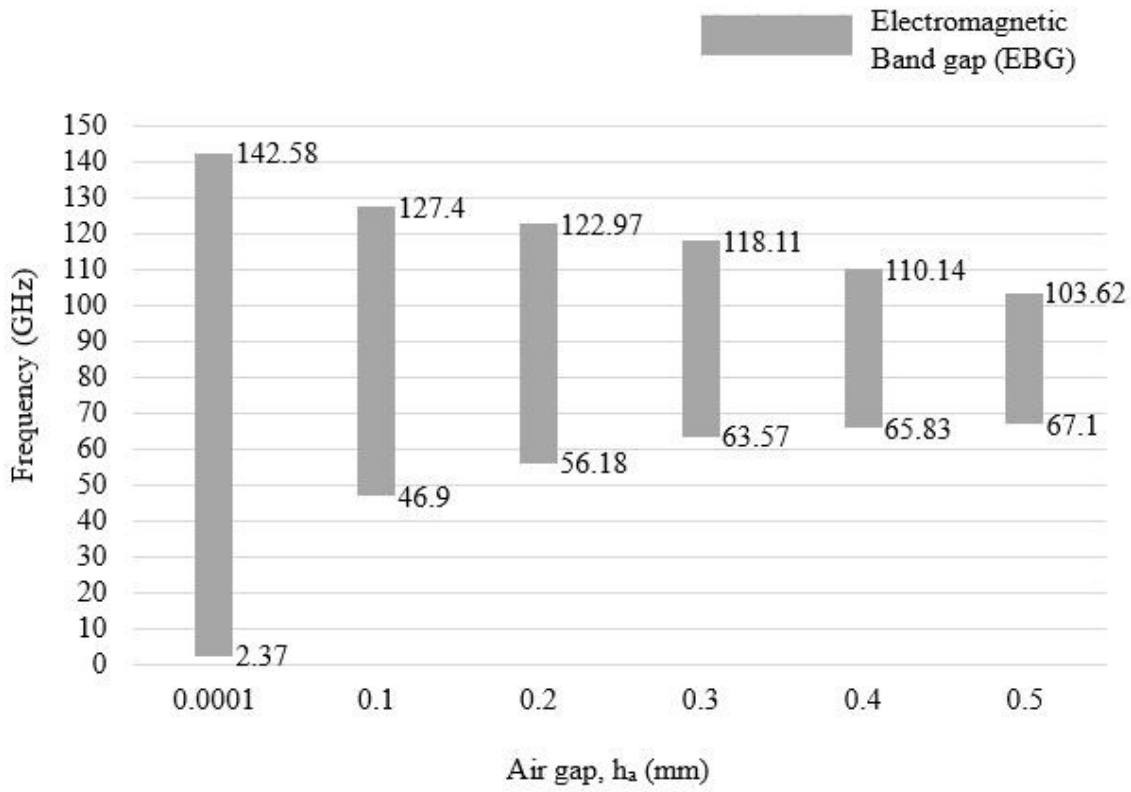

Fig.-3.3: Parametric study for an air gap (h_a) between nails and upper PEC plate while keeping other parameters constant

3.1.3 Standard Circular Waveguide With Respect to Operating Frequency

As previously mentioned, the operating frequency is selected for the multiband frequency range of 50- 110 GHz, which covers both V-band (50- 75 GHz) and W-band (75- 110 GHz). For circular waveguides, there are different standard diameters assigned to these frequency groups. Different circular waveguide diameters with different frequency ranges within the desired frequency band are shown in Table 3.2. In addition, Figure 3.4 represents a diagram of a general circular waveguide with waveguide opening diameter (represented by D) along with few screw holes for alignment.

Table 3.2: Standard Circular Waveguide Parameter and their Operating Frequency

Frequency Band	Frequency Range (GHz)		Circular Waveguide Diameter, D (mm)
V	Low	50-58	4.19
	Mid	58-68	3.58
	High	68-75	3.18
W	Low	75-88	2.84
	High	88-110	2.39

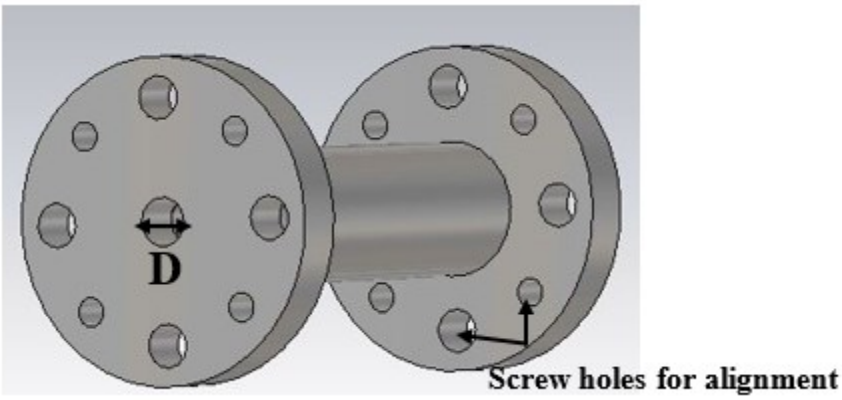

Fig.-3.4: Circular Waveguide (D= Diameter of the waveguide opening)

3.1.4 Different Contactless Waveguide Adaptor for Various Frequency Range

As mentioned earlier, a standard UG-387/U round waveguide flange is modified for the proposed contactless adaptor. Thus, the adaptor's size and bandwidth are already determined according to the standard flange and waveguide. For each frequency range mentioned in Table 3.2, a new adaptor for each standard circular waveguide diameter is designed every time.

The results shown in Figure 3.5 correspond to a waveguide inter-connection consisting of two standard circular waveguides with the proposed contactless adaptor between them, as depicted in Figure 3.1 (b). Figure 3.5 combines the scattering parameters of five different circular waveguide diameters within the frequency range of 50- 110 GHz (V-band and W-band).

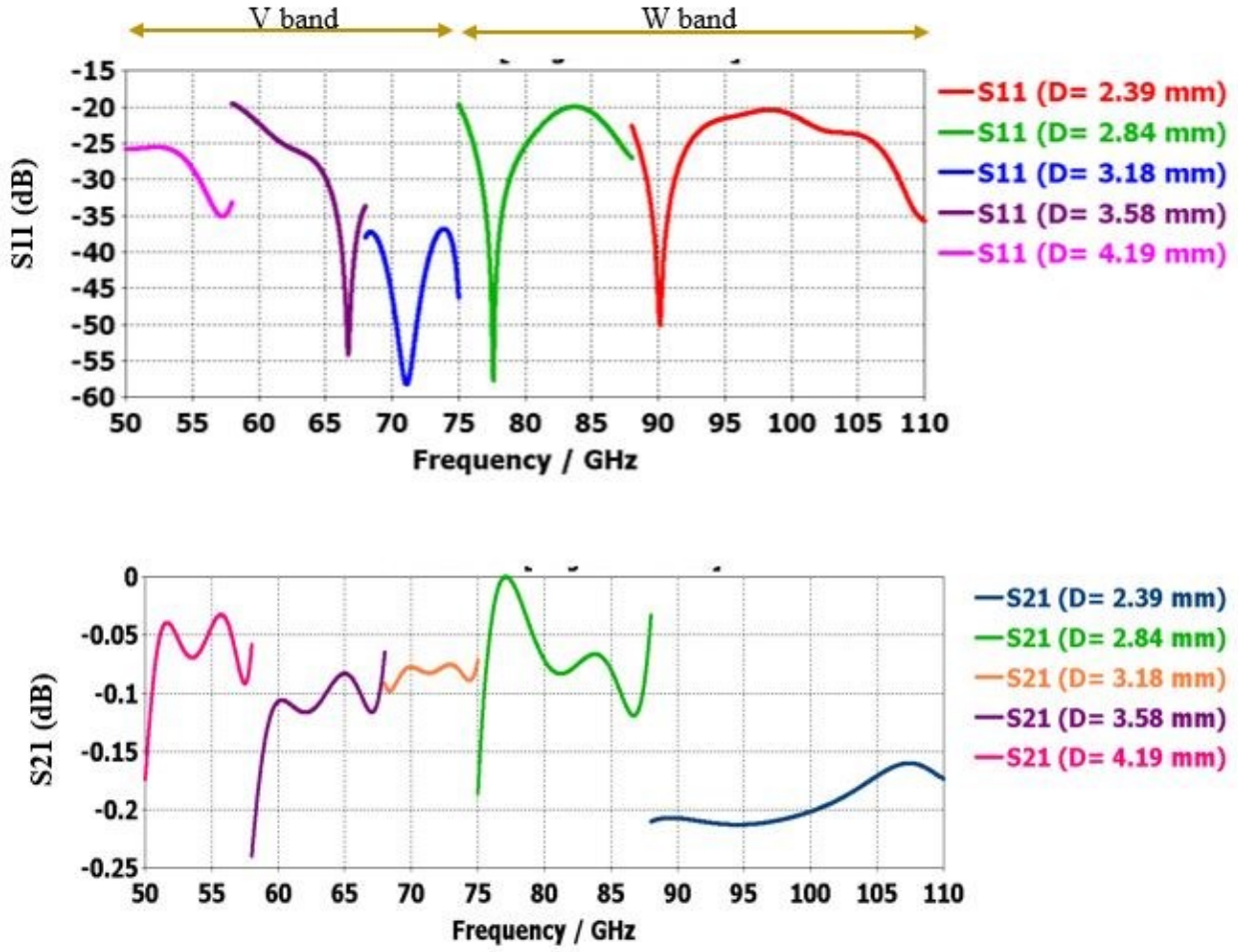

Fig.-3.5: Simulation result of the proposed structure for different adaptors of various circular waveguide diameters (D= circular waveguide diameter)

It is clearly visible that the return loss is better than 20 dB throughout the entire frequency bandwidth, which is an excellent matching level. Similarly, the transmission coefficient is well above -0.25 dB, which means negligible loss and leakage at the connection.

3.1.5 Same Contactless Waveguide Adaptor for Various Frequency Range

In the previous section, a gasket-like adaptor that has a circular waveguide surrounded by a bed of pins around the waveguide opening from both sides is suggested. It is possible to design a different adaptor for each waveguide diameter. To limit the manufacturing cost and archive, the products for developing a new adaptor for each frequency range, a single adaptor with the same pins lattice but varying waveguide diameters, are possible. The latter case can immensely reduce the manufacturing period as well as resources.

Figure 3.6 shows how a single adaptor can be utilized with the same pins lattice but varying the waveguide diameters for each frequency range, keeping the nail position constant. For instance, the initial waveguide diameter is 2.39 mm for the frequency range of 88-110 GHz. Keeping all the pin positions constant, if the waveguide diameter is increased to 2.84 mm for a frequency range of 75-88 GHz, and it ends at a diameter of 4.19 mm for the frequency range of 50-58 GHz.

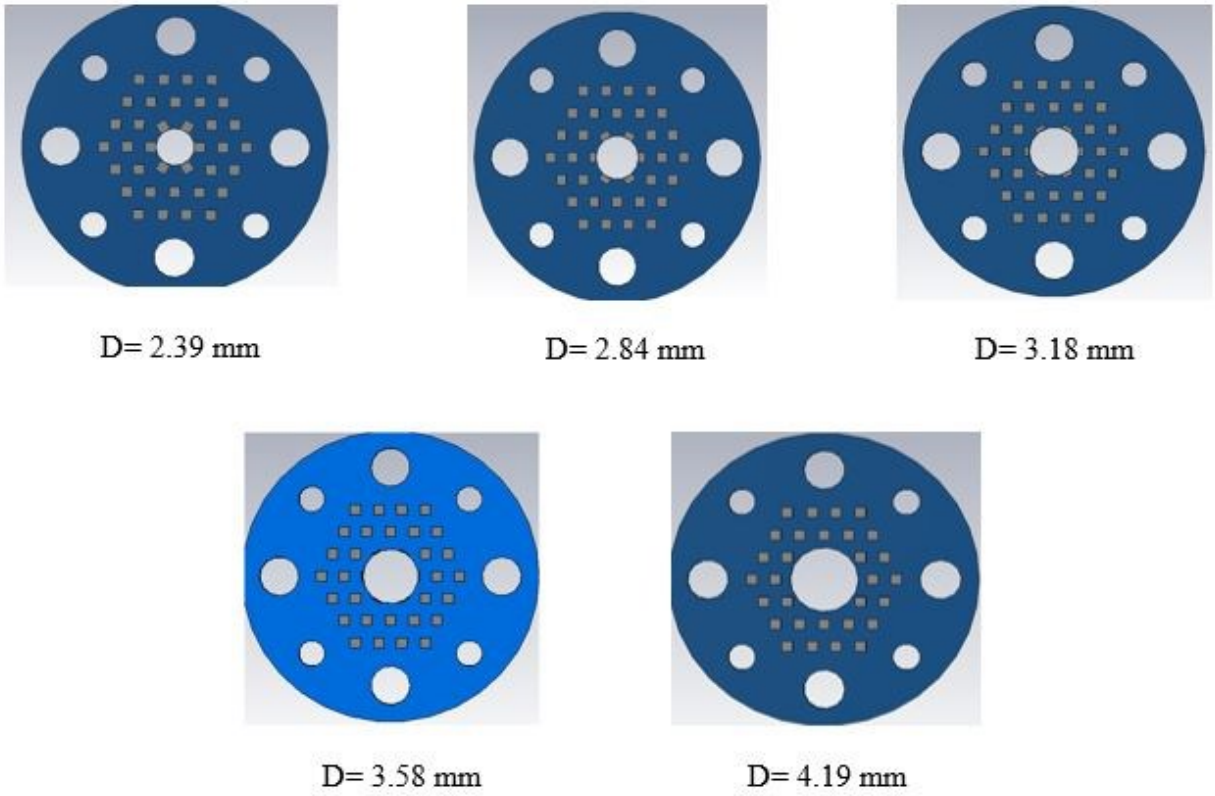

Fig.-3.6: Single adaptor with the same pins lattice, but varying the waveguide diameters keeping the nail position constant (initial waveguide diameter, D= 2.39 mm)

The responses of the same circular waveguide adaptor according to various waveguide diameters within the proposed frequency range are given in Figure 3.7. In this case, the return loss is better than 18.5 dB, and the insertion loss is within 0.27 dB.

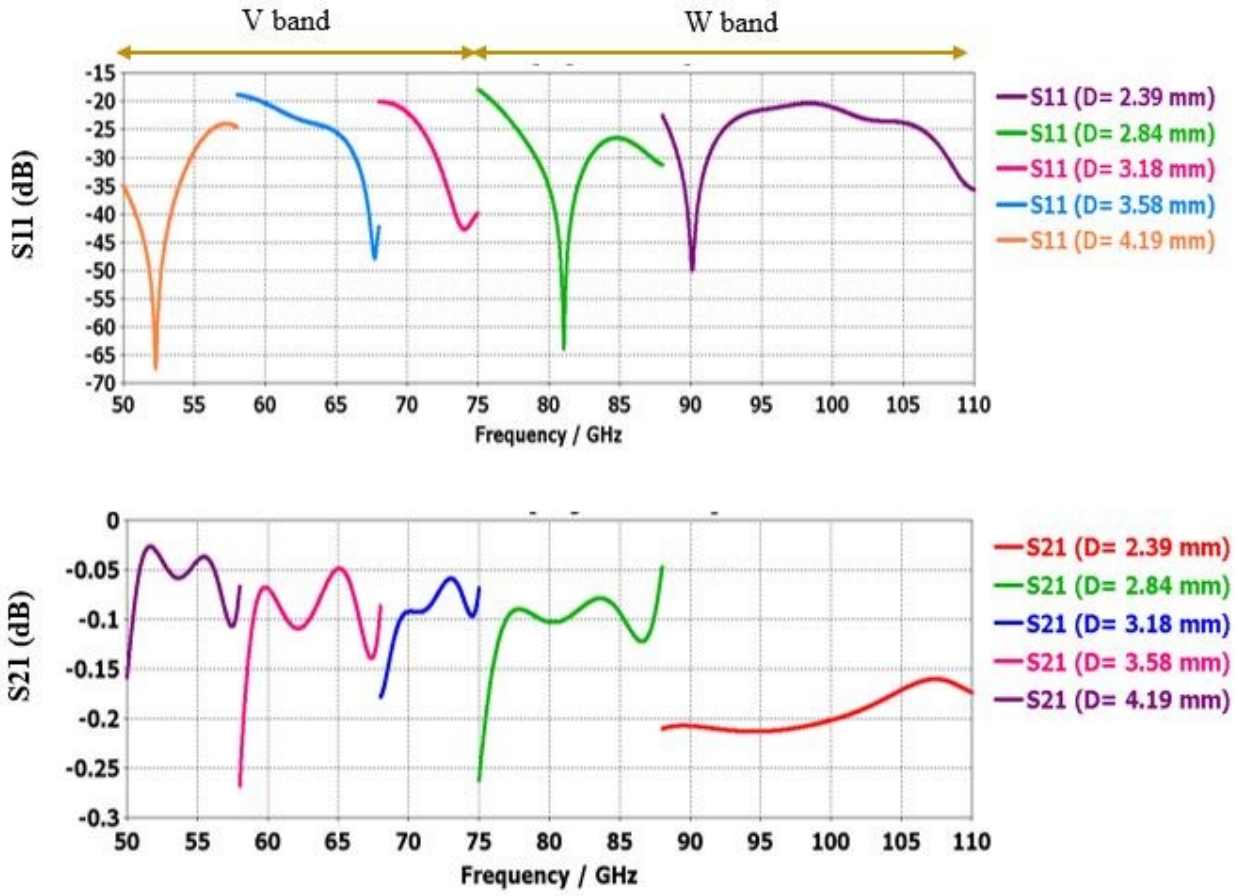

Fig.-3.7: Simulation result of the proposed structure for same adaptors of various circular waveguide diameters (D= circular waveguide diameter)

3.2 Surface Roughness

The conductor surface roughness might interrupt the current flow and eventually impact the wave propagation of interconnects. The surface roughness effect can be substantial at high frequency due to the skin effect. At the VHF range, where the skin depth is comparable to the root-mean-square (RMS) value of the rough surface height, the effect of conductor surface roughness becomes a critical factor to consider when designing waveguide connectors [75-79].

It should be stated that the use of the adaptor makes it possible to have a rough waveguide flange surface. Allowing for a rough waveguide flange does not require polishing the flange surface and thus reduce the manufacturing cost of the standard flanges. So roughness (0.2 x 0.2 x 0.2 μm^3) on random places of the waveguide flange as well as inside the waveguides was applied using VBA macro and random function of CST MWS. Then we measured the response of contactless waveguide adaptor for different circular waveguides within the frequency range, and the simulated result is showed in Figure 3.8. The return loss is better than 20 dB, and the insertion loss is better than 0.28 dB throughout the entire frequency range for different circular waveguide adaptors after adding surface roughness.

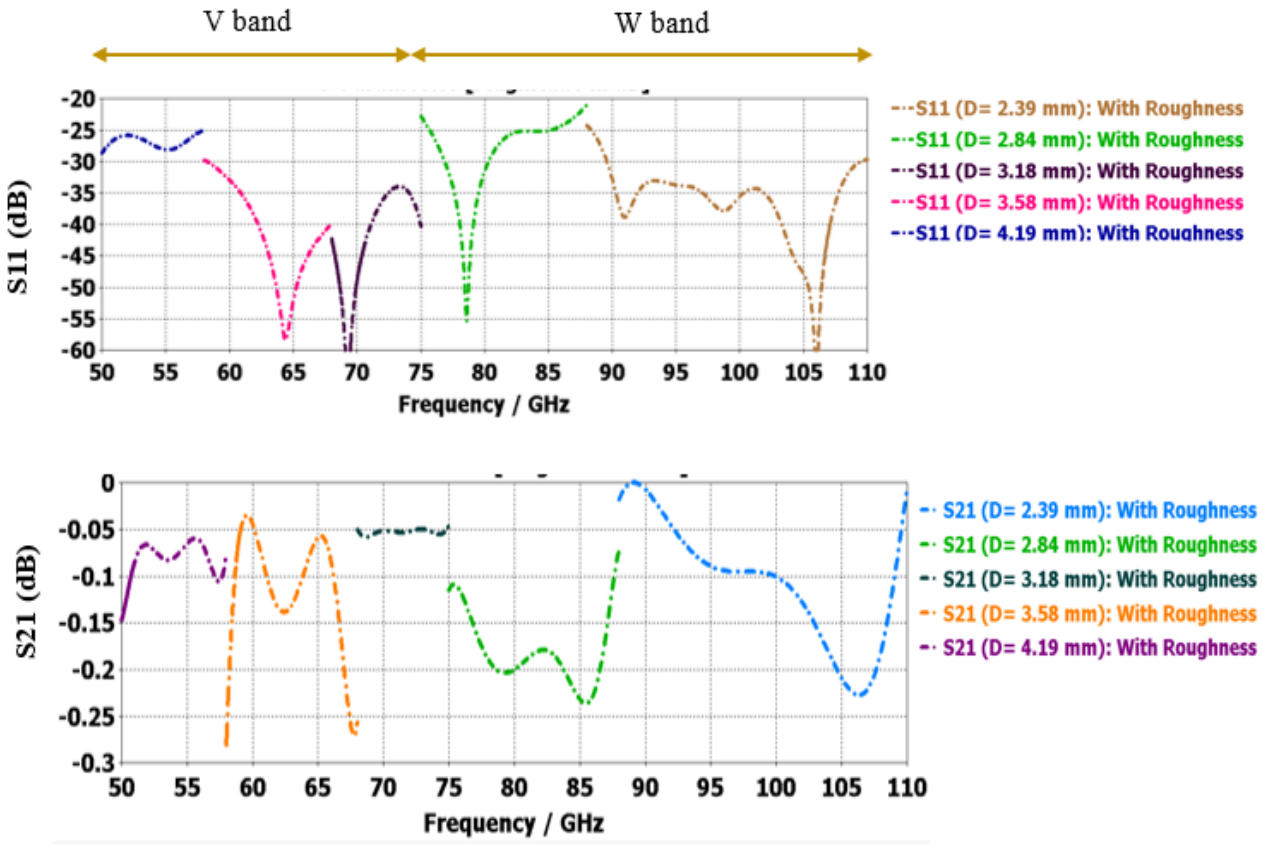

Fig.-3.8: Simulation result after adding surface roughness on the proposed structure for different adaptors for various circular waveguide diameters (D= circular waveguide diameter)

Figure 3.8 represents response after implementing surface roughness on random locations for different adaptors designed for each frequency range. Also, after adding surface roughness on random locations of the waveguide for the same circular waveguide adaptor and keeping the position of the pins constant, if we change the waveguide diameter, the response is given in Figure 3.9. Both the reflection coefficient and the transmission coefficient represent a better matching level throughout the entire frequency range, even after adding surface roughness.

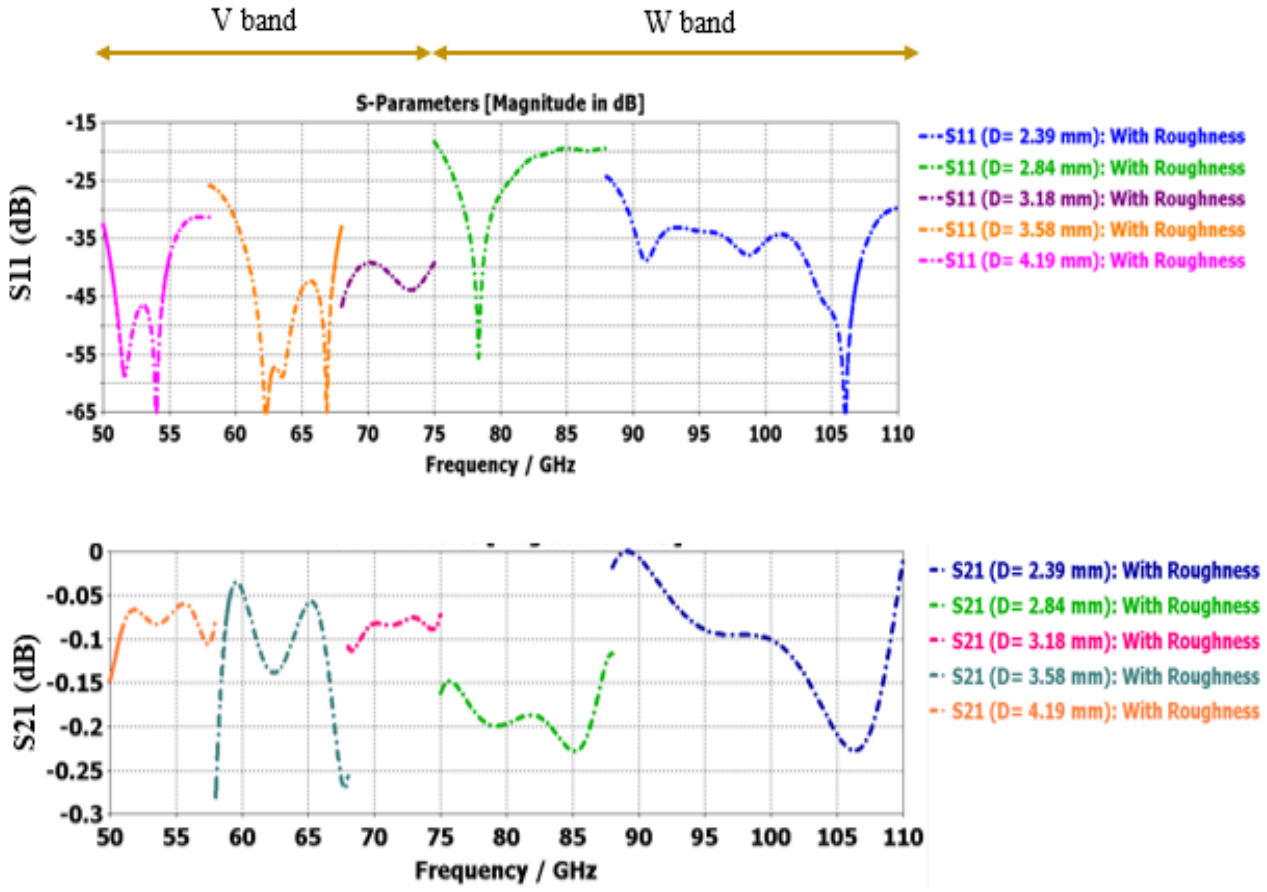

Fig.-3.9: Simulation result after adding surface roughness on the proposed structure for same adaptors with respect to various circular waveguide diameters (D= circular waveguide diameter)

The circular waveguides' results demonstrated good performance even when relatively large airgaps between the pins and upper PEC surface were considered, e.g., 0.1 mm, along with surface roughness. It is worth noting that the proposed contactless adaptor is not limited to circular

waveguides, but it can be designed for other mm-wave standard waveguide flange interconnects, such as rectangular waveguides.

3.3 Contactless Waveguide Adaptor (CWA) for Rectangular Waveguide

Rectangular waveguide adaptor is also designed for both ideal cases (which is a smooth surface) and after adding surface roughness. Table 3.3 indicates a standard rectangular waveguide parameter and their operating frequency range. Figure 3.10(a) shows a general rectangular waveguide diagram with inner dimensions represented by A and B for length and width, respectively. Figure 3.10(b) demonstrates pin orientation on the contactless rectangular waveguide adapter, where the nails were distributed uniformly using square lattice around the rectangular waveguide opening.

Table 3.3: Standard Rectangular Waveguide Parameter and their Operating Frequency

Frequency band	**Waveguide name**	**Frequency range (GHz)**	**Cutoff frequency (GHz)**	**Inner dimensions of waveguide opening**	
			Lowest order mode	**A (mm)**	**B (mm)**
V	WR15	50-75	39.875	3.7592	1.8796
W	WR10	75-110	59.015	2.54	1.27

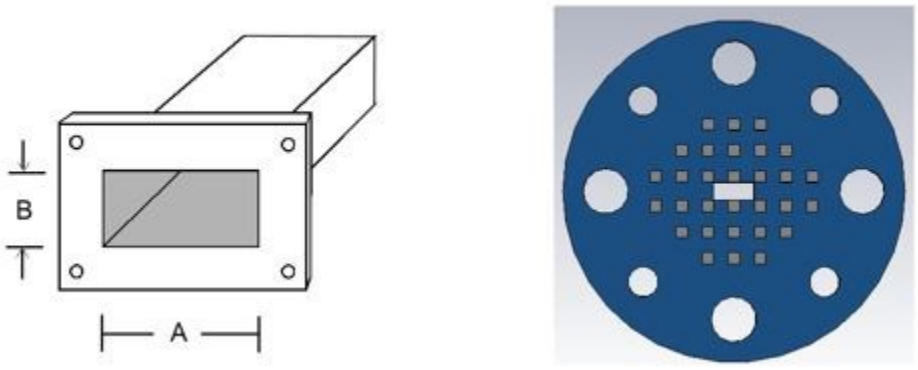

(a) (b)

Fig.-3.10: (a) General rectangular Waveguide (A, B= inner dimensions of the waveguide opening) and (b) pin orientation on the contactless rectangular waveguide adaptor

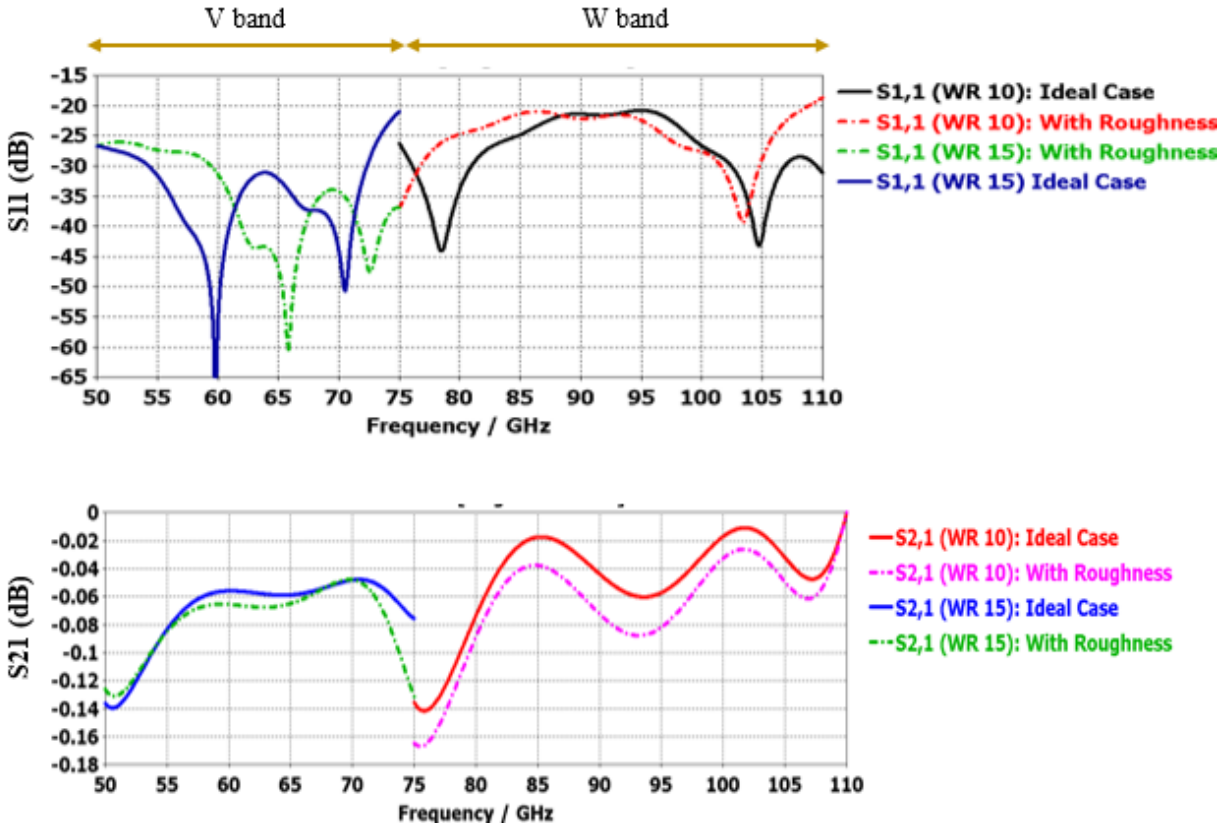

Fig.-3.11: Simulation results after adding surface roughness on the proposed structure for different adaptors for multiple frequency bands of rectangular waveguide

Figure 3.11 displays a comparison between the ideal case (which is a smooth surface, i.e., without surface roughness) and after adding surface roughness for different dimensions of rectangular waveguides according to their frequency range. Here different rectangular waveguides for different frequency ranges were implemented, as it was simulated for circular waveguides in earlier sections.

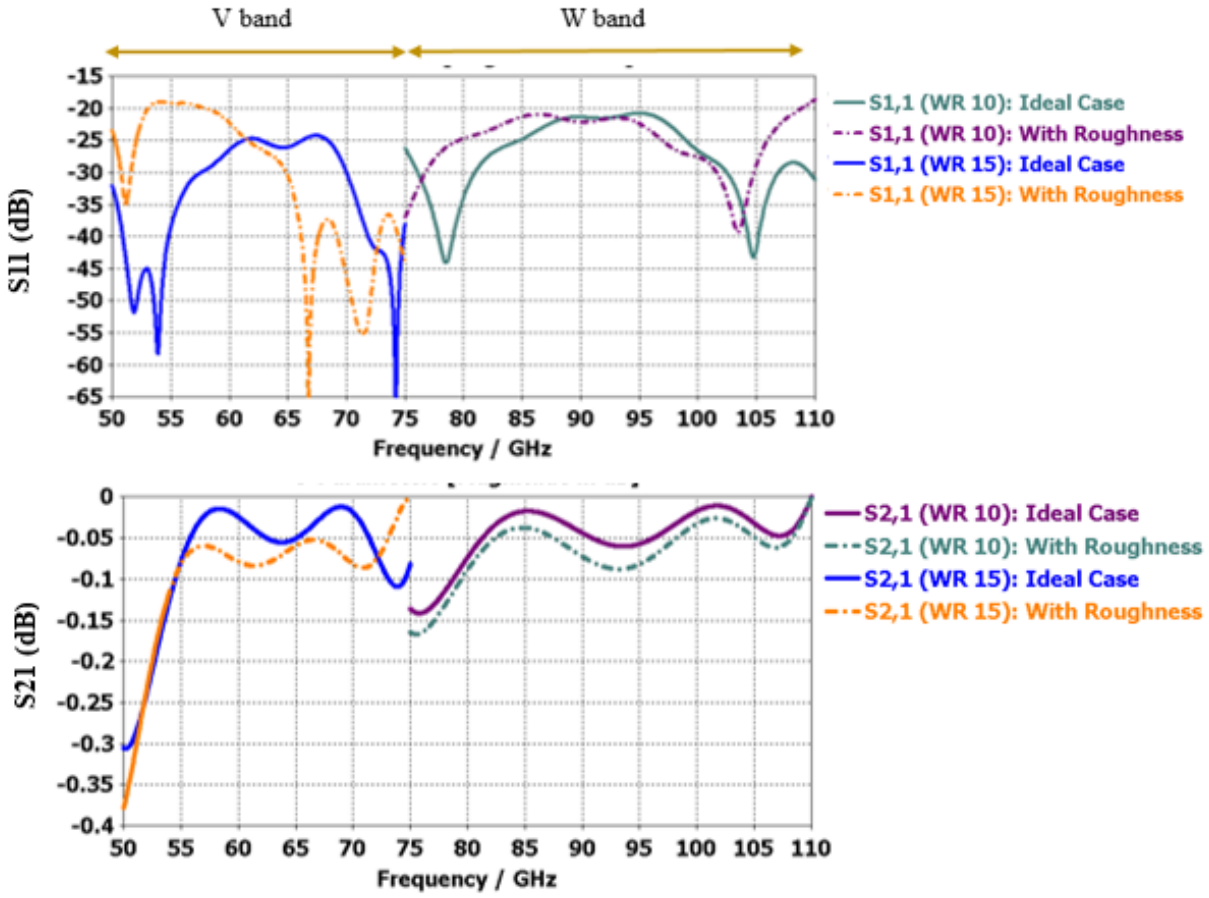

Fig.-3.12: Simulation results after adding surface roughness on the proposed structure for same adapters for multiple frequency bands of rectangular waveguide

Figure 3.11 represents simulation results after applying surface roughness on random places for different adaptors of different rectangular waveguide dimensions according to each frequency range. Also, after adding surface roughness on random locations of the waveguide for

the same rectangular waveguide adaptor and keeping the position of the pins constant, if we change the waveguide dimensions, the response is given in Figure 3.12. Both return loss and insertion loss represent a better matching level throughout the entire frequency bandwidth, even though surface roughness was added.

3.4 Validation of Results for the Proposed CWA

Electromagnetic solvers are based on resolving Maxwell's equations in different forms. The Time-domain solver of CST MWS operates by FDTD (Finite Difference Time Domain) method to solve Maxwell's equations, whereas the Frequency-domain solver utilizes FIM (Finite Integral Method) method to solve Maxwell's equation. Thus, these two solvers use two different methods to simulate the same structure. However, both solvers are originally from the FIT (Finite Integration Technique) that operates on the Integral Forms of Maxwell's Equations [80]. Therefore, it is expected that both solvers provide similar results with differences related to their numerical solution accuracy. For further validation, Time-domain and Frequency-domain have been used to simulate the proposed structure for both circular and rectangular standard waveguides. The simulation results presented in the earlier subchapters were achieved by Time Domain Solver of CST Microwave studio.

3.4.1 Result Validation for Circular Waveguides

The return loss of the proposed CWA has been compared for different adaptors within the operating frequency range, as well as the same adaptors varying the waveguide diameter with respect to different frequency ranges and illustrated in Figure 3.13. It should be stated that, in both situations, roughness has been added at random places of the structure, including flanges and inside the waveguide.

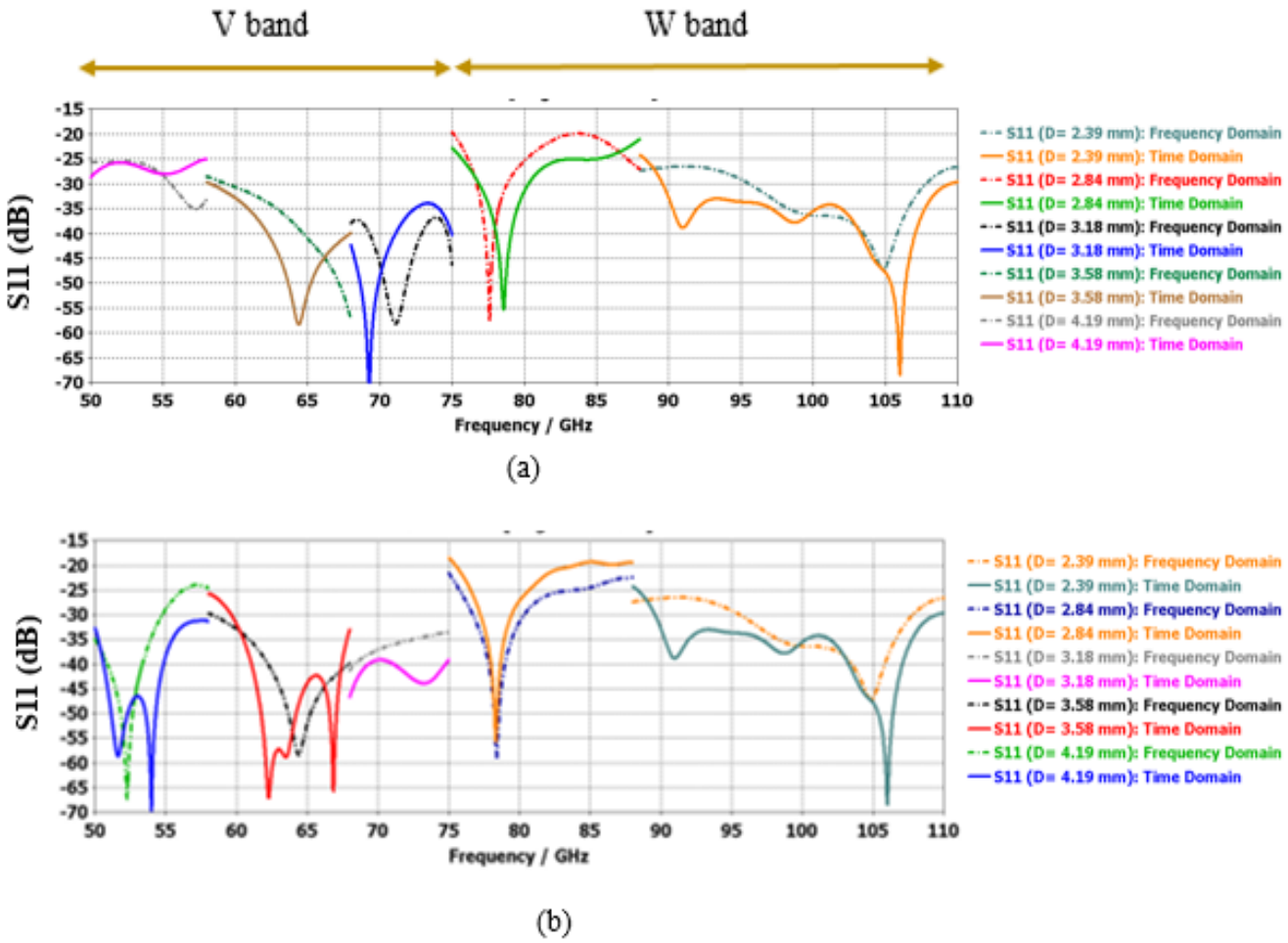

Fig.-3.13: Return loss of the proposed CWA structure for (a) Different adaptors and (b) Same adaptors with respect to various circular waveguide diameters (D) for both Time Domain and Frequency Domain Solver of CST MWS

3.4.2 Result Validation for Rectangular Waveguides

Similar to the previous subsection, the return loss has been compared for both the Time-domain and the Frequency-domain solver of CST MWS for standard rectangular waveguides after adding roughness on random locations and depicted in Figure 3.14. Like the circular waveguides, rectangular waveguides also demonstrate similar results in both solvers, along with outstanding matching level.

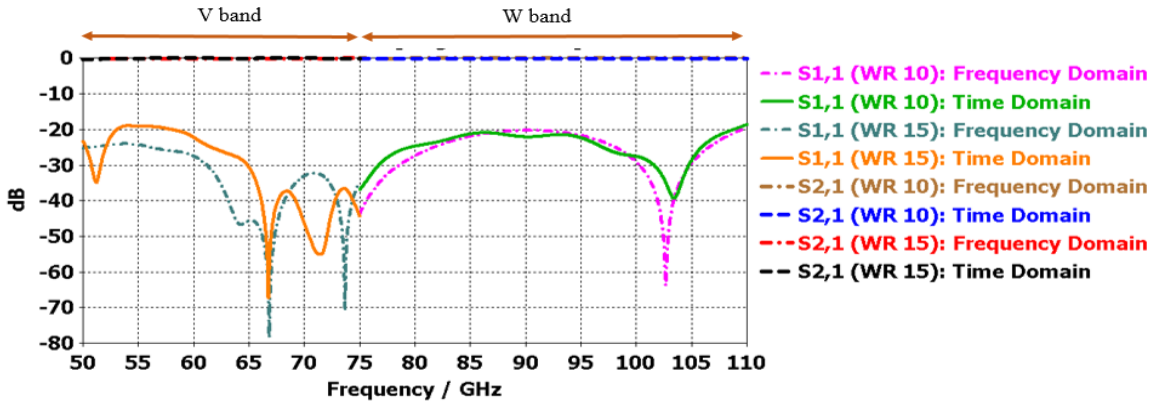

(a)

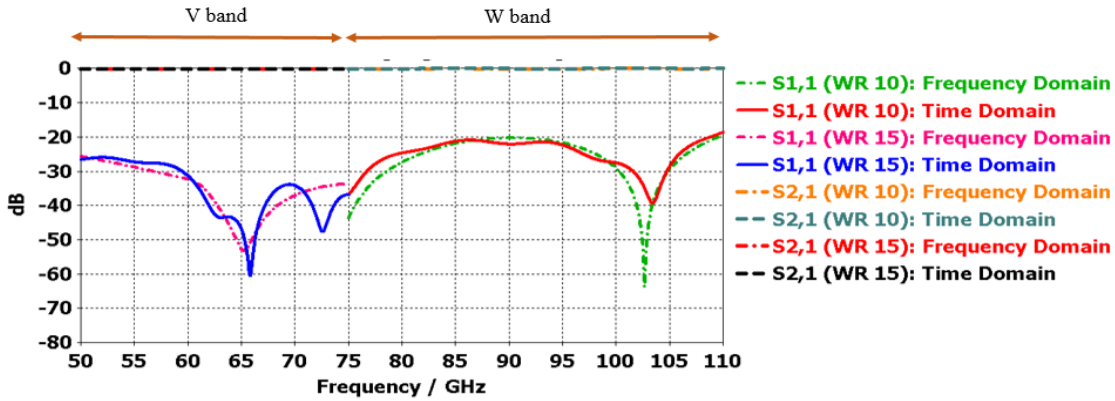

(b)

Fig.-3.14: Return loss of the proposed CWA structure for (a) different adaptors and (b) same adaptors with respect to various rectangular waveguide dimensions for both Time Domain and Frequency Domain Solver of CST MWS

This chapter represents how the connection between two standard circular waveguide flanges can be made without possible leakage, even with no electrical contact assurance. This has been assured by inserting an adapter like an mm-wave gasket between them. There was no need to alter the original structure of the standard waveguide flange. It is possible to have a different adaptor for each waveguide diameter. However, here a single adapter with the same pins lattice but varying the waveguide diameters have also been proposed. Besides, surface roughness has also

been implemented. Finally, simulated results for a smooth surface and rough surface for both circular and rectangular waveguides are found to be almost similar to each other.

Chapter 4

Contactless and Flangeless Pipe Contact for Standard Waveguides

The waveguide is one of the most widely used microwave transmission systems due to its benefit of low loss and high power dealing capacity. The waveguide flange is the most common connecting concept for different components certainly has a larger dimension than the waveguide and requires perfect alignment and contacts. This outsize might have some adverse effects for a compact design, especially for satellite and space application systems with strict limitations of volume and weight. Besides, the requirements for an improved connection between waveguides are very crucial to ensure leakage-free wave propagation. Lately, several rectangular waveguide connectors have been presented based on gap waveguide (GW) technology focusing on millimeter-wave applications [81- 85]. However, all the mentioned waveguide connection structure reported above have larger volume compared to the waveguide itself. This chapter proposes to reduce the volume and weight of the traditional waveguide flange, contactless, and flangeless pluggable waveguide connection based on gap waveguide technology.

4.1 Contactless Waveguide Connector (CWC) for Circular Waveguide

4.1.1 Design Methodology

A contactless and flangeless circular waveguide pipe contact made of a bed of pins is proposed in this chapter. The bed of pins is surrounding a circular waveguide opening from one end to be connected to another circular waveguide end of a similar structure. The bed of pins surface is making an artificial magnetic conductor (AMC), and the smooth pipe covering the pins acting as

a perfect electric conductor (PMC). Aligning these openings together and covering those symmetrically with the smooth pipe prevent signal leakage even if no contact is assured. No flange is required for the pipe contact, and it can be used for circular waveguides covering multiple mm-wave frequency bands between 50 and 110 GHz.

The 3D geometry of the proposed solution is illustrated in Figure 4.1. The elementary structure consists of a circular waveguide covered by three rows of equal gap pins connected to another waveguide with similar pins and a smooth surface pipe covering all the pins. The pipe's inner diameter is equal to the outer diameter of the circular waveguide along with pin height.

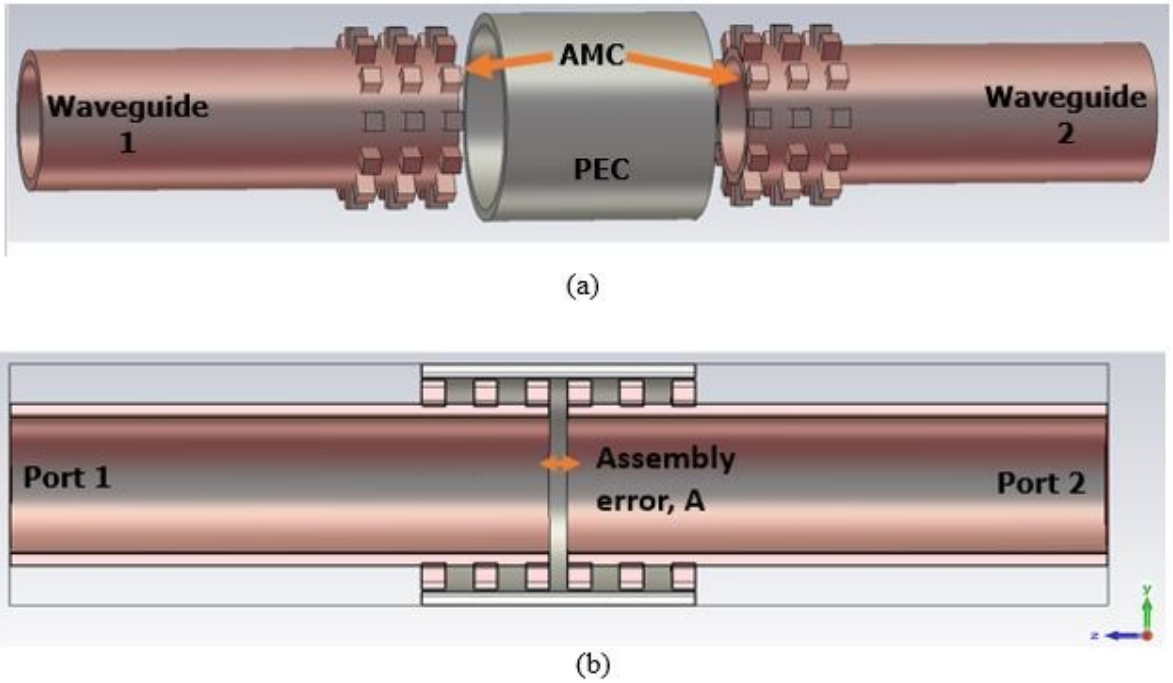

Fig.-4.1: Structure geometry of contactless and flangeless circular waveguide pipe contact (a) 3D view and (b) Cross-sectional view.

The smooth inner surface of the pipe contact acting as a PEC ensures a seamless transition for circular waveguide connection. Since surface roughness and machining error is unavoidable

during the manufacturing process, a certain airgap of 0.1mm between the AMC and PEC surface is assumed in this design to account for any accidental miss contact. The corrugated structure's pin dimension is precisely the same as the unit element and dispersion diagram discussed in Chapter 3 of this thesis. Moreover, different circular waveguide diameters with different frequency ranges within the desired frequency band are given in Table 3.2. For this proposed structure analysis, the same waveguide dimensions are followed.

4.1.2 Effect of Assembly Errors on the CWC

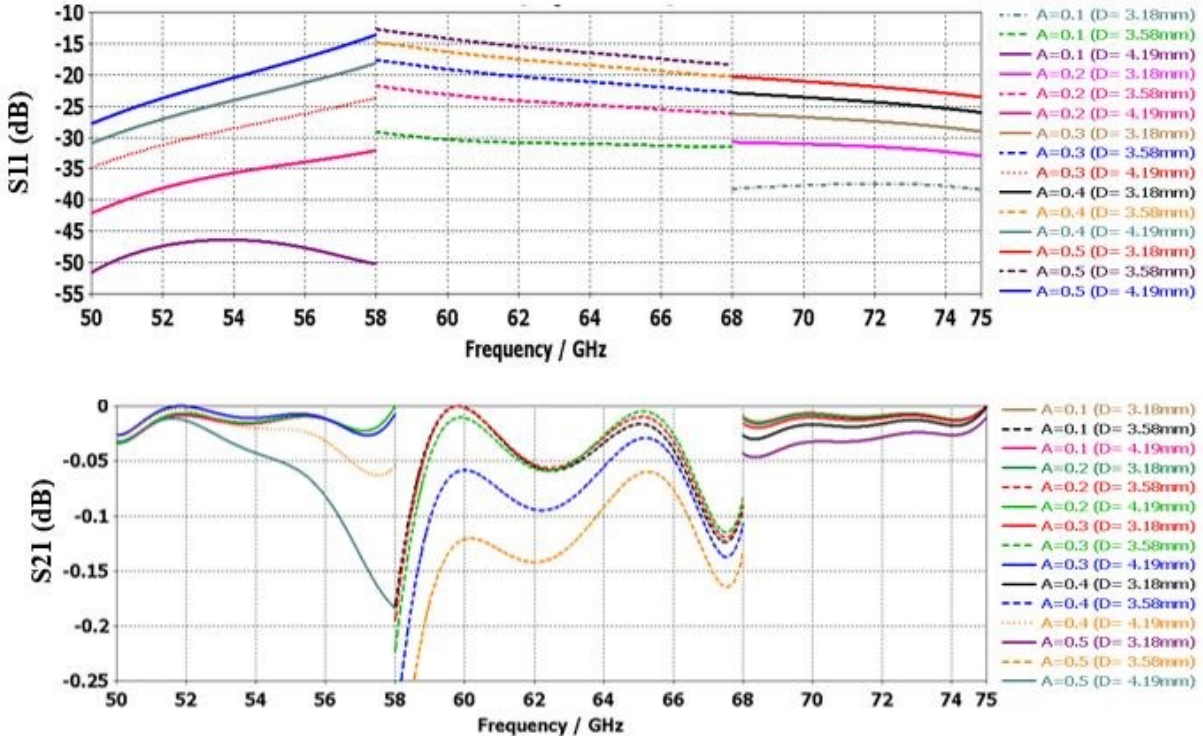

Fig.-4.2: Parametric study for Assembly Error, **A** from 0.1 mm to 0.5 mm with a step of 0.1 mm to estimate the cut-off value (D= diameter of circular waveguide opening) for V-band

Assembly error, defined with A, is a possibility while inserting the corrugated waveguides (AMC) into the smooth pipe (PEC). It could be created by surface curvature, dirt, or human error. At high frequencies, this gap can be crucial as the operating wavelength is short. Hence, smaller gaps can be comparable to wavelength and might create significant leakage.

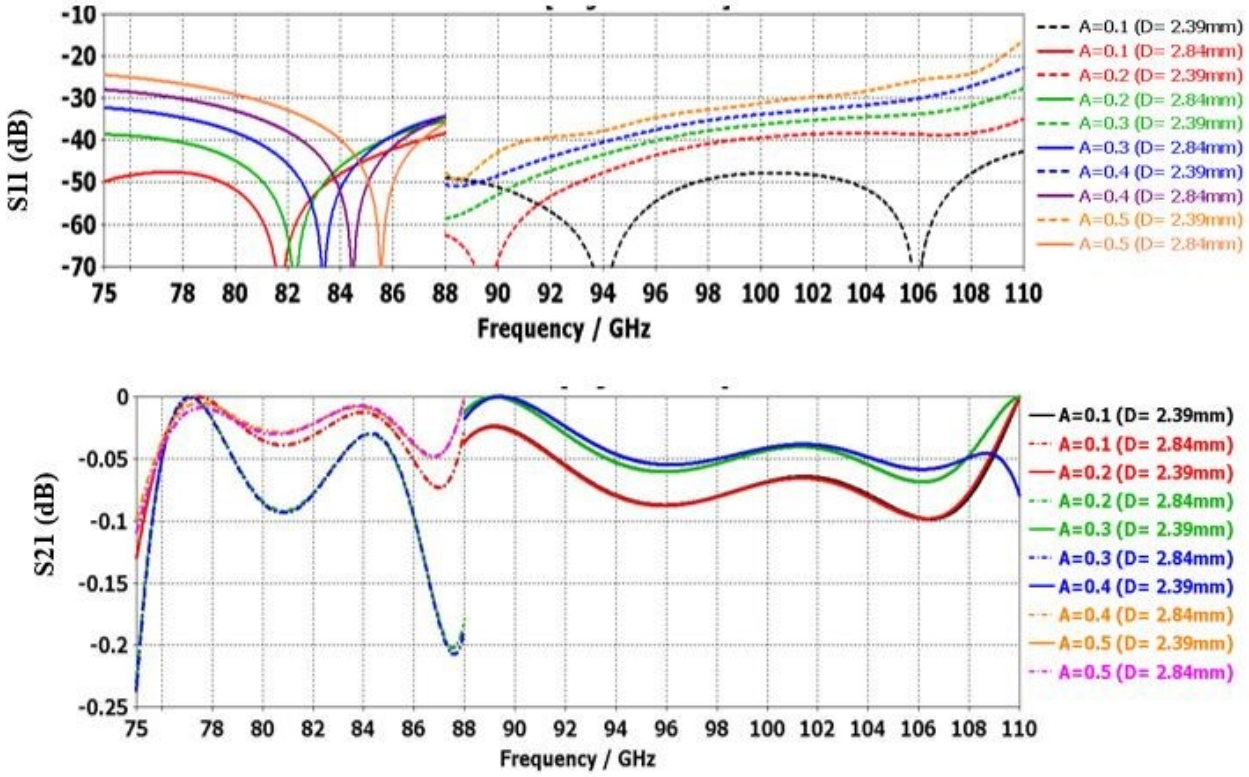

Fig.-4.3: Parametric study for Assembly Error, **A** from 0.1 mm to 0.5 mm with a step of 0.1 mm to estimate the cut-off value (D= diameter of circular waveguide opening) for W-band

To evaluate the transmission performance with an assembly error A, a parametric study from 0.1 to 0.5 mm with a step of 0.1 mm is performed on CST Microwave Studio. The airgap between the AMC and PEC surface is considered as 0.1 mm for this study. It states that when assembly error is less than 0.2 mm, the simulated return loss and insertion loss are better than 20 dB and 0.2 dB, respectively, for the entire bandwidth, which is an excellent transmission performance. This study's results are presented in Figure 4.2 for the V-band and in Figure 4.3 for

the W-band, respectively. Though the threshold value for assembly error, A, is 0.2 mm according to the simulation result, it is considered as 0.1 mm throughout the operational frequency range for further analysis of the proposed structure.

4.1.3 Impact of Alignment on the Proposed Structure

Since two circular waveguides of similar AMC structures are connected inside a pipe, there is a possibility that the pins of the two waveguides may not be perfectly aligned with each other.

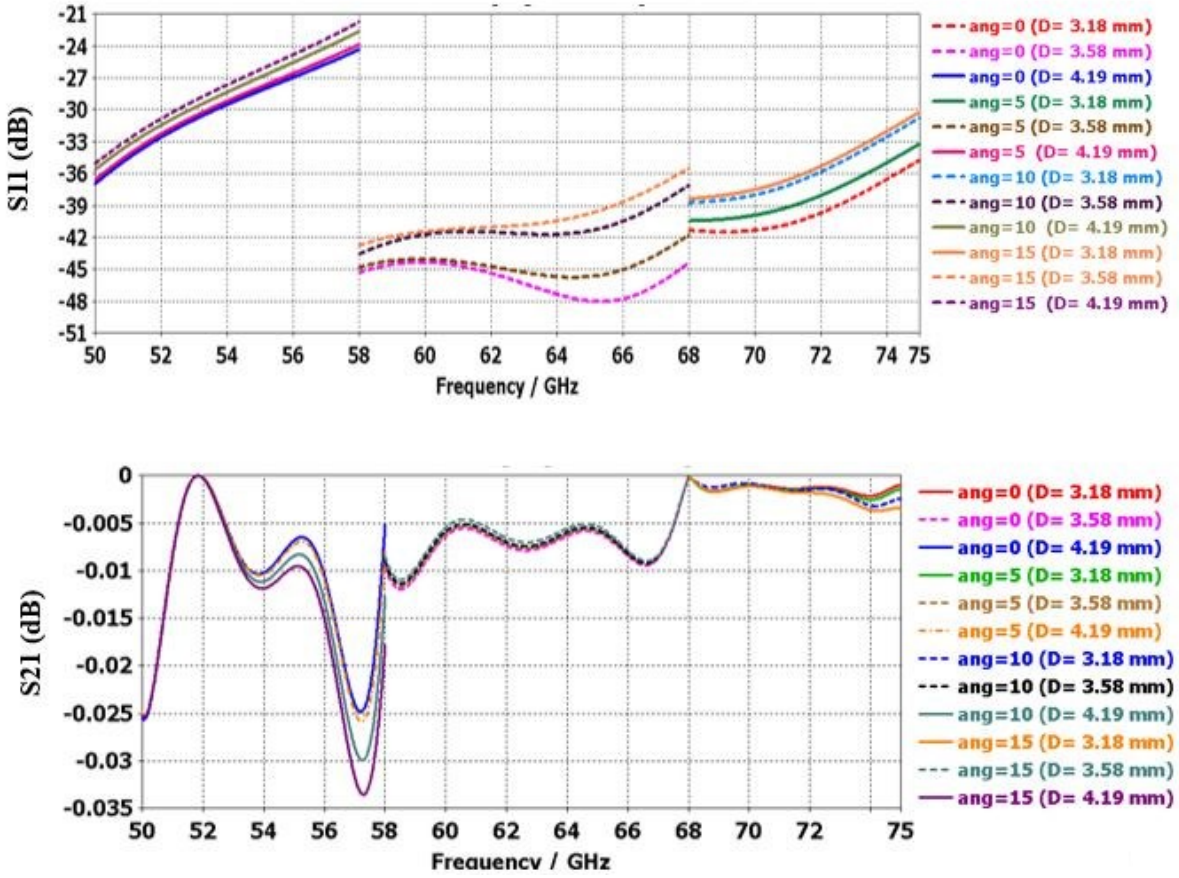

Fig.-4.4: Simulation result of the proposed structure for V-band based on various circular waveguide diameter, D with respect of angle of misalignment (ang).

A parametric study for the misalignment is performed for the entire frequency range, as shown in Figure 4.4 for V-band with a step of 5-degree misalignment. It is evident that, even though the pins are misaligned, the return loss is always better than 20 dB and the insertion loss is better than 0.035 dB. The assembly error, A, and the airgap between the AMC and PEC structures are considered as 0.1 mm and 0.1 mm, respectively, for this parametric study.

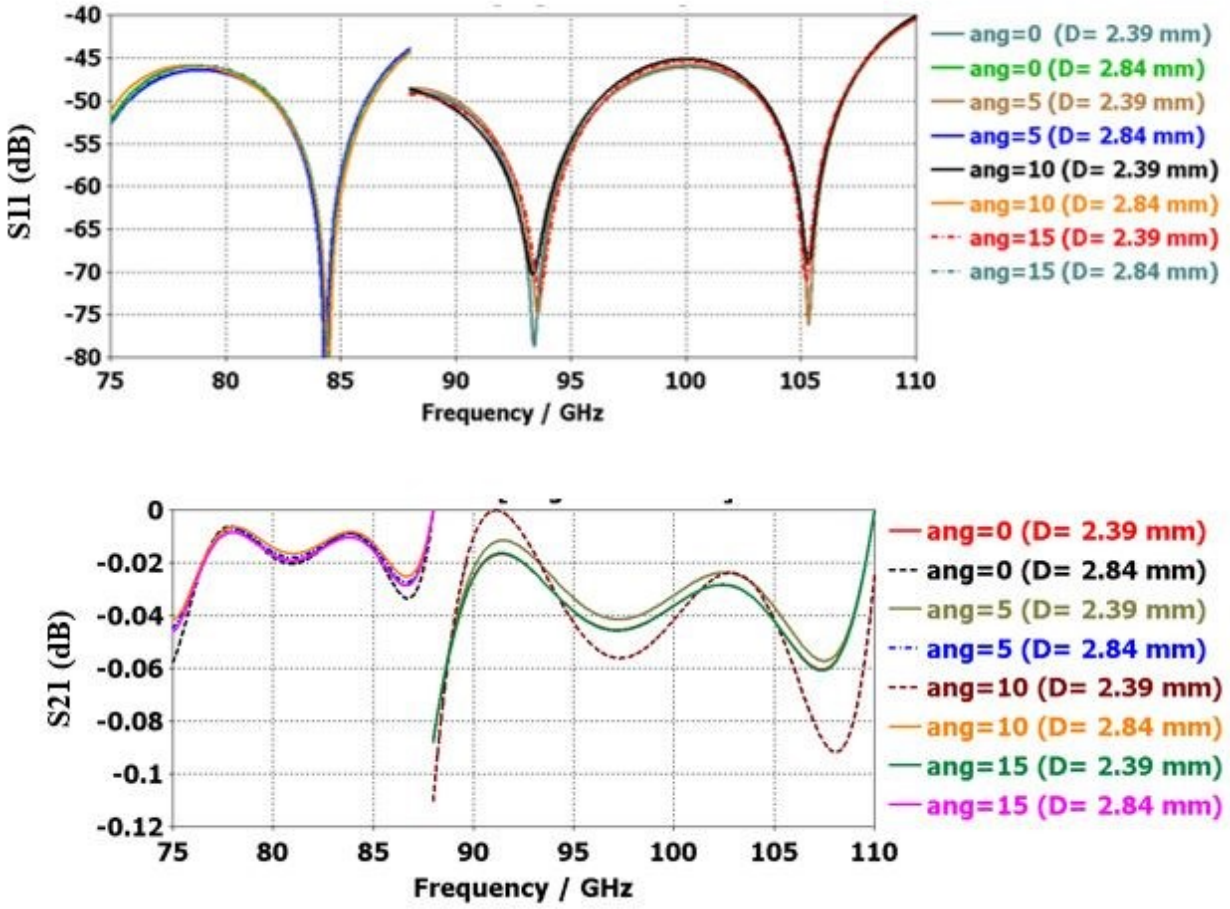

Fig.-4.5: Simulation result of the proposed structure for W-band based on various circular waveguide diameter, D with respect of angle of misalignment (ang).

Similarly, a misalignment study is performed for the entire operating frequency range, as shown in Figure 4.4, for W-band with a step of 5-degree misalignment. It is clearly visible that,

even though the pins are misaligned, the return loss is always better than 40 dB and the insertion loss is better than 0.11 dB. The assembly error, A, and the airgap between the AMC and PEC structures are considered as 0.1 mm and 0.1 mm, respectively, for this parametric study.

4.1.4 Electric Field Distribution based on Pins' Alignment

The periodically placed nails in the AMC structure cancel the field propagation transverse to the ridge direction. Theoretically, there should not exist any propagating field transverse to the ridge direction along the magnetic boundary. However, since no real magnetic surface exists in nature, some field components transverse to the ridge direction exist.

A tiny air gap exists between the AMC and PEC surface due to surface roughness and machining error during the manufacturing process. Additionally, Assembly error is another possibility while inserting the AMC structures into the PEC one. Suppose electromagnetic (EM) waves leak from these tiny gaps, the EM transmission of the waveguide might be adversely affected, especially at higher frequencies. To prevent this EM leakage from the gaps, the AMC structure's dimensions have to be appropriately designed to form a forbidden band, which should cover the operating frequency range of the waveguides.

Figure 4.6 illustrates the electric field distribution behavior of the proposed contactless and flangeless pipe contact for two corrugated circular waveguides when the pins are perfectly aligned. Five different frequencies have been chosen to demonstrate the electric field distribution according to their standard waveguide diameter, D. It is evident that the AMC structure prevents the EM leakage significantly within the airgap between the pins and PEC surface, as well as assembly error between two circular waveguides. Therefore within the operating bandgap, the EM wave is guided properly along the waveguides without significant leakage.

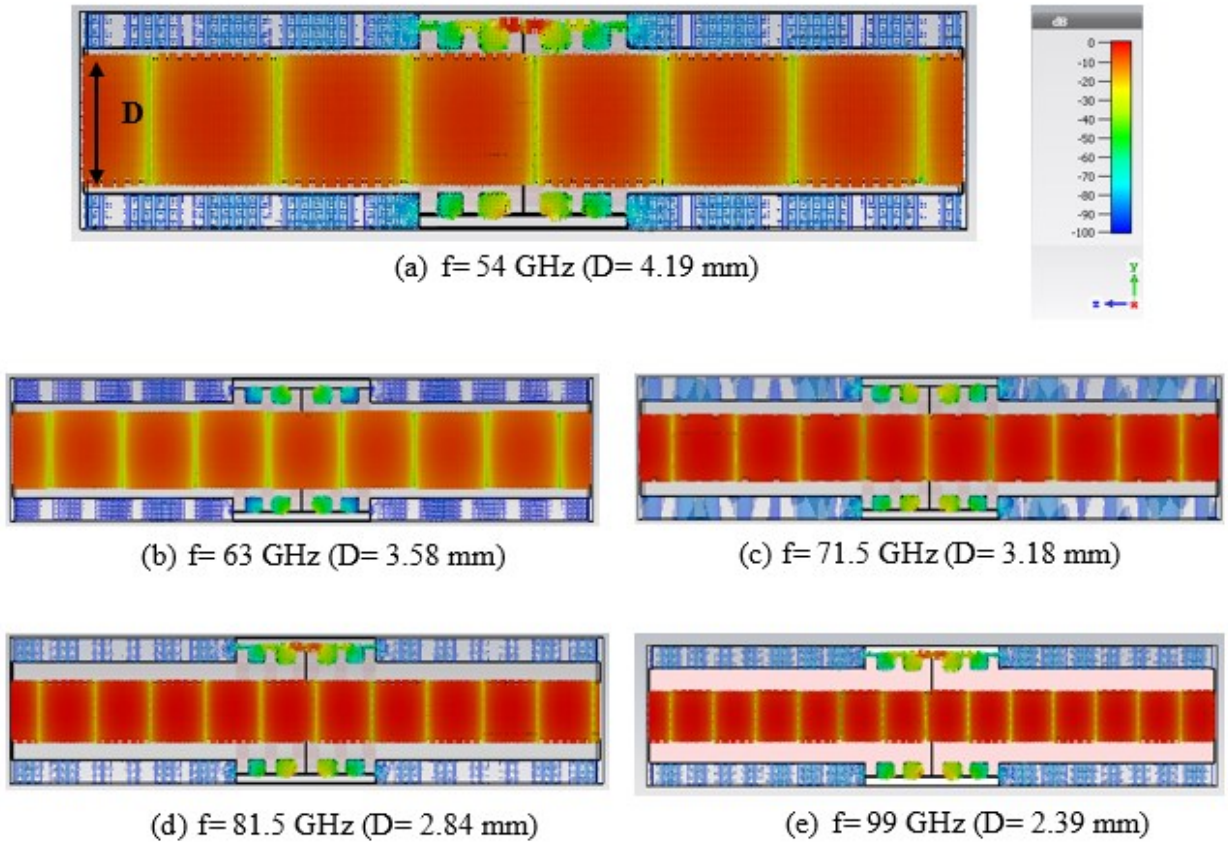

Fig.-4.6: Electric field distribution (across plane A) of contactless flange-free pipe contact for circular waveguides at various frequencies and different waveguide diameters (D) when pins of both waveguides are perfectly aligned

Figure 4.7 represents the electric field distribution behavior of the proposed contactless and flangeless pipe contact for two corrugated circular waveguides at two different frequencies when the pins on each waveguide are misaligned at 15-degree from each other. It shows that the pins' misalignment does not affect the EM propagation between the waveguides because of the perfectly designed AMC structure. The signal leakage beyond the third row of pins and the smooth pipe is below -70 dB, as demonstrated in Figure 4.6 and Figure 4.7.

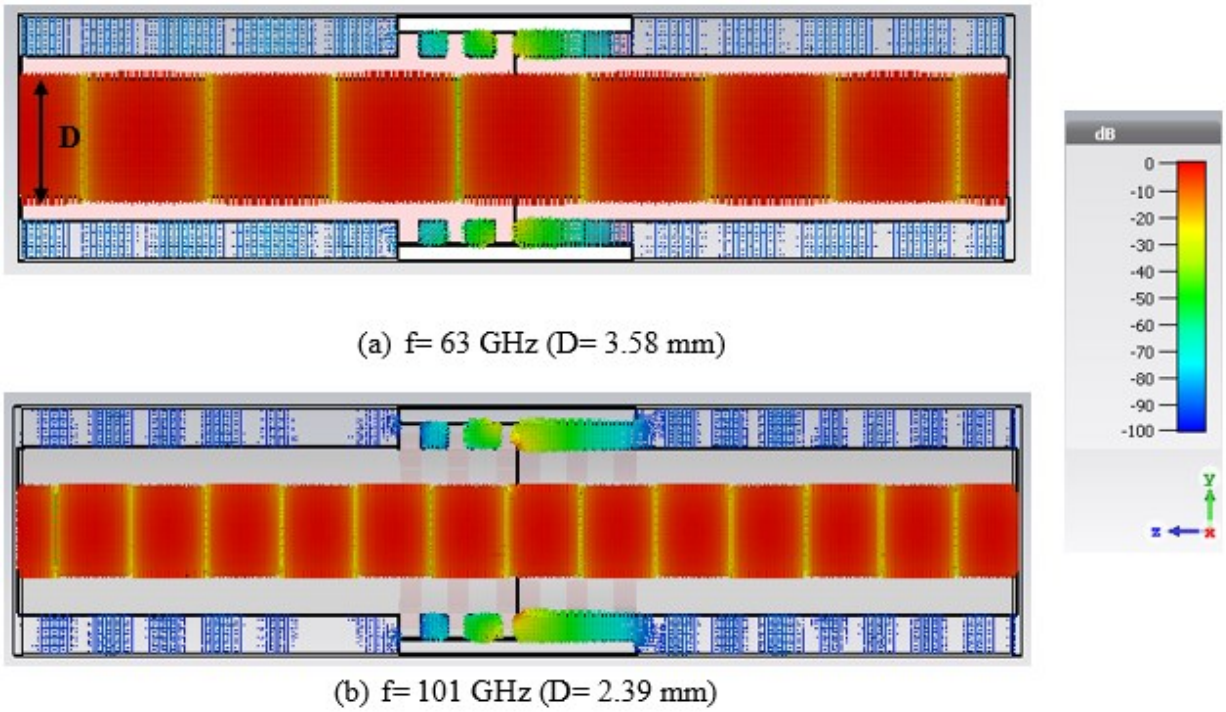

(a) f= 63 GHz (D= 3.58 mm)

(b) f= 101 GHz (D= 2.39 mm)

Fig.-4.7: Electric field distribution (across plane A) of contactless flange-free pipe contact for circular waveguides at various frequencies and different waveguide diameters (D) during 15-degree misalignments between the pins of (a) V-band and (b) W-band waveguides

4.2 Contactless Waveguide Connector (CWC) for Rectangular Waveguide

Flange-free contactless pipe contact for rectangular waveguides is designed. The standard rectangular waveguide parameter and their operating frequency range for V-band and W-band are specified in Table 3.3.

Figure 4.8 shows the geometrical structure of the proposed design for standard rectangular waveguides within the operating frequency range. Assembly error, A, and the airgap between the AMC and PEC structures are considered as 0.1 mm and 0.1 mm, respectively, for this structure.

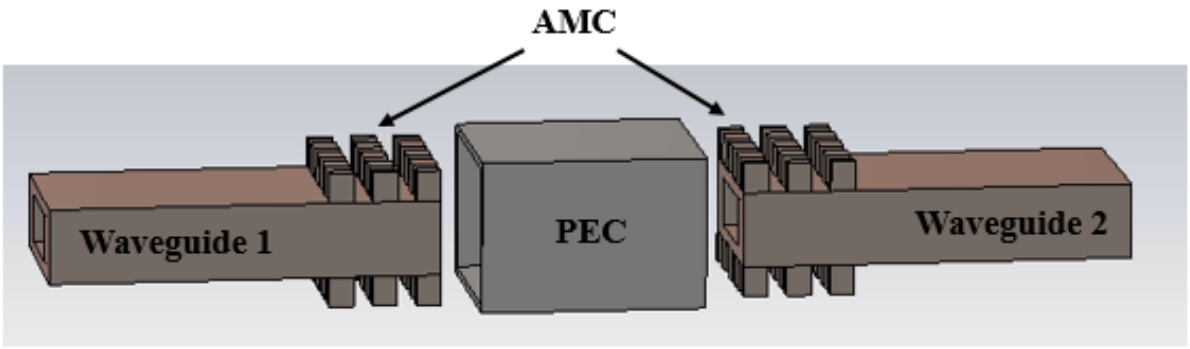

(a)

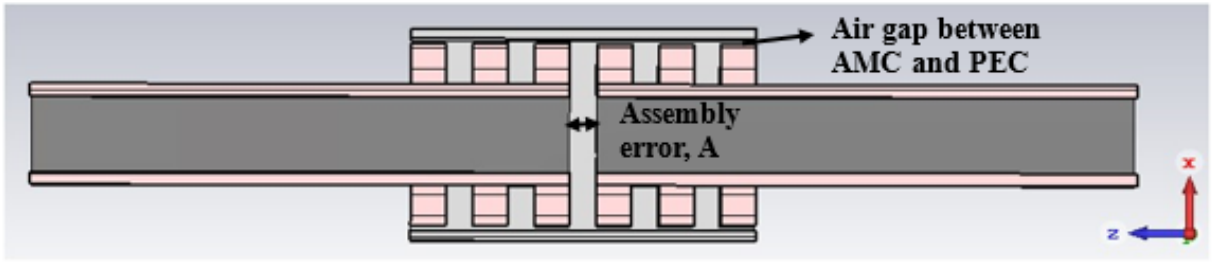

(b)

Fig.-4.8: Structure geometry of contactless and flangeless rectangular waveguide pipe contact (a) 3D view and (b) Cross-sectional view.

The pins at each corner of the corrugated structure are modified to adjust with the periodic assembly. Figure 4.9(a) shows the perspective view of one side of the AMC structure, and Figure 4.9(b) represents the pin orientation as well as rectangular waveguide opening from the front view of the AMC structure.

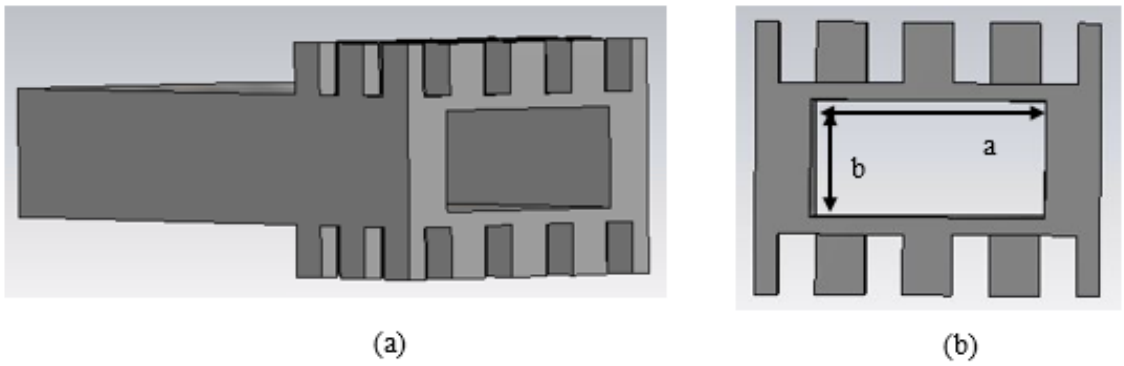

Fig.-4.9: Pin orientation of the proposed structure for rectangular waveguide (a) Perspective view of the corrugated structure and (b) Front view of the waveguide opening (a,b = rectangular waveguide dimension)

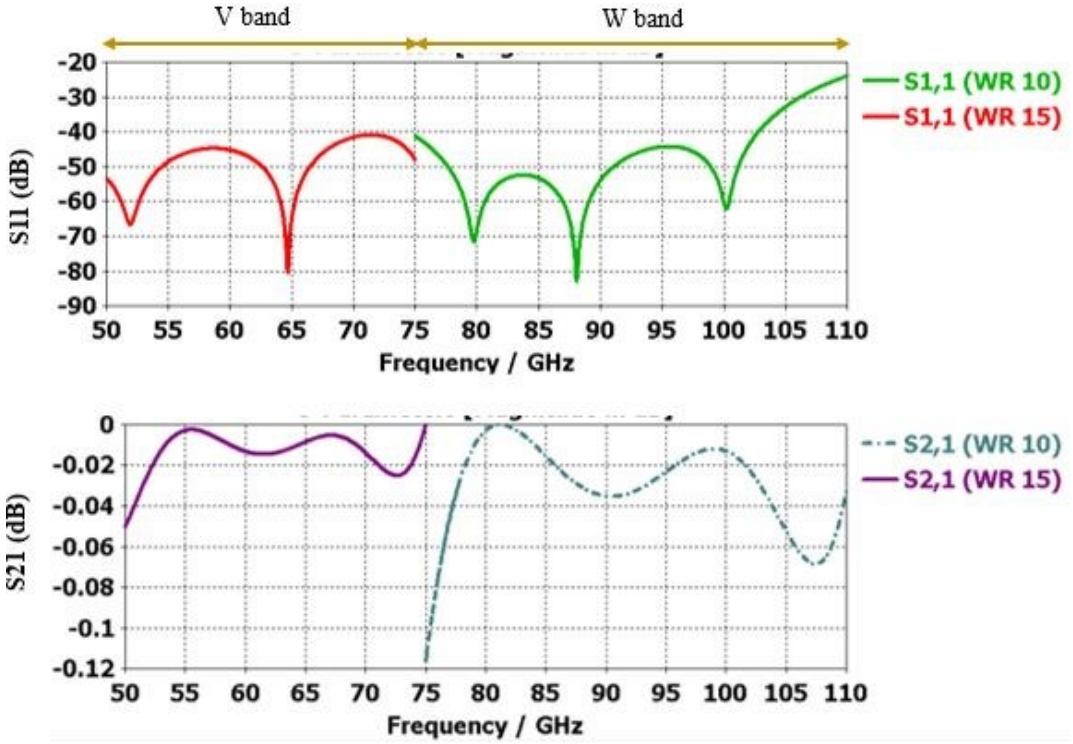

Fig.-4.10: Simulated results for contactless and flangeless pipe connector for rectangular waveguide (V-band and W-band)

The simulation result for standard rectangular waveguide pipe contact is mentioned in Figure 4.10. It shows that return loss is better than 20 dB and insertion loss is better than 0.12 dB throughout the entire frequency range.

The E-field distribution of the proposed contactless and flangeless pipe contact for the rectangular waveguide is shown in Figure 4.11 for the V-band and W-band at 62.5 GHz and 92.5 GHz, respectively. It can be depicted that the electric fields are confined mostly within the second row (out of three rows) of the periodic cells.

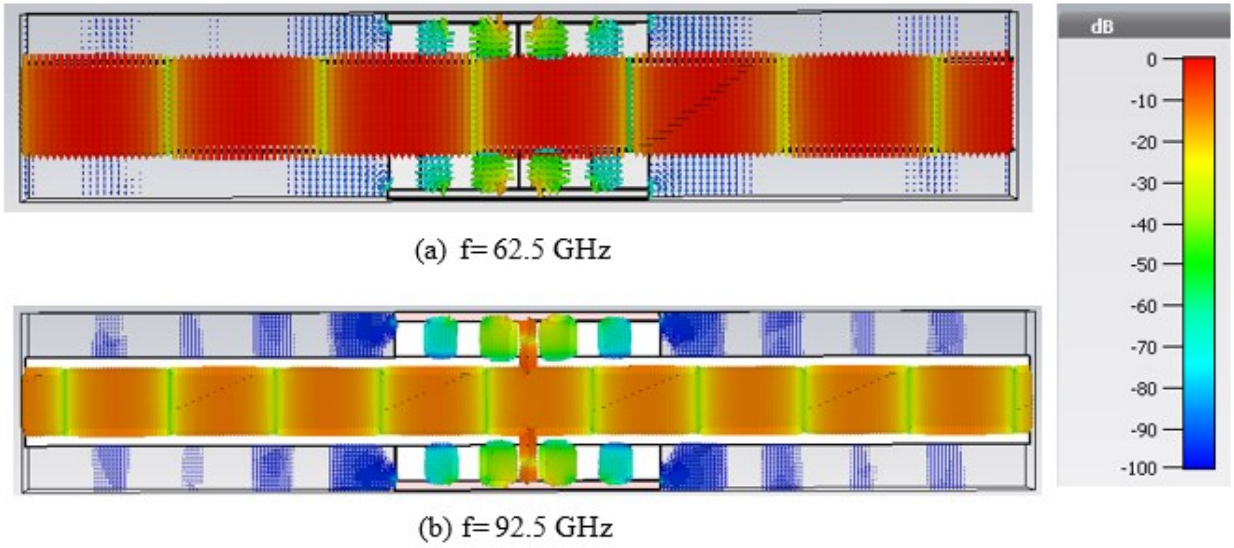

Fig.-4.11: E- field distribution (across plane A) of contactless and flangeless pipe contact for rectangular waveguide for (a) V-band at 62.5 GHz and (b) W-band at 92.5 GHz

The periodic cells are blocking the unwanted leakage caused by the assembly error, A and airgap, h_a between the periodic cells and smooth cover. With this corrugated structure, it is possible to suppress the unwanted leakage, which improves the overall transmission from one port to another port.

4.3 Comparison of Dimensions between Waveguide Flange and CWC

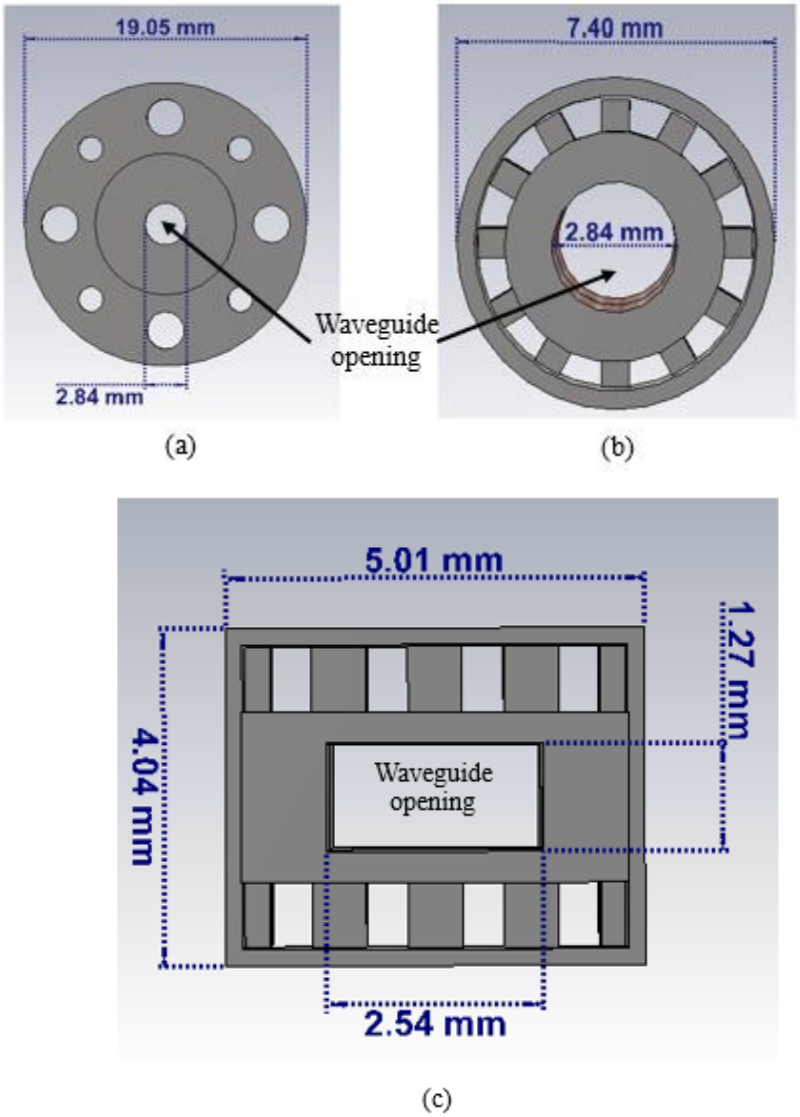

Fig.-4.12: Sectional size comparison of (a) standard UG-387/U round waveguide flange, (b) CWC for circular waveguide (W-band), and (c) CWC for rectangular waveguide (W-band)

Figure 4.12 illustrates the sectional size comparison of standard UG-387/U round waveguide flange and the proposed contactless and flangeless circular and rectangular waveguides. For both circular and rectangular waveguides covering V-band and W-band, the standard UG-387/U round waveguide flange is being implemented regularly. In Figure 4.12, only

the dimensions for W-band waveguides are being compared, the overall dimensions for V-band and W-band (in both circular and rectangular waveguides) are the same. Only the waveguide opening diameter is varied with respect to the selected frequency range. Compared to traditional UG-387/U waveguide flange diameter, the contactless and flangeless circular waveguide diameter reduces from 19.05mm to 7.4mm, decreasing by more than 60%, thus achieving outstanding miniaturization of circular waveguide connection. Likewise, the flangeless rectangular waveguide connection's sectional dimensions are decreased to 6.69×4.14 mm^2, which is another significant reduction of the rectangular waveguide assembly.

4.4 Connection Method of Proposed CWC

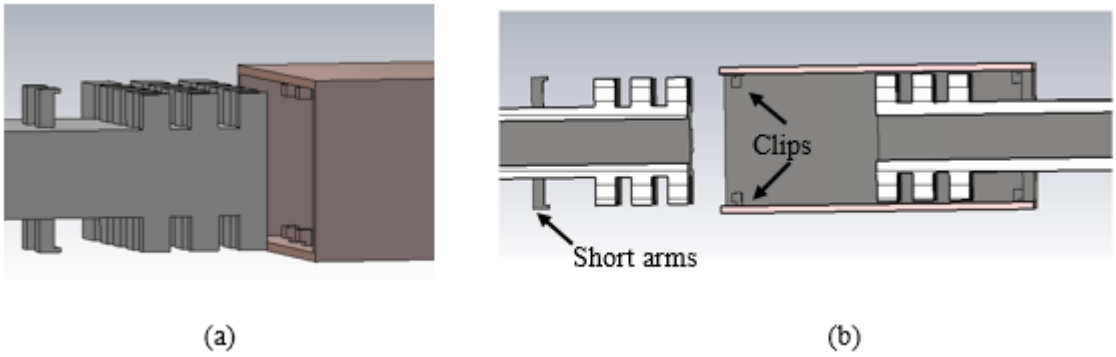

Fig.-4.13: Additional short arms for connecting corrugated structures of a rectangular waveguide with a smooth cover (a) Partial 3D view and (b) Cross-sectional view

Since no flange or screws are being used in the proposed structure, four additional short arms on each side of the corrugated structures are designed for fixation. Similar clips are added inside the smooth pipe to make them connected to the short arms of the AMC structures. The short arms do not perturb the periodicity of the nails on the AMC structures. Figure 4.13 represents the connection method of the proposed structure for flangeless rectangular waveguide contact. The

clips inside the smooth pipe are positioned carefully in between the corrugated structure's periodic nails, so there is no contact between the nails and the clips while inserting the AMC structure inside the PEC one.

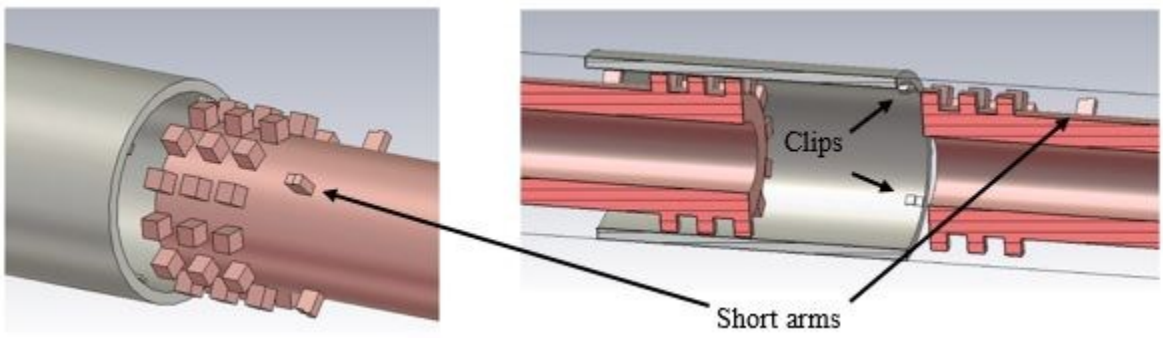

(a) (b)

Fig.-4.14: Additional short arms for connecting corrugated structures of a circular waveguide with a smooth pipe (a) Partial 3D view and (b) Cross-sectional view

Figure 4.14 signifies the connection method of the proposed structure for flangeless circular waveguide pipe contact. Four short arms on each side of the AMC structure is placed along with four clips on each side inside the PEC structure for connection. Similar to rectangular waveguide contact, the clips inside the smooth pipe are positioned carefully in between the periodic nails of the AMC structure, so they don't touch the periodic nails while injecting the AMC structure into the PEC one.

4.5 Result Validation of Proposed CWC

For more verification, two different solvers (Time-domain and Frequency-domain) are utilized in CST Microwave Studio and shown for standard circular waveguides in Figure 4.15 (a) and (b) for V-band and W-band, respectively. The results represent a similar S-parameter, which validates the response of the proposed structure for standard circular waveguides covering V-band and W-band. Assembly error, A, and the airgap between the AMC and PEC structures are considered as 0.1 mm and 0.1 mm, respectively, for this calculation.

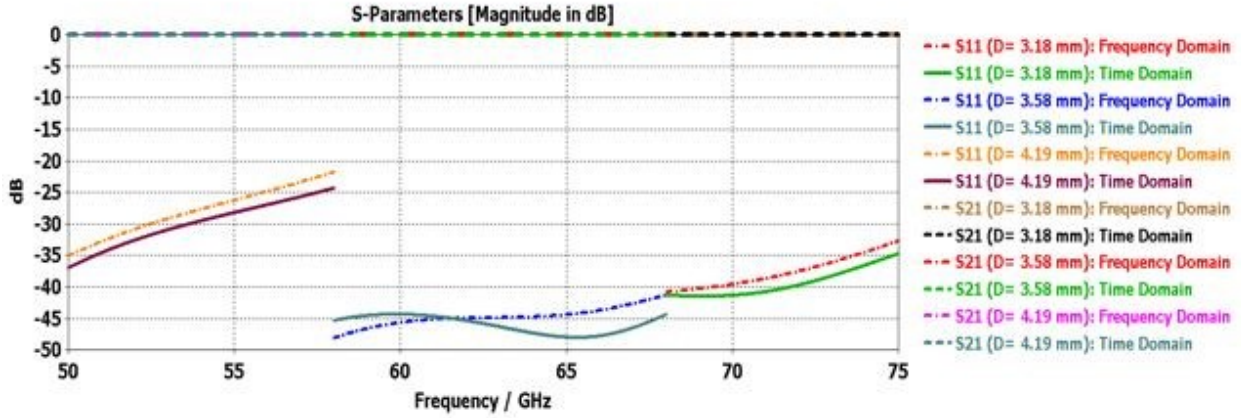

(a)

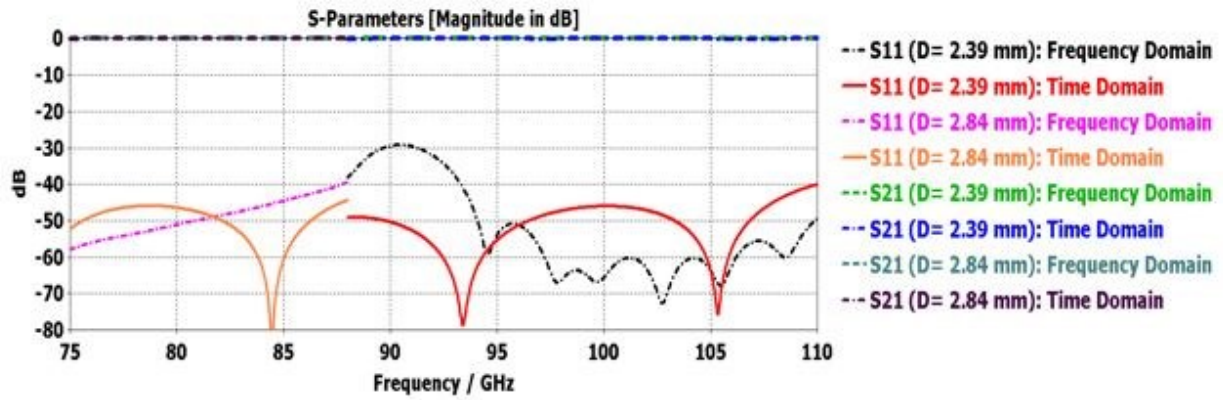

(b)

Fig.-4.15: Scattering Parameter of the proposed CWC for Standard Circular Waveguides (a) V-band and (b) W-band

Figure 4.16 exhibits the response for contactless and flangeless pipe contact for standard rectangular waveguides simulated in the Time-domain and Frequency-domain solver of CST MWS. Similar to the circular waveguide scenario, the assembly error and the airgap are considered as 0.1 mm and 0.1 mm, respectively. Both solver result demonstrates a similar scattering parameter for better validation.

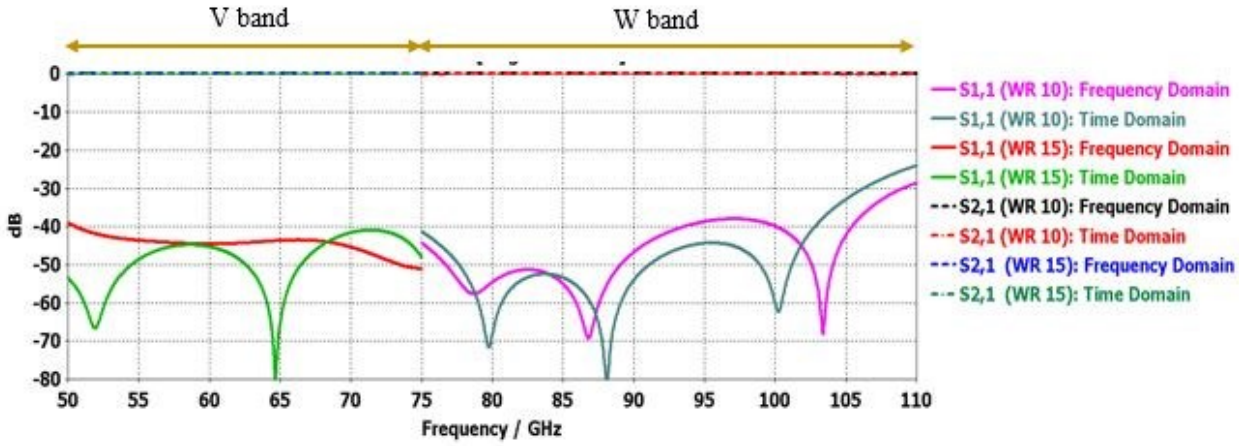

Fig.-4.16: Scattering Parameter of the proposed CWC for Standard Rectangular Waveguides

We aim to show how the connection between two slightly modified flangeless standard waveguides can be made without possible leakage, even with no electrical contact assurance. This has been assured by inserting the waveguides inside a smooth metal pipe. Also, to reduce the size of traditional waveguide flange and make fast waveguide connection without connecting screws, a unique solution of flangeless and contactless waveguide connection for both circular and rectangular waveguides is suggested using gap waveguide technology. A pluggable flangeless structure is designed where a contactless EBG structure is formed to prevent possible EM leakage from the trivial air gap of the pipe contact. In the meantime, the size of the traditional waveguide

flange is dramatically reduced by this flangeless structure. The design is simple as well as cost-effective, validating an impressive return loss and insertion loss.

Chapter 5

Wide Ka-band Gap Waveguide Orthomode Transducer

Reciprocal devices that are responsible for combining and dividing two orthogonal polarized signals are discussed in this chapter, which is defined as Orthomode Transducers (OMT). Basically, an OMT is a polarization filter that separates two orthogonal polarizations within the same frequency band, and vice versa. OMTs are crucial devices attached to the antenna system and primarily used for the antenna feeding structures that support two propagating modes focusing on maximizing the bandwidth efficiency of communication channels.

In general, an OMT is electrically a four-port device, though it reveals only three physical ports. The common port is generally a square or circular cross-section that provides two electrical ports that are allocated to the independent orthogonal dominant modes: TE_{10} and TE_{01} modes for the square waveguide and a 90^{o} rotated or orthogonal TE_{11} and TE_{11} modes for the circular waveguide. The remaining two ports are formed by a standard waveguide or coaxial ports, aiding only the respective fundamental single signal mode. It should be noted that the excitation of higher-order modes can adversely distress the matching and isolation performance of an OMT design, especially within the physical branching region due to discontinuities. This eventually affects the radiation pattern of the antenna. A careful definition of the common port cross-section and using symmetries in the structure reduces the generation of higher-order modes to a certain extent.

The proposed OMT structure is a high-performance compact symmetric OMT comprising E-bend and H-bend along with a combination of ridge gap and groove gap waveguide technology.

The design is performed through multiple steps that include the OMT core, transitions from OMT core output to RGW, 270˚ E- plane bend, 90˚ H- plane bend, power divider, and groove gap to standard waveguide port transition. These steps have been discussed in detail in the upcoming sections. Due to the gap waveguide technology used in the design of the proposed OMT, it avoids any electrical contact and operates efficiently without any leakage issue.

5.1 Guiding Structures of Orthomode Transducer

The proposed orthomode transducer design is symmetric, with a combination of ridge gap waveguide (RGW) and groove gap waveguide (GGWG) guiding structure. Section 5.1.1 deliberates the proposed RGW guiding structure and its simulation results, followed by GGWG guiding structure along with its simulation results discussed in Section 5.1.2.

5.1.1 Proposed Ridge Gap Waveguide Guiding Structure

One of the selected guiding structures for the OMT is the Ridge Gap Waveguide (RGW). This guiding structure supports the quasi- TEM mode, even if the electrical connection is not present. It can be said that other modes are not barred from propagation due to the guiding structure; rather, they are not excited within the bandgap of the proposed guide. The characteristics of the gap waveguide are evidently understandable from its dispersion diagram. The key assignment is to determine the lower and upper cut-off frequency of the EBG stopband. These cut-off frequencies can then be studied as a function of the periodic surface's geometrical parameters, the airgap height between the periodic nails and upper conducting plate (PEC), to find an acceptable solution. The RGW geometry and the simulated results are presented in Figure 5.1. A ridge gap waveguide row containing unit cell and a ridge with infinite periodic boundaries is simulated for accurate calculation of the EBG using CST Microwave Studio Eigenmode Solver, as shown in Figure 5.1. The unit cell's periodic structure results in a high surface impedance at the bottom of the textured

surface, which does not allow wave propagation. The periodic pins act like an Artificial Magnetic Conductor (AMC), where a normal electric field does not exist. The ridge height (h_r) has been kept slightly shorter than the pin height (h_p) for a better matching level of the RGW. The bandgap is considered as the operating bandwidth of the ridge gap waveguide, which is 15 to 48 GHz according to the dispersion diagram in Figure 5.1 (b). The solid continuous black line of the dispersion diagram in Figure 5.1 (b) represents the quasi-TEM mode propagating along the ridge. The vertical E-field distribution of the desired quasi-TEM mode is nearly constant across the ridge. The simulated results in Figure 5.1(c) embodies that the guide has an acceptable matching and transmission level over the Ka-band, from 27 to 40 GHz.

Table 5.1: Dimensions of the RGW structure

Parametric Symbols	**Value (mm)**
h_p	2.7
h_a	0.1
w_p	1.6
w_r	2.9
h_r	2.62
g	1.5

The dimensions of the RGW structure are shown in Table 5.1, where w_p is the pin width, w_r is the ridge width, h_r is the ridge height, g is the gap between two consecutive pins, h_p is the pin height, and h_a is the airgap between the pins and upper PEC layer. The thickness of the upper and lower conducting metal plate (PEC) is 0.05 mm.

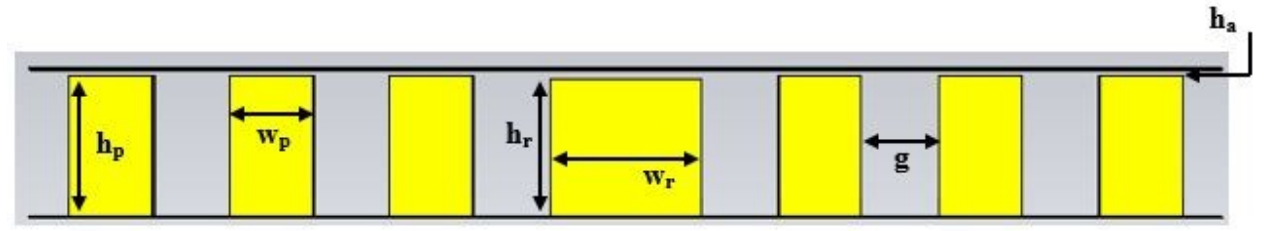

(a)

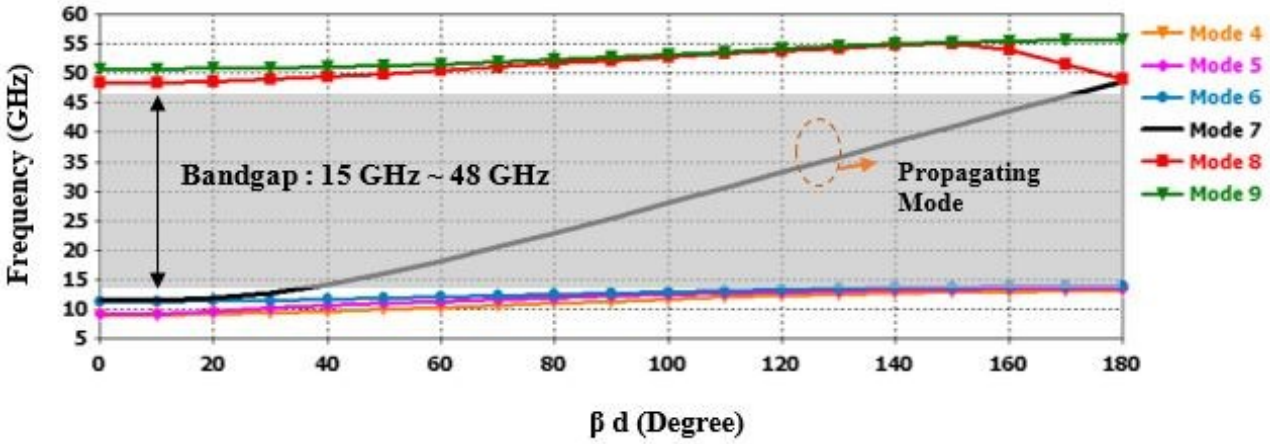

(b)

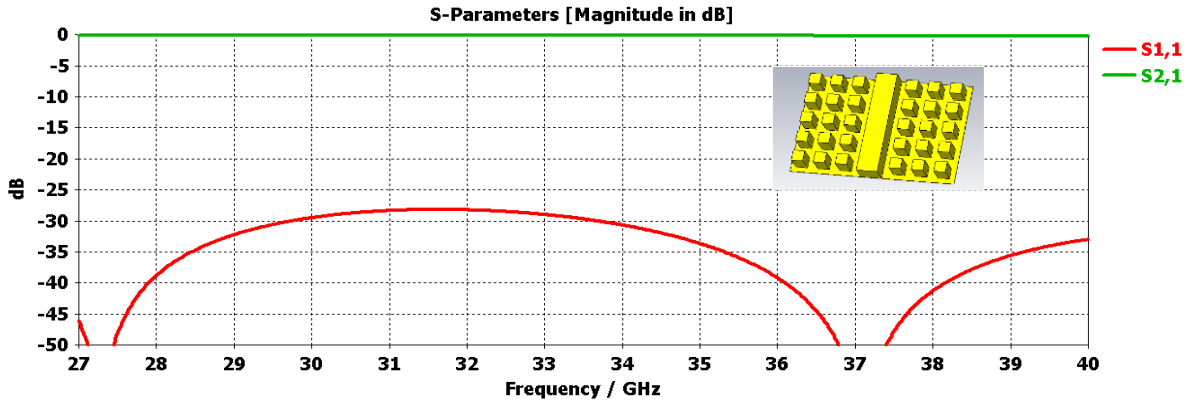

(c)

Fig.-5.1: RGW structure: (a) One row with the geometrical parameters, (b) Dispersion diagram with EBG, and (c) Reflection and transmission coefficients along with 3D view (top conducting metal plate is hidden).

5.1.2 Proposed Groove Gap Waveguide Guiding Structure

Another guiding structure for the OMT is Groove Gap Waveguide (GGWG). This guiding configuration is similar to RGW, with the ridge removed, forming a groove. GGWG supports the TE_{10} mode similarly to the rectangular waveguide, even if the top and bottom conductors are not

electrically connected. Like RGW, other modes are not forbidden from propagation due to the guiding structure; rather, they are not excited at the stopband of the GGWG. The GGWG one-row structure and the simulated results are presented in Figure 5.2 (a). The dispersion diagram in Figure 5.2 (b) represents a wide bandgap that is almost from 15 to 48 GHz. The solid black line of the dispersion diagram in Figure 5.2 (b) represents the TE_{10} mode propagating through the groove. The transmission results in Figure 5.2 (c) indicates that the GGWG has an acceptable return loss and insertion loss over the operating frequency range of 27- 40 GHz. The dimensions of the GGWG structure are shown in Table 5.2.

Table 5.2: Dimensions of the GGWG structure

Parametric Symbols	**Value (mm)**
h_p	2.7
h_a	0.1
w_p	1.6
w_g	7.97
g	1.5

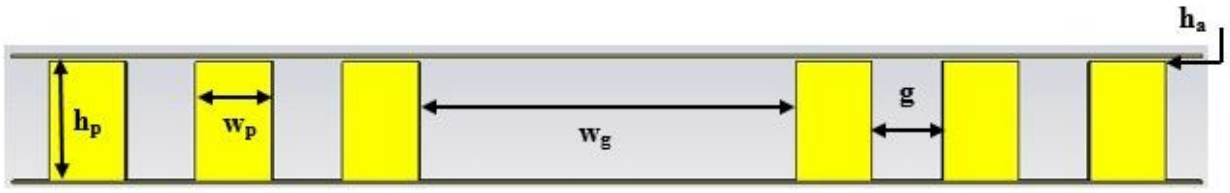

(a)

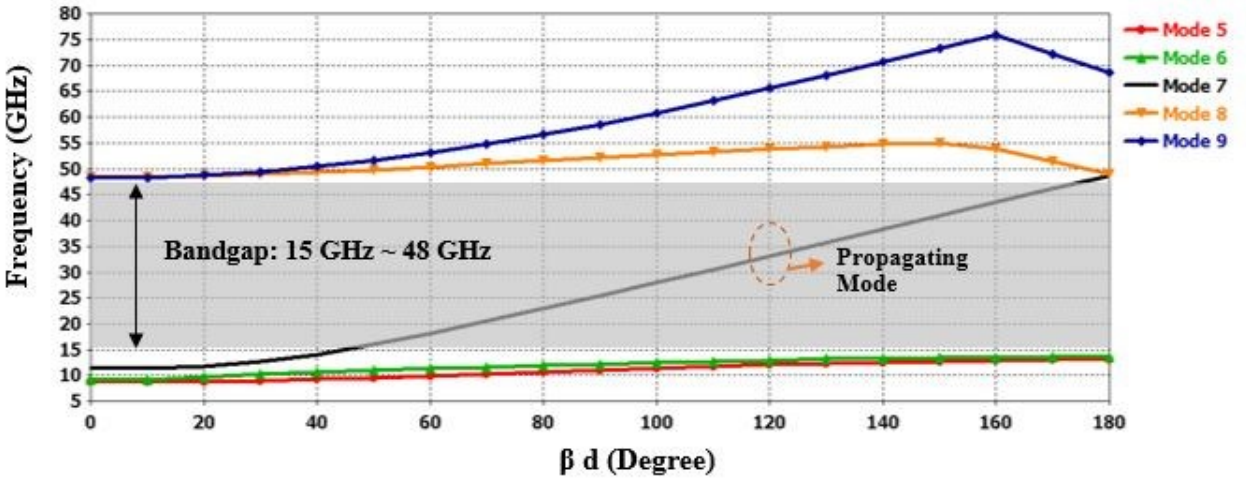

(b)

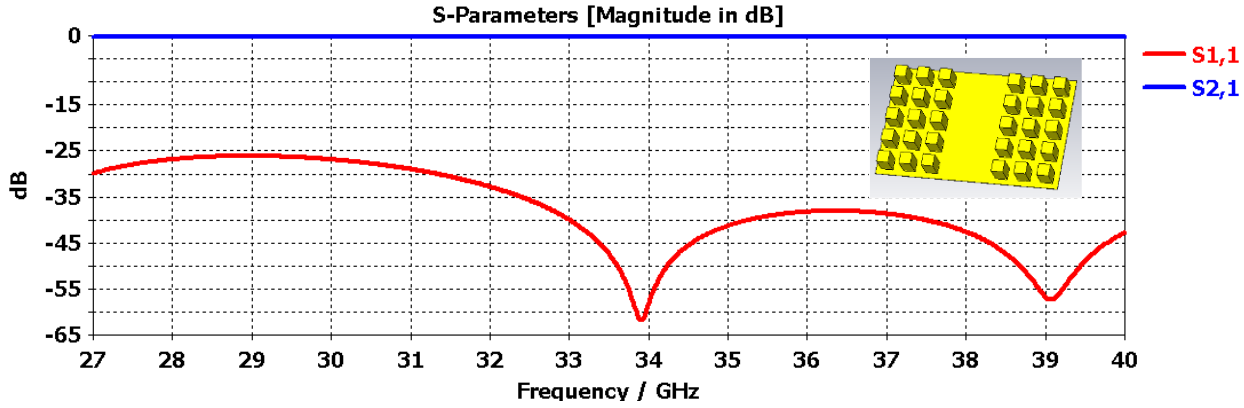

(c)

Fig.-5.2: GGWG structure: (a) One row with the geometrical parameters, (b) Dispersion diagram with EBG, and (c) Reflection and transmission coefficients along with 3D view (top conducting metal plate hidden).

5.2 Core of the Orthomode Transducer

The proposed OMT is deploying a turnstile junction in order to separate/ merge two orthogonal polarizations within the same frequency band. The guiding structure implemented on the OMT core is the previously mentioned GGWG. The OMT core input consists of a nonstandard circular waveguide of diameter 7.2 mm, as a common port of the OMT structure. The common port diameter supports TE_{11} mode at 24.4 GHz, TM_{01} mode at 31.9 GHz, and TE_{21} mode at 41 GHz. Due to the planned differential feeding, the odd mode TM_{01} is suppressed. Thus, the available band is 24.4 to 41 GHz, which accommodates the whole Ka-band as an operating frequency band without any disruption.

The turnstile junction is a key element of the OMT design in terms of better reflection coefficient as well as isolation among the polarizations. The common port supports two orthogonal polarizations of TE_{11} mode. Each of the two incoming polarization is equally divided into two 180˚ out of phase RF signals by the turnstile junction. For instance, Ports 2 and 4 support the same mode with a 180˚ phase difference, whereas Ports 3 and 5 support the orthogonal mode with a 180˚ out of phase. For high performance OMTs with high polarization isolation, the return loss at the common port input must be cautiously optimized by implementing a matching component located at the center of the turnstile junction. Given the fact that the turnstile is made of two GGWG waveguide intersections, two stacked cylinders are overlaid as matching structures for better reflection coefficient (S11) throughout the entire bandwidth. The turnstile sections' dimensions are tabulated in Table 5.3, where d_m and h_m are the diameter and height of the superimposed cylinders, respectively. Sections 1 and 2 represent the lowest and top cylinders in that order.

Table 5.3: Dimensions of the Turnstile Sections

Turnstile Sections (Lowest to top)	Cylinder Diameter, d_m (mm)	Cylinder Height h_m (mm)
1	7.84	0.68
2	4.2	1.29

The core structure of the OMT is shown in Figure 5.3, and its simulated results are displayed in Figure 5.4.

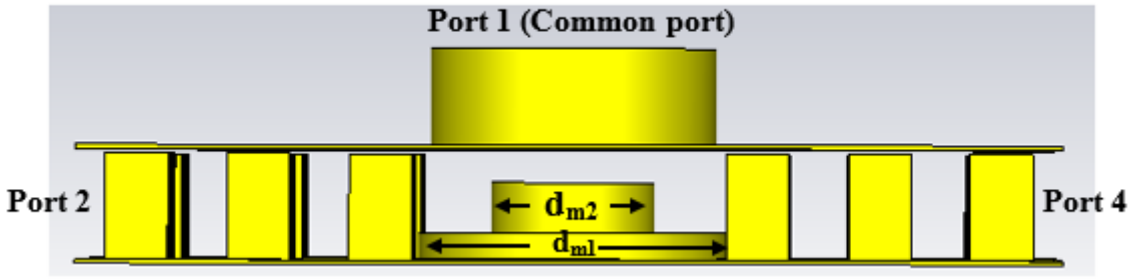

(a)

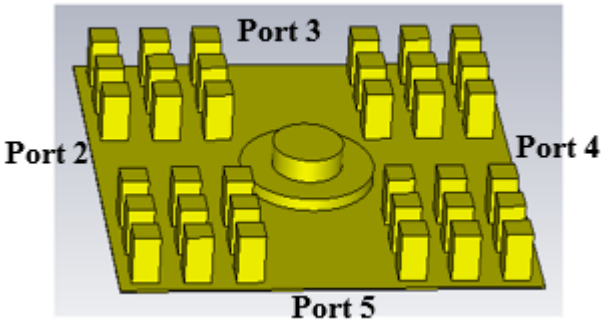

(b)

Fig.-5.3: Proposed OMT core including port numbers (a) Side view indicating turnstile junction diameters: d_{m1} and d_{m2} and (b) 3D view showing port numbers (top metal plate and circular waveguide, i.e., common port hidden)

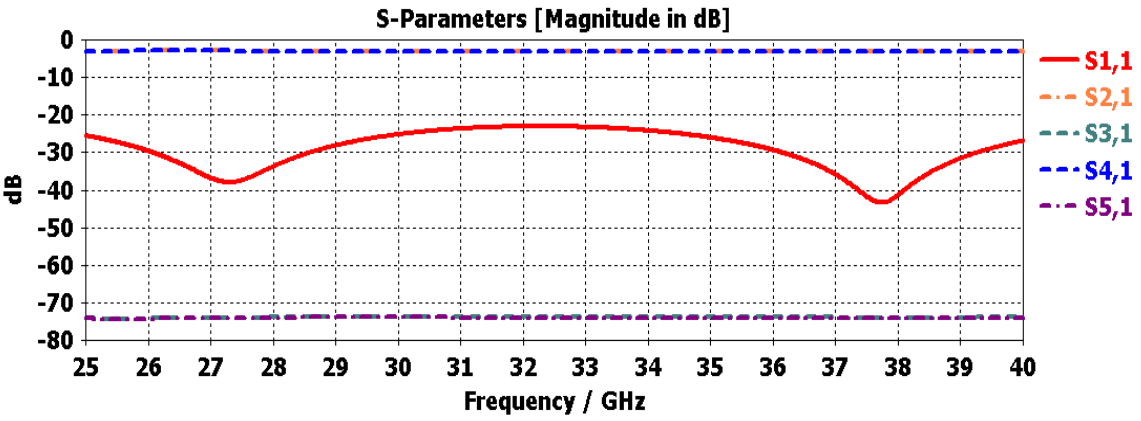

(a)

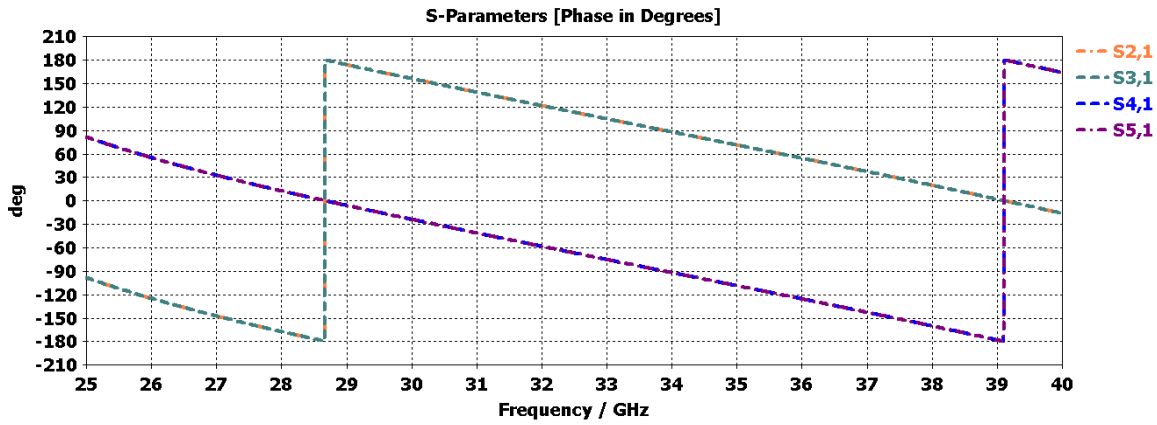

(b)

Fig.-5.4: Simulated results of the proposed OMT core (a) Scattering parameter of the OMT core and (b) Phase difference between each pair of the opposite output ports of OMT core

According to the scattering parameters displayed in Figure 5.4 (a), it is clearly visible that the reflection coefficient of the OMT core is better than -20 dB throughout the entire bandwidth while maintaining excellent isolation between opposite pair of OMT core output ports. Additionally, each pair of the opposite output ports are 180˚ out of phase, as illustrated in Figure 5.4 (b). It should be mentioned that the positioning of the matching element at the midpoint of the turnstile junction is very crucial to ensure efficient separation of the two orthogonal polarizations entering through the common port (Port 1) of the OMT core. Otherwise, RF performance can substantially deteriorate.

5.3 Transition from OMT Core Output Port to RGW

As mentioned earlier, the guiding structure of the OMT core is chosen to be a groove gap waveguide. Since the proposed OMT is a combination of GGWG and RGW, a transition between these two guiding structures has been designed. It should be stated that the dominant modes for GGWG and RGW are TE_{10} and quasi-TEM mode, respectively. As shown in Figure 5.5(a), multiple matching steps have been included at the end of the ridge to achieve an acceptable matching from the transition. The simulated response of a single transition is presented in Figure 5.5(b) that demonstrates an excellent matching level.

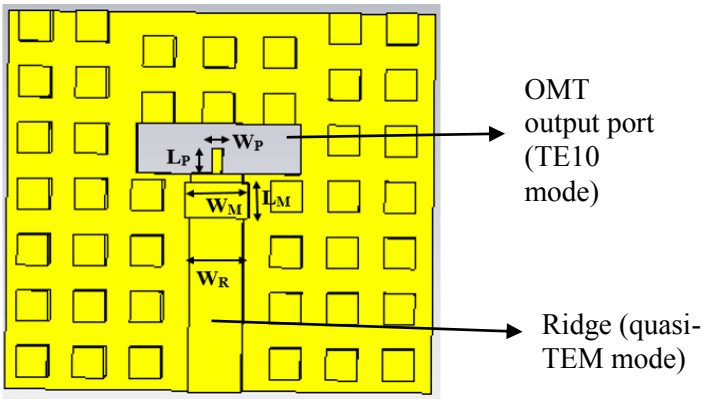

(a)

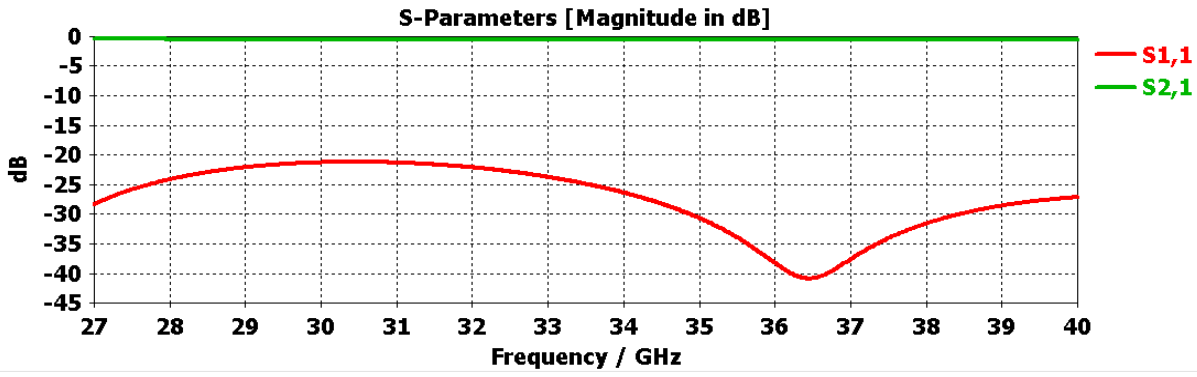

(b)

Fig.-5.5: Transition from OMT core output port to RGW (a) Structure of the transition and (b) Simulation result of a single transition

The dimensions of the matching steps indicated in Figure 5.5 (a) are presented in Table 5.4. The dimension of the OMT output port is identical to the measurement of the groove in the previously mentioned GGWG, and the dimension of the ridge is precisely similar to the ridge of the formerly stated RGW in Section 5.1.

Table 5.4: Dimensions of the Matching Steps of Transition

Parametric Symbols	Value (mm)
L_P	1.48
W_P	0.47
L_M	1.94
W_M	3.38
W_R	2.9

5.4 E-plane Bend and H-plane Bend

For each polarization of the OMT, a pair of E-plane bend and H-plane bend have been implemented. E- and H-plane bends make it possible to design a compact OMT structure. The proposed 270° E-plane bend is dissimilar to the traditional planer ridge gap waveguide. This bend exists on the ridge as well as on the upper and lower PEC plate, as depicted in Figure 5.6. According to Figure 5.6 (a), the ridge's bend shape is similar to the alphabet “L” with a smooth 270° bend at the corner. Pins at the bend are modified to adjust with the rest of the pins on both planes of the E-plane bend.

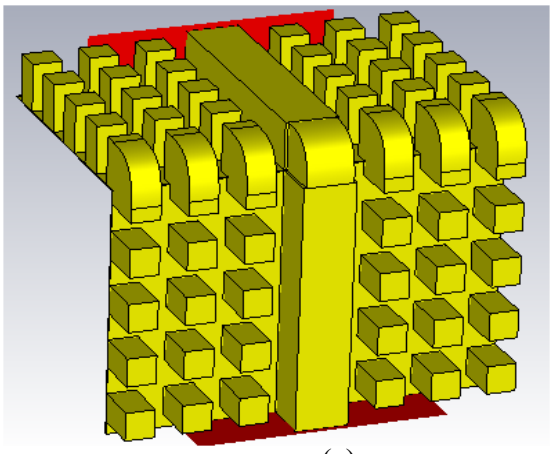

(a)

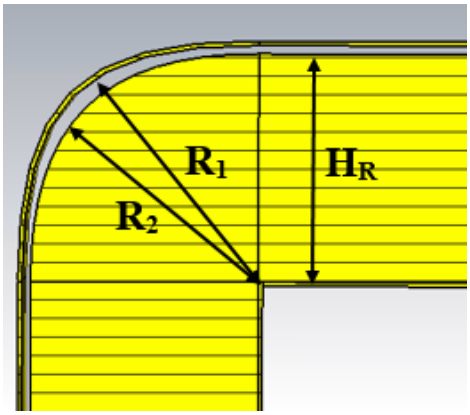

(b)

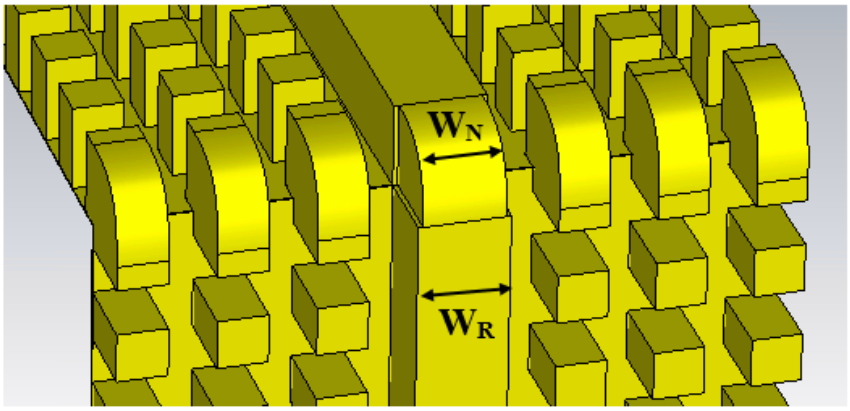

(c)

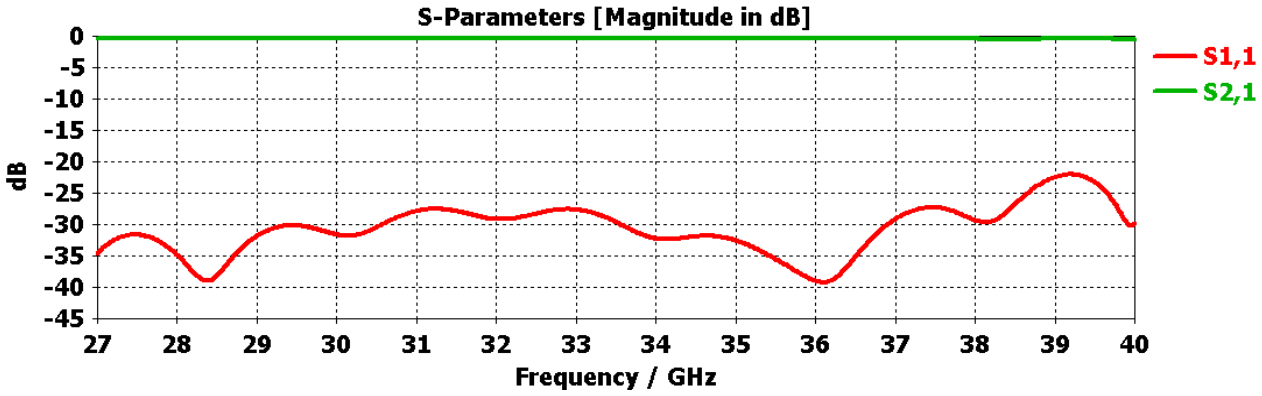

(d)

Fig.-5.6: 270˚ E-plane bend (a) Full structure (upper PEC plate hidden), (b) Enhanced cross-sectional side view of the ridge indicating radius of the bends, (c) Partial view of the E-plane bend comparing the ridge and bend's width, and (d) Simulation result of the 270˚ E-plane bend

To achieve a better matching level, the ridge height and width have been reduced at the curve of the 270˚ E-plane bend. Figure 5.6 (b) represents the cross-sectional view of the ridge, where R_1 is the radius of the top PEC plate, R_2 is the radius of the ridge bend, and H_R is the height of the ridge (excluding the bend). Figure 5.6 (c) demonstrates the partial view of the E-plane bend, where W_N is the narrow width of the ridge at the bend, and W_R is the ridge width (without the bend). All these mentioned values are tabulated in Table 5.5. Additionally, Figure 5.6 (d) displays an excellent return loss that is better than 20 dB all over the entire bandwidth (27- 40 GHz).

Table 5.5: Dimensions of the 270˚ E-plane bend

Parametric Symbols	**Value (mm)**
R_1	3
R_2	2.91
H_R	2.62
W_N	2.56
W_R	2.9

The periodically placed nails cancel the field propagation transverse to the ridge direction. Theoretically, there should be no propagating wave transverse to the ridge direction as the magnetic boundary is applied. However, since no real magnetic surface exists in nature, some trivial field components transverse to the ridge direction are present. Although there are no non-planar bends on the ridge as well as on the upper and bottom PEC plate, it does not distress the overall power transfer of the RGW. Thus, it is suitable for developing power dividers, orthomode transducers, couplers, and other microwave components.

Like E-plane bend, a pair of 90° H-plane bend is utilized for each polarization of the OMT structure, as shown in Figure 5.7 (a). The pins' position around the 90° bend has been slightly modified near the bend, which does not disrupt the H-plane bend's periodicity. The simulation result in Figure 5.7 (b) shows that the reflection coefficient is better than -25dB throughout the frequency band of interest.

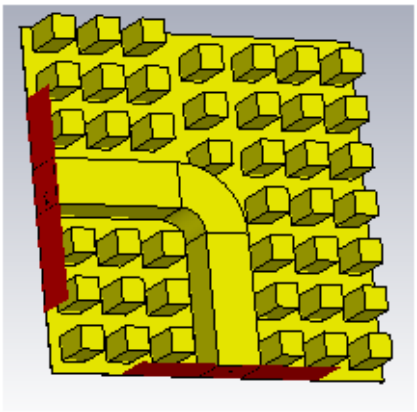

(a)

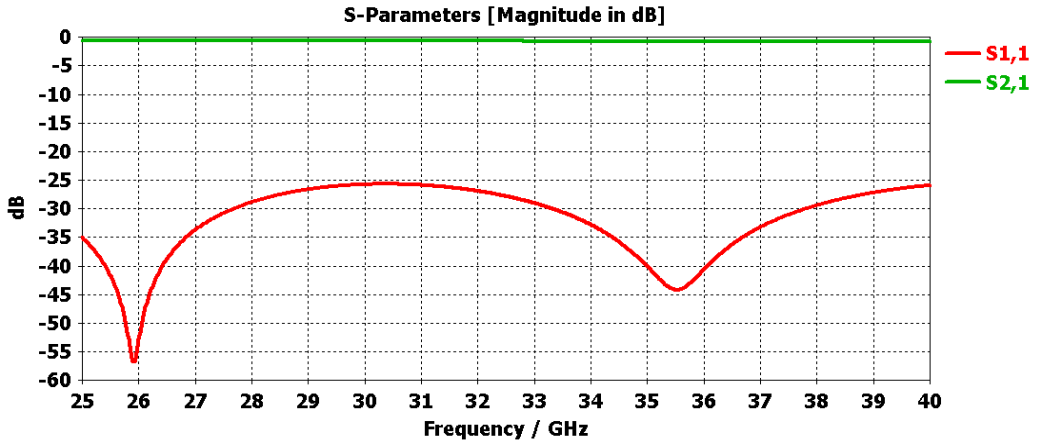

(b)

Fig.-5.7: 90˚ H-plane bend (a) 3D view (upper PEC layer hidden) and (b) Simulation result of the 90˚ H-plane bend

5.5 GGWG to WR-28 Power Combiner and Transition

The fundamental concept of any power divider is to combine multiple signals from different ports to one port. These signals could be of any magnitude and phase. For each polarization of the OMT structure, one power divider has been designed to merge two signals into one and then transmit to the standard WR-28 rectangular waveguide. The standard WR-28 waveguide parameters, along with its operating frequency, are presented in Table 5.6.

Table 5.6: Standard WR-28 Waveguide Parameter and its Operating Frequency

Frequency band	**Waveguide name**	**Frequency range (GHz)**	**Cutoff frequency (GHz)**	**Inner dimensions of waveguide opening**	
			Lowest order mode	**A (mm)**	**B (mm)**
Ka	WR-28	26.5-40	21.077	7.112	3.556

The signals divided by the OMT core's turnstile junction consist of the same magnitude but are 180° out of phase. Hence, to counteract the phase difference between two signals, the power combiner should operate at a similar phase difference. The proposed power combiner is based on a slot placed on the top PEC plate, where two lines are feeding the slot from two opposite directions. It should be stated that the power combiner consists of both RGW and GGWG, along with the stepped transition between them. For improved matching and lesser reflections, a metallic cuboid with a rectangular cross-section is placed at the power combiner's center. This metallic cuboid located at the center of the slot acts like a turnstile for the propagating signal.

Additionally, the slot dimension is identical to the WR-28 waveguide. Furthermore, to prevent signal leakage while connecting the OMT to the standard waveguide flange, pins are

placed around the slot to generate a periodic structure. The dimensions of these pins are the same as the pins used in the RGW and GGWG of this power combiner. A standard UG599/U rectangular flange has been used at the output port (WR-28) of the power combiner. The standard flange design is shown in Figure 5.8, and the dimensions of the flange are presented in Table 5.7.

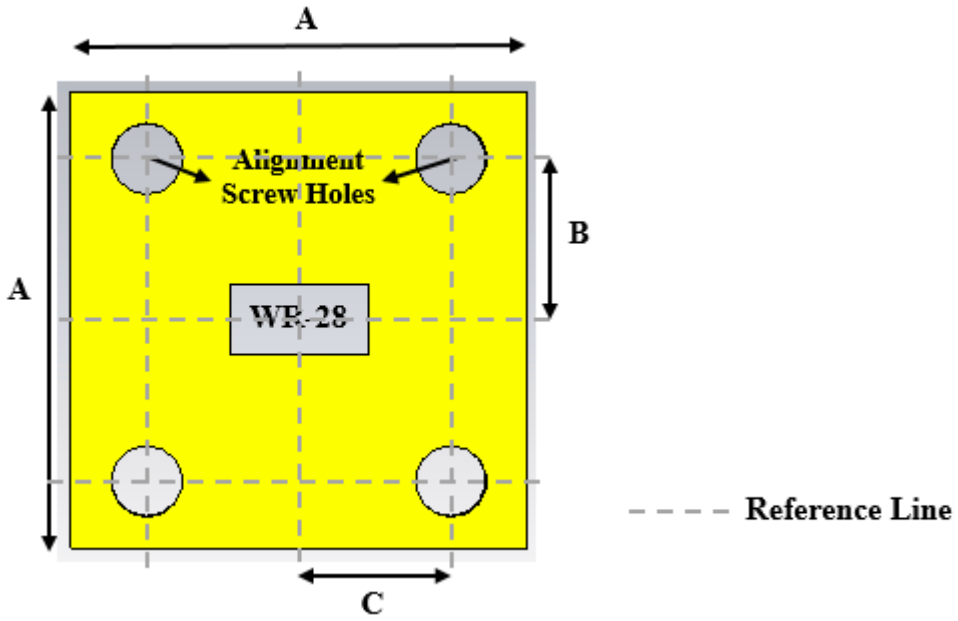

Fig.-5.8: Standard UG599/U rectangular waveguide flange for WR-28

Table 5.7: Dimensions of Standard UG599/U Flange

Parametric Symbols	Value (mm)
A	19.05
B	6.73
C	6.35
Diameter of Screw Holes	2.98

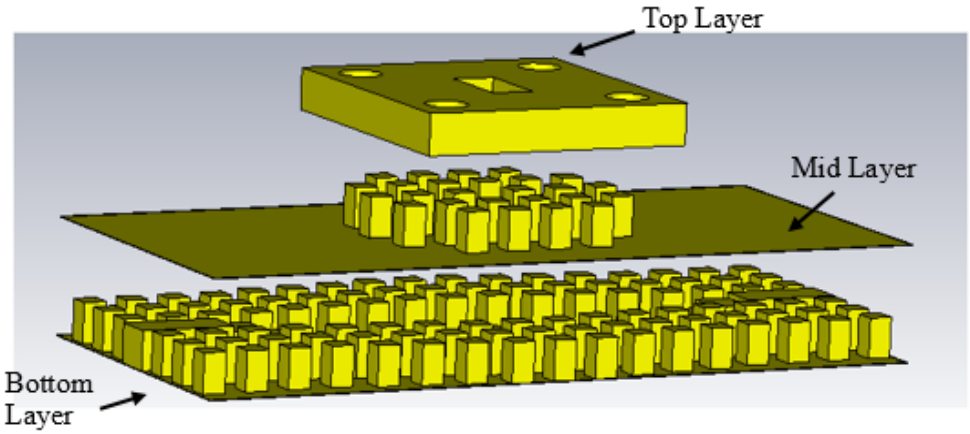

(a)

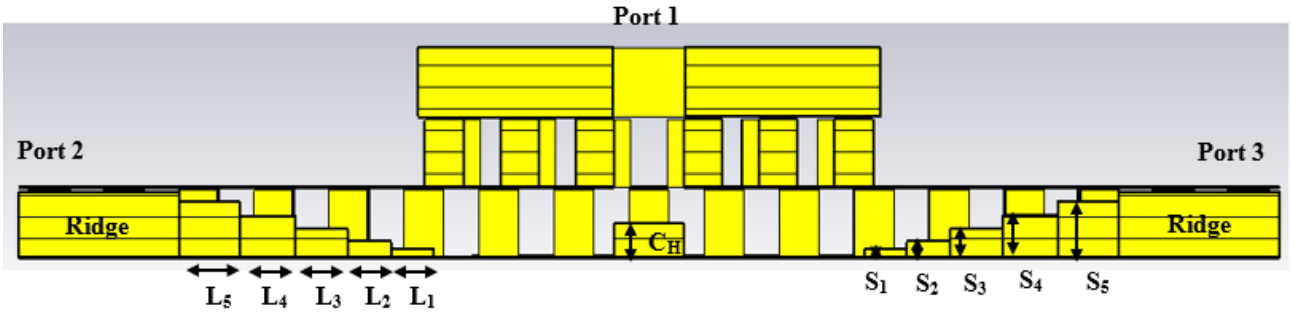

(b)

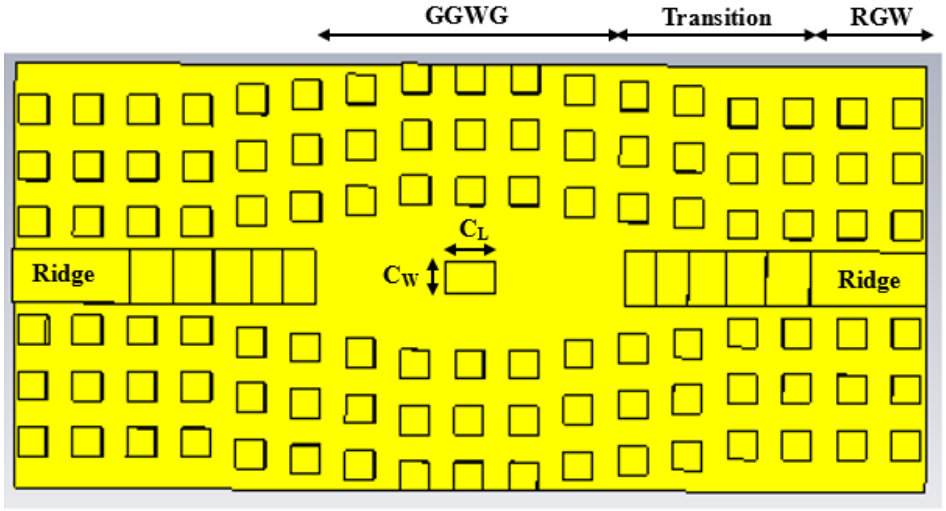

(c)

Fig.-5.9: GGWG to WR-28 power combiner and transition (a) 3D view along with standard flange (top layer) of the waveguide for connecting to the port (Enhanced airgap between each layer), (b) Cross-sectional side view, and (c) Bird's-eye view of the bottom layer (hidden upper layers)

The proposed power combiner's geometrical structure is presented in Figure 5.9, and the simulation results are illustrated in Figure 5.10. Figure 5.9 (a) shows that the airgap between layers has been increased to visualize the 3D view better. The top layer is the standard UG599/U flange mentioned earlier, whereas the bottom layer holds the GGWG and RGW of the power divider. The middle layer contains the upper metal plane of the bottom layer's gap waveguide structure along with the periodic pins located around the slot to prevent signal leakage. Figure 5.9 (b) shows the cross-sectional view from the side, indicating the transition parameters as well as height (C_H) of the metallic cuboid placed at the center of the power combiner. Finally, Figure 5.9 (c) represents the bird's eye view of the power combiner's bottom layer. Figure 5.9 (c) shows that the groove width has gradually reduced to match the ridge width, which was followed to avoid sudden discontinuity of the structure. All the notations mentioned in Figure 5.9 are stated in Table 5.8.

Table 5.8: Dimensions of the GGWG to WR-28 Power Combiner and Transition

Parametric Symbols	**Value (mm)**	**Parametric Symbols**	**Value (mm)**
L_1	1.78	S_3	1.15
L_2	1.84	S_4	1.66
L_3	2.17	S_5	2.24
L_4	2.34	C_H	1.36
L_5	2.48	C_L	7.112
S_1	0.35	C_W	3.556
S_2	0.64		

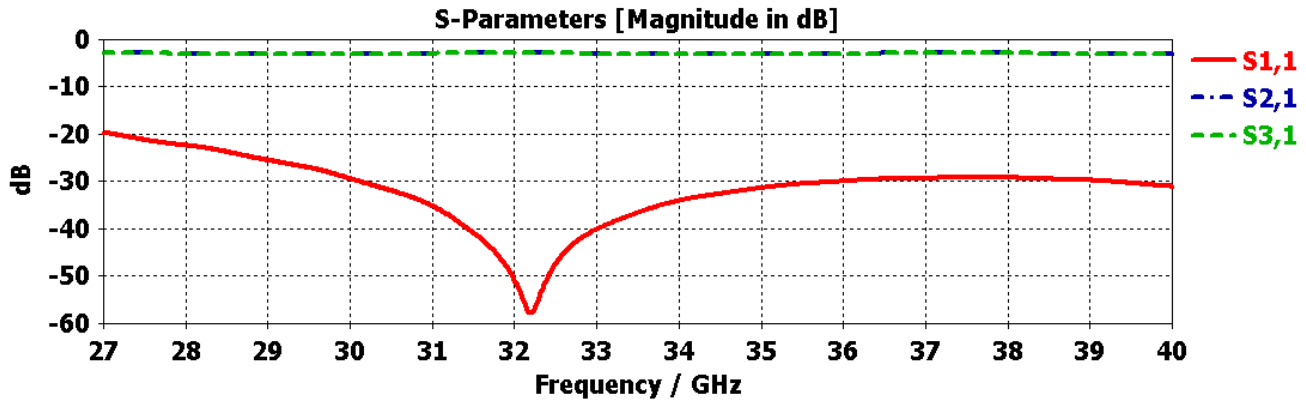

(a)

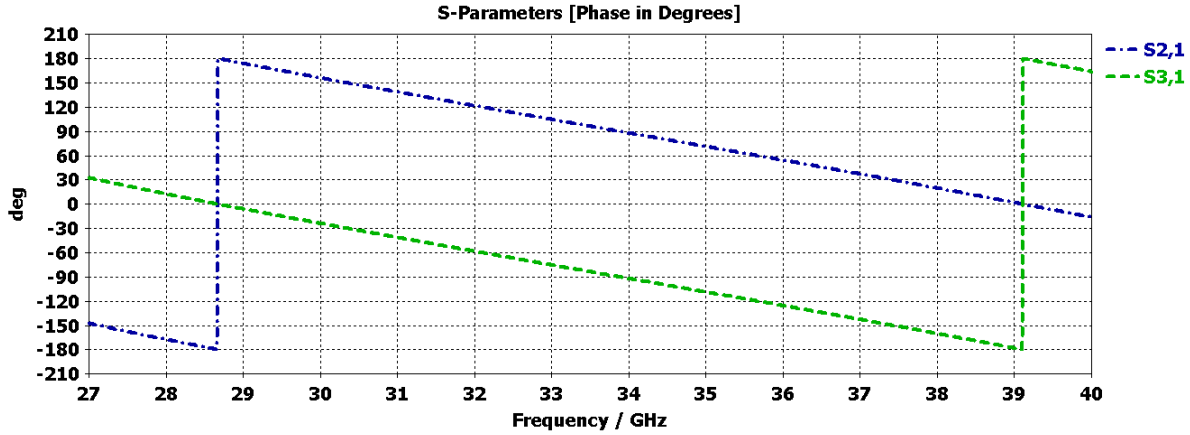

(b)

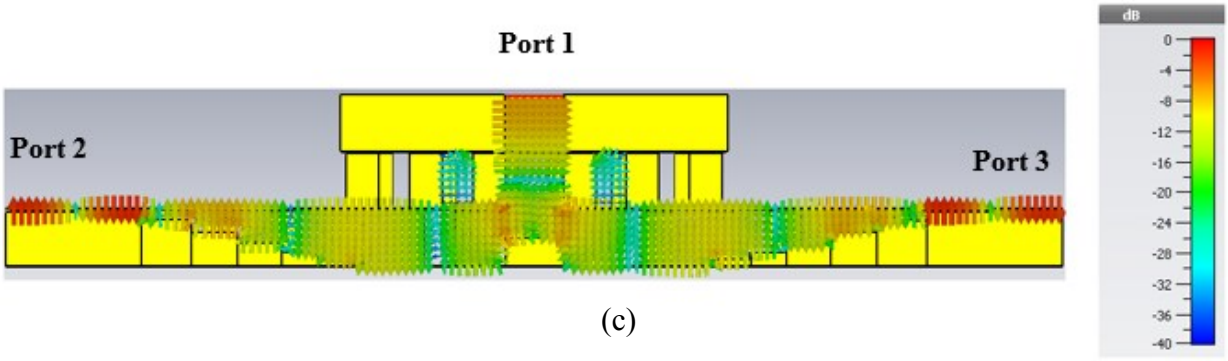

(c)

Fig.-5.10: Simulation Results for GGWG to WR-28 power combiner and transition (a) Reflection and transmission coefficient, (b) Phase difference between port 2 and port 3, and (c) Electric field distribution at 33.5GHz at plane-A cross-section

The simulation results of the power combiner are shown in Figure 5.10. It is evident that the return loss is better than 20 dB over the entire band. The magnitude of the signals of Port 2 and Port 3 are equal (around -3 dB), while the phase difference between these signals is 180° that is required to provide the 180° difference required by the turnstile junction of the OMT core. Moreover, to show that the two feeding ports are out of phase, the electric field distribution at 33.5 GHz is shown in Figure 5.10 (c). This power combiner is applied twice within the OMT structure, once for vertical polarization and then horizontal polarization.

5.6 Complete OMT Structure

The overall OMT structure is discussed in this Section. The OMT core has four output ports; each pair are assigned for one polarization signal, as declared earlier. The OMT complete structure is shown in Figure 5.11, while the simulation results for vertical and horizontal polarizations of the full OMT are displayed separately in Figure 5.12. The E-plane bend and the H-plane bend result in fitting around a block to ensure a compact OMT configuration. OMT core is placed in the middle, from which each polarization is transmitted to opposite directions. Two of the OMT core outputs that correspond to one polarization signal are combined and transferred to the WR-28 standard waveguide through the power combiner proposed in the previous subsection. Meanwhile, the other pair of output signals are transferred to the other polarization structure. The final OMT structure has three physical ports: one is the common port, i.e., nonstandard circular waveguide; the other two ports are standard WR-28 rectangular waveguides transverse to each other, representing each polarization. It is worth stating that there is no need for any electrical contacts between the OMT layers (parts), thus no need for any metal screws for connection, but for assembly. Since the OMT core is designed following gap waveguide technology, each polarization

section can be fabricated separately and then merged together. The overall dimensions of the entire OMT are 65.3 x 65.3 x 60 mm^3.

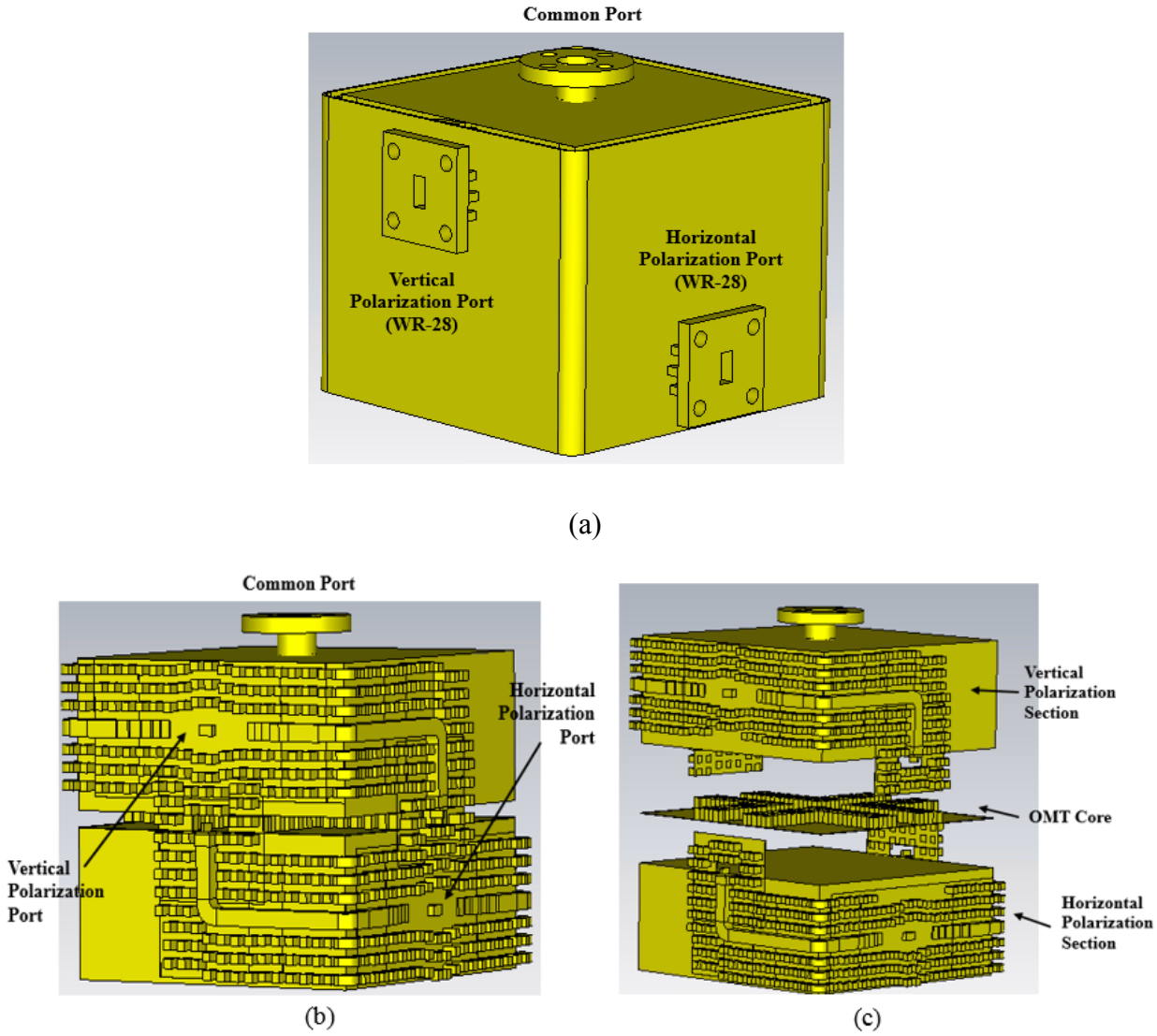

Fig.-5.11: Complete OMT Structure (a) 3D view indicating all three physical ports, (b) Perspective view (upper PEC and rectangular waveguide flange hidden), and (c) Airgap enhanced between each layer of the OMT; each polarization section and OMT core specified (upper PEC and rectangular waveguide flange hidden)

According to the simulation results in Figure 5.12, it achieves a return loss better than 18 dB throughout the bandwidth for both horizontal and vertical polarizations. The isolation between the two polarizations is better than 70 dB over the entire band. In addition, the insertion loss has a level better than 0.5 dB over the frequency band.

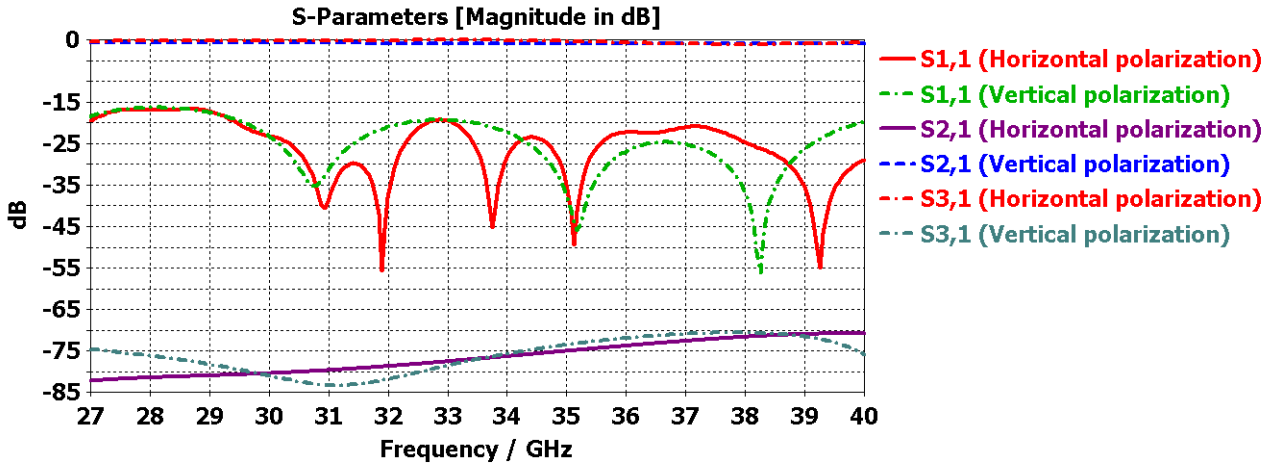

Fig.-5.12: Simulation results for the complete OMT structure excited through a common port

5.7 Back-to-Back Setup for Further Verification

For additional validation of the complete OMT structure, several methods can be implemented. Firstly, the OMT's common port can be connected to a matched load that can absorb all the propagating modes [88]. The second method is to replace the matched load with a conical horn antenna operating in the same frequency band of the OMT. The third setup connects two OMTs in a back-to-back manner through the common ports, without any rotation and rotating one OMT by 90° to ensure that there are no higher-order modes exited due to any asymmetry created during manufactures. Similar insertion loss levels with or without rotation is an indication of that. Of course, the simulation does not show that because of the perfect dimensions. The third method is

followed to validate the OMT structure since it is simple and reliable in terms of our structure as there are four measuring ports, each with one propagating mode. As mentioned earlier, measurements are taken twice: initially, the two OMTs are aligned imaging each other without any rotation connected through the common ports, while the second setup is by rotating one OMT by 90° from the other one [86-88]. In the back-to-back setups, four ports are numbered, as shown in Figure 5.13, and the simulation results for each setup are presented in Figure 5.14. The simulation results for each back-to-back setup represent an agreeable similarity, with a very good matching level.

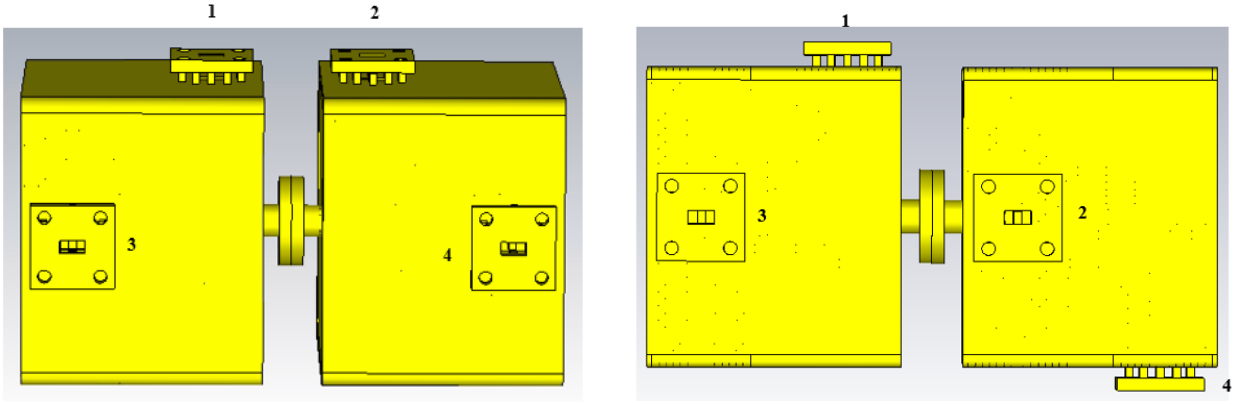

(a) (b)

Fig.-5.13: OMT back-to-back setup. (a) Without rotation and (b) With 90° rotation

5.8 Result Validation of Proposed OMT

For more verification, two different solvers: Time-domain (TD) and Frequency-domain (FD), are utilized in CST Microwave Studio and shown for proposed OMT for Ka-band in Figure 5.15 for reflection coefficient of horizontal and vertical polarization. The results represent a similar S-parameter, which validates the proposed structure's response for the entire frequency band of interest.

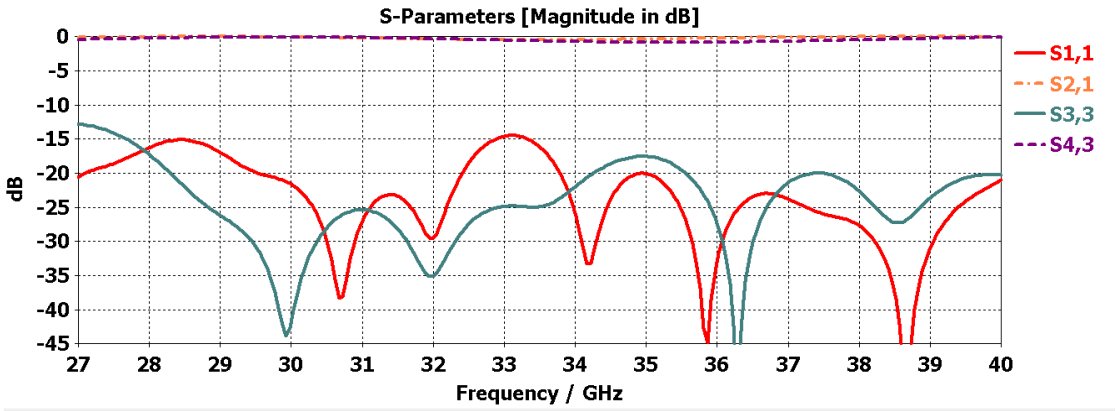

(a)

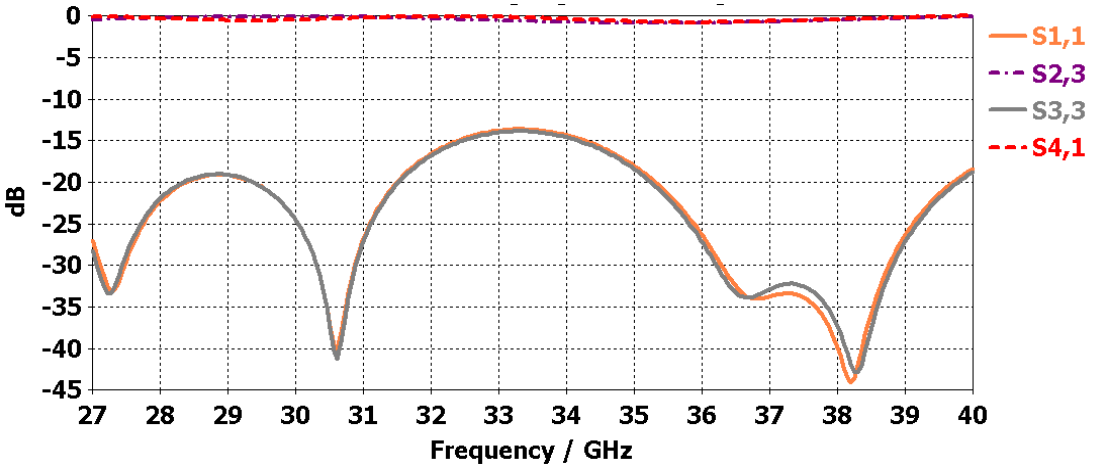

(b)

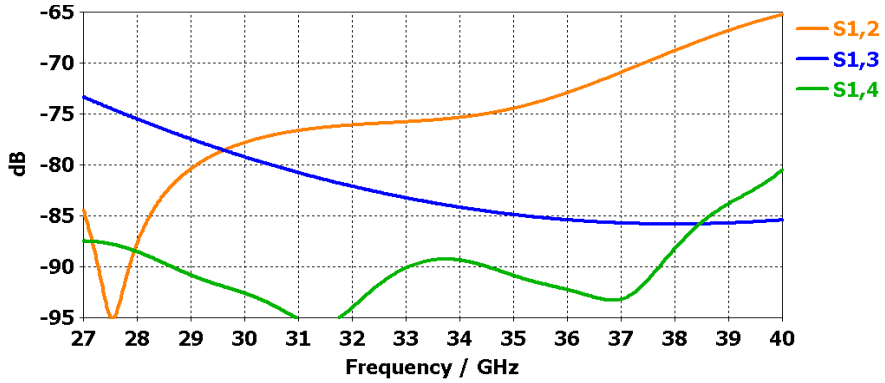

(c)

Fig.-5.14: OMT simulation results using a back-to-back setup (a) Without rotation (matching and insertion loss), (b) With 90° rotation (matching and insertion loss), and (c) Isolation coefficients with 90° rotation

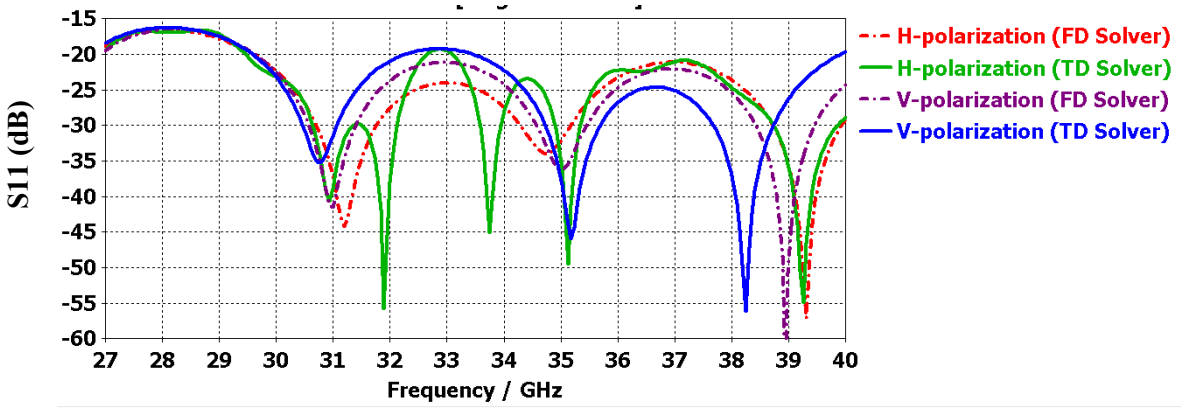

Fig.-5.15: Comparison between reflection coefficients (S_{11}) for horizontal and vertical polarizations of entire OMT structure using CST MWS time-domain (TD) solver and frequency-domain (FD) solver

5.9 Evaluation of Proposed OMT

A comparison between proposed OMT and some of the other published OMTs is presented in Table 5.9. It summarizes the main features and tradeoffs of the OMTs provided in this chapter with other references, for various frequency bands and for parameters that can be compared between different topologies. The quantitative dimensions normalized to the center frequency wavelength (λ_0) have been included in Table 5.9 as well. The mentioned references in Table 5.9 represent the main concept of the turnstile (twofold symmetric) OMTs, each having a diverse realization by implementing various components.

Table 5.9: Comparison between mm-Wave OMTs

References	Bandwidth, (GHz) / %, λ_0 (mm)	Average Return Loss, dB	Average Insertion Loss, dB	Average Isolation, dB	Dimensions, λ_0
[91]	12.6- 18.25 / 36.6, 19.45	< 28	< 0.11	> 40	3.6 x 1.44 x 1.03
[92]	220- 330 / 40, 1.1	< 22	< 0.6	> 60	9.17 x 9.17 x 0.83
[93]	13.5- 18.1 / 29.1, 19	< 18	< 0.2	> 50	7.0 x 4.53 x 2.79
[55]	18- 26 / 36.3, 13.64	< 19	< 0.15	> 48	6.52 x 6.52 x 4.26
[89]	31- 45 / 36.8, 7.89	< 25	< 0.2	> 50	8.61 x 6.59 x 4.31
This work	27- 40 / 38.8, 8.96	< 18	< 0.5	> 70	7.29 x 7.29 x 6.7

(λ_0 = wavelength at the center frequency)

It is possible to exclude the thickness of the two rectangular flanges and the common port extension that could make the present OMT seem smaller.

5.10 Size Reduction of the Proposed OMT

It is possible to downsize the proposed OMT by modifying a few components, for instance, embedding the pins around the common port or reducing the ridge length of the out-of-phase power divider. This size-reduction results in improved insertion loss due to less conductor loss of the overall OMT structure. Table 5.10 represents the comparison between the initial and downscaled OMT structures, which indicates that the new OMT structure is $1.4\lambda_0$ times smaller on each side and $0.68\lambda_0$ times shorter on the height compared to the initial OMT.

Table 5.10: Comparison between initial and downsized OMTs

References	**Bandwidth, (GHz) / %, λ0 (mm)**	**Average Return Loss, dB**	**Average Insertion Loss, dB**	**Average Isolation, dB**	**Dimensions, λ_0**
Initial OMT	27- 40 / 38.8, 8.96	< 18	< 0.5	> 70	7.29 x 7.29 x 6.7
Downsized OMT		< 18	< 0.37	> 72	5.89 x 5.89 x 6.02 **($1.4\lambda_0$ reduction)**

(λ_0 = wavelength at the center frequency)

The overall structure of the downscaled OMT is illustrated in Figure 5.16. It shows that the pins around the common port are embedded into the OMT surface following a triangular lattice orientation. Besides, the ridge length has been reduced by $1.4\lambda_0$ on each side of the power divider. Screw holes around the common port have been placed through which the OMT will be connected to the antenna flange. The antenna flange's smooth surface will act as the upper PEC layer for generating a gap waveguide for the pins placed around the common port.

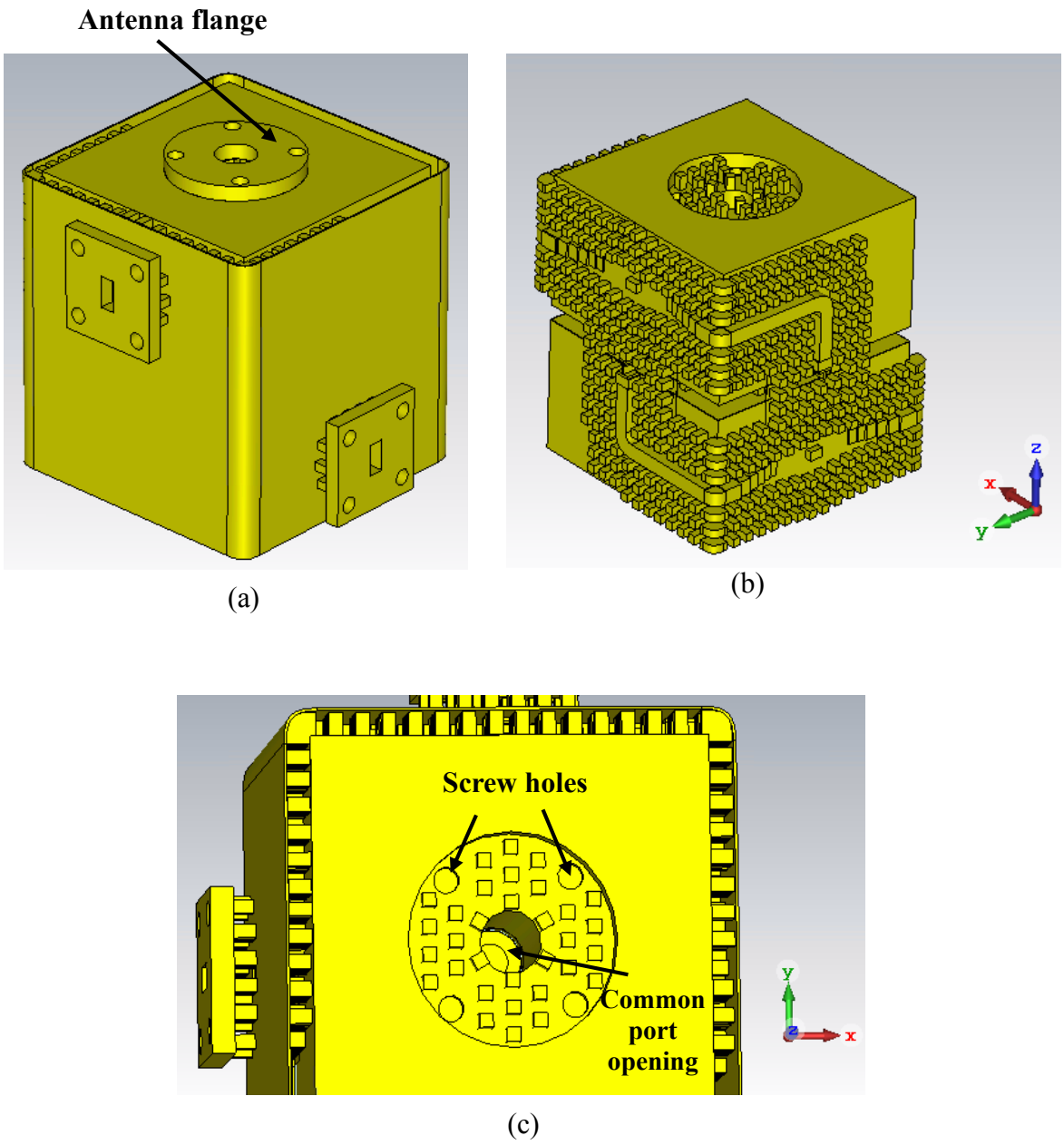

Fig.-5.16: Downsized OMT Structure (a) 3D view indicating all three physical ports, (b) Perspective view (upper PEC and waveguide flange hidden), and (c) Enhanced view of the common port region indicating pins' orientation and screw holes (for connection) around the common port opening

According to the simulation results in Figure 5.17, it achieves a return loss better than 18 dB throughout the bandwidth for both horizontal and vertical polarizations. The isolation between the two polarizations is better than 72 dB over the entire band. Additionally, the insertion loss has a level better than 0.37 dB over the frequency band.

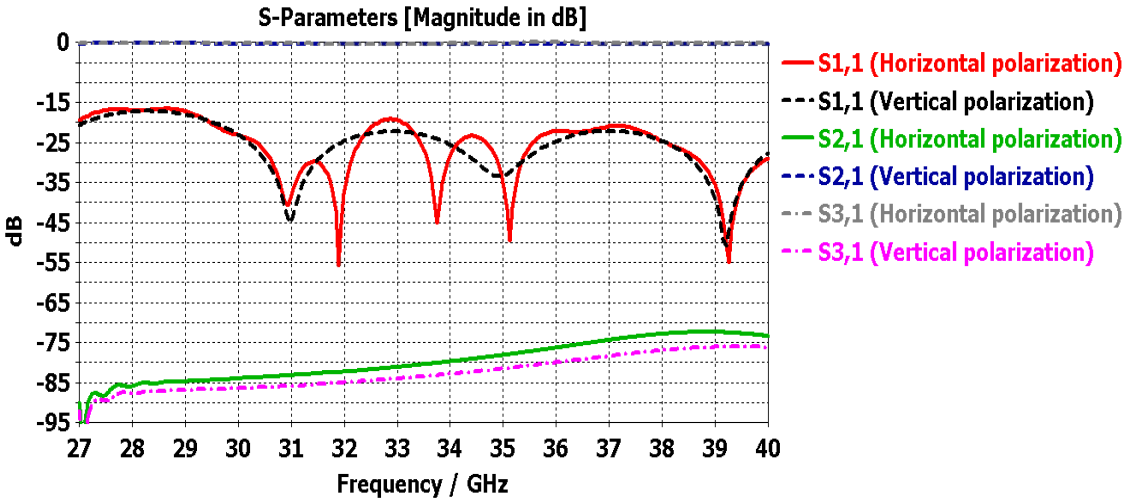

(a)

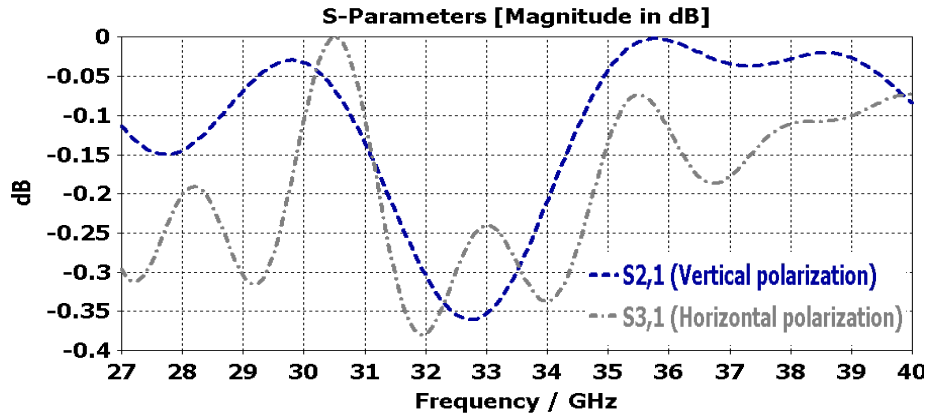

(b)

Fig.-5.17: (a) Simulation results and (b) Insertion loss for both polarizations of downsized OMT structure excited through a common port

In the back-to-back setups, four ports are numbered, as shown in Figure 5.18, and the simulation results for each setup are presented in Figure 5.19. For the back-to-back setups, the OMTs are connected through an antenna flange, which acts as the upper PEC layer (of both OMTs) for the pins positioned around the common ports. The simulation results for each back-to-back setup represent an agreeable resemblance, with a very good matching level.

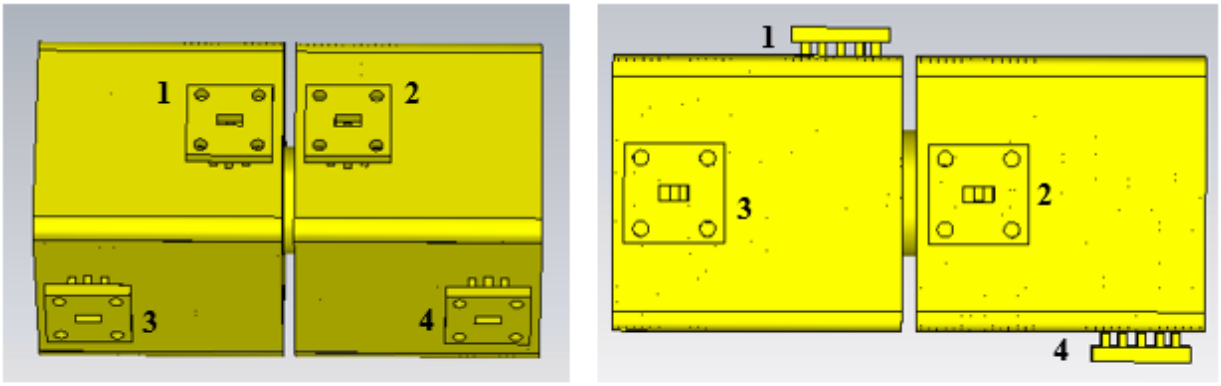

Fig.-5.18: Downsized OMT back-to-back setup (a) Without rotation and (b) With 90° rotation

For further verification, two different solvers: Time-domain (TD) and Frequency-domain (FD), are utilized in CST Microwave Studio and shown for downsized OMT for Ka-band in Figure 5.20 for reflection coefficient of horizontal and vertical polarization. The results demonstrate a similar S-parameter, which validates the proposed structure's response to the entire frequency band of interest.

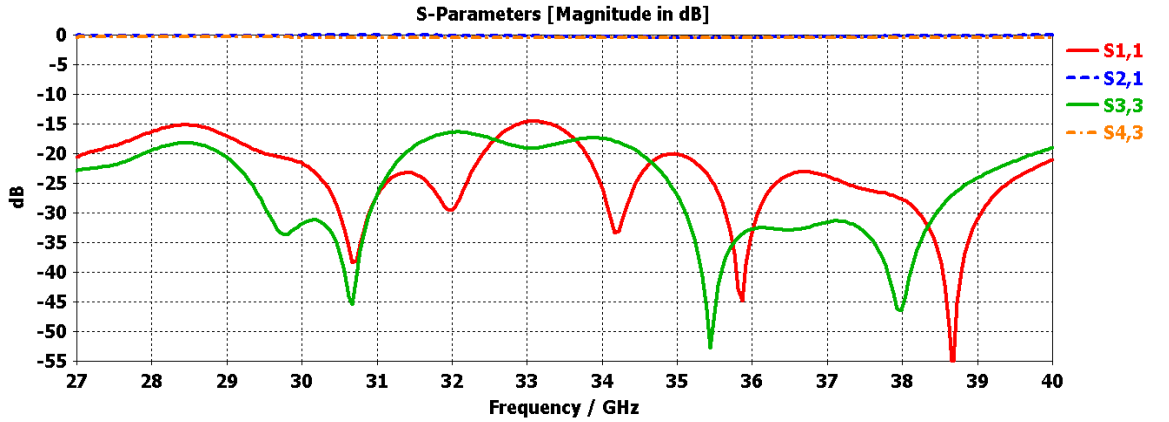

(a)

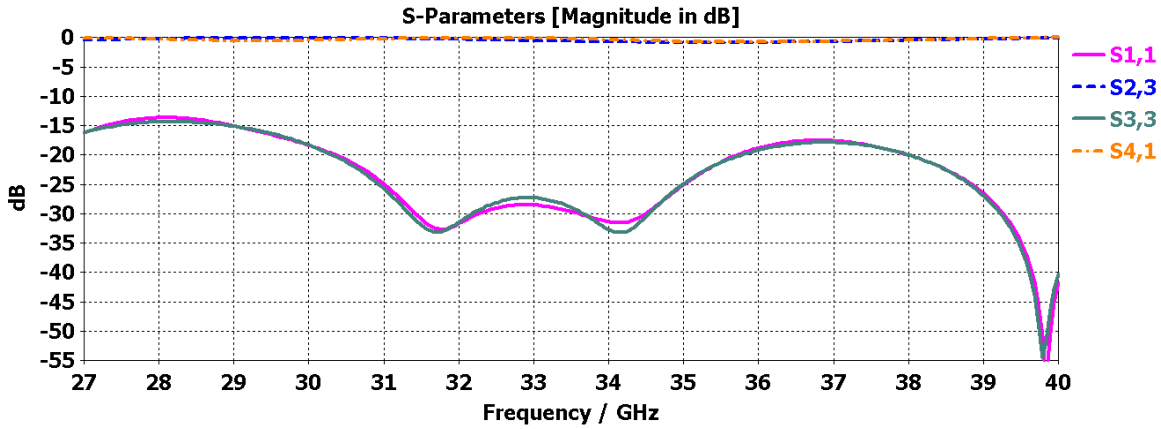

(b)

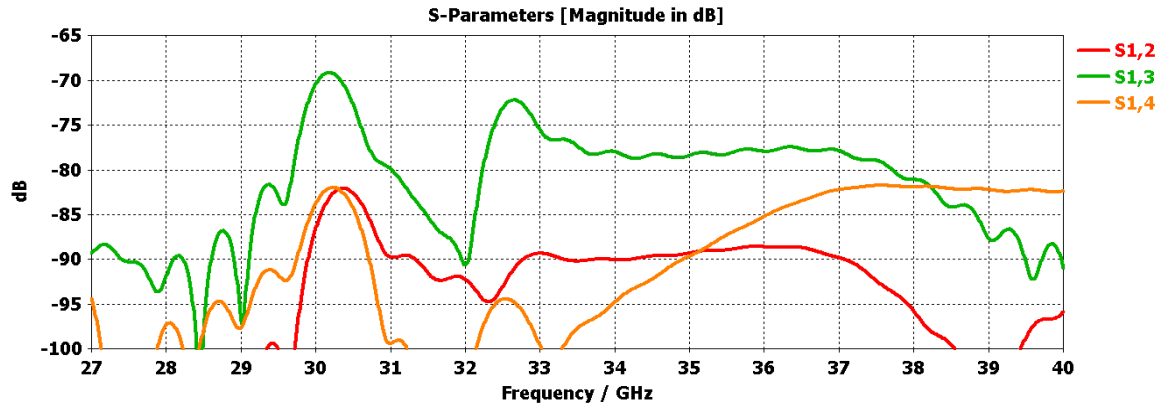

(c)

Fig.-5.19: Downsized OMT simulation results using a back-to-back setup (a) Without rotation (matching and insertion loss), (b) With 90° rotation (matching and insertion loss), and (c) Isolation coefficients with 90° rotation

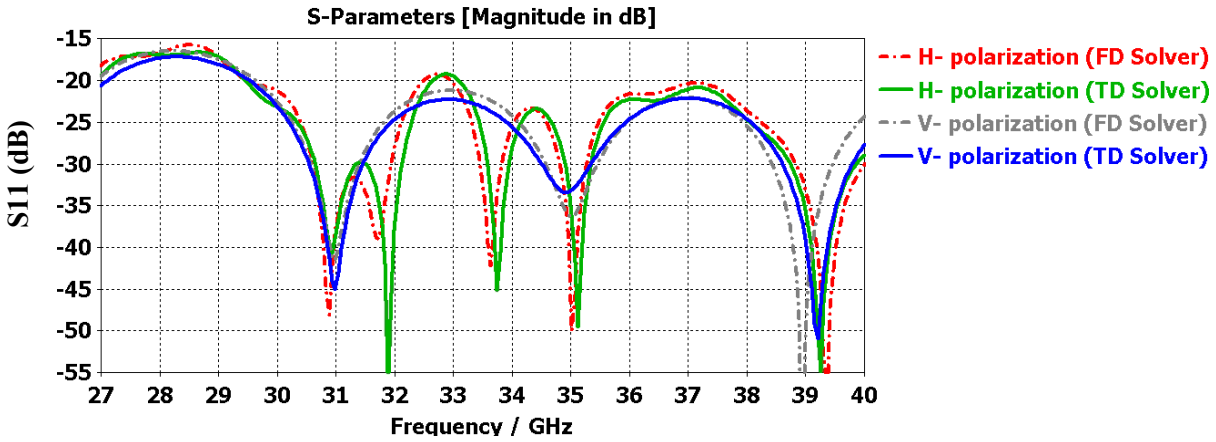

Fig.-5.20: Comparison between reflection coefficients (S_{11}) for horizontal and vertical polarizations of downsized OMT structure using CST MWS time-domain (TD) solver and frequency-domain (FD) solver

A unique structure of symmetric OMT has been designed and validated in this chapter. The selected implementation technology was a combination of RGW and GGWG due to their massive benefits over other conventional technologies at the millimeter frequency band. The proposed OMT's operating band has been selected from 27 to 40 GHz, covering almost the entire Ka-band. The two orthogonal ports have been selected as WR-28 standard rectangular waveguide to expedite the measurements, thus making the connection of the proposed structure convenient for standard equipment.

Chapter 6

Conclusion and Future Possibilities

Gap waveguide technology has gained its prominence for millimeter and submillimeter-wave applications. Here, a consistent approach has been followed towards designing various devices using periodic structures for the millimeter-wave frequency band. Several RF devices have been proposed and validated. The first structure represented a contactless adaptor between two standard waveguide flanges for leakage-free wave propagation. The proposed design does not require any modification to the standard waveguide flange. This proposed structure has also demonstrated an excellent return loss and insertion loss of better than 20 dB and 0.3 dB, respectively, for both standard circular and rectangular waveguides, irrespective of a smooth or rough surface. The second structure has focused on the connection between two slightly modified flange-free standard waveguides, even without any electrical contacts, alongside a 60% downsizing of the proposed structure compared to the traditional UG-387/U waveguide flange. In addition, a compact orthomode transducer has been designed based on gap waveguide technology covering the Ka-band to combine/divide two orthogonal polarizations. Since the gap waveguide technology has been utilized in the OMT structure, it has validated an efficient operation without any electrical contact or leakage issue. Besides, a decent matching level of better than -18 dB and an isolation level of 70 dB have been achieved from this compact OMT structure. All the simulated results have been verified by the time-domain and frequency-domain solver of CST Microwave Studio. Besides, a back-to-back setup measurement for the OMT has been performed for further validation. The simulated results have acceptable levels for both mentioned solvers of CST MWS.

6.1 Main Contributions

Based on the proposed structures, the contributions of the thesis can be outlined as the following:

- A contactless adaptor without modifying the standard waveguide flanges for circular and rectangular waveguides covers a wide frequency band.
- Roughness considered on the adaptor surface and demonstrated outstanding transmission results, thus reducing the cost and effort of leveling the surface while manufacturing.
- Flange-free pluggable contactless waveguide connector designed for both circular and standard rectangular waveguides for an extensive frequency bandgap.
- Introducing a high-performance symmetric compact OMT by implementing E-plane and H-plane bend.
- A novel orthomode transducer combining the ridge gap and groove gap waveguide technology is designed. Additionally, the proposed OMT demonstrates a very wideband throughout the operating frequency range.

6.2 Future Possibilities

The technology consisting of periodic structures with high impedance surfaces, such as the ridge gap waveguide and the groove gap waveguide, are expected to play a vital role in the new-age communication system. The main reason behind such a reputation is the high performance of these technologies, especially at high-frequency bands. Furthermore, their insusceptibility against high losses and leakage issues is another reason for the prominence. The future work suggested based on this research work can be summarized by the following ideas:

- Introduce stepped impedance transformation at the connection of the pipe contact's two waveguides to convert standard waveguide (AMC section) to size- reduced end. The AMC structure can then be organized on the compact end's outer surface, thus reducing the dimension of the pipe contact.
- The pins on the standard waveguide pipe contact can be fabricated on the smooth structure's internal surface, thus keeping the waveguide structures unperturbed, as illustrated in Figure 6.1.

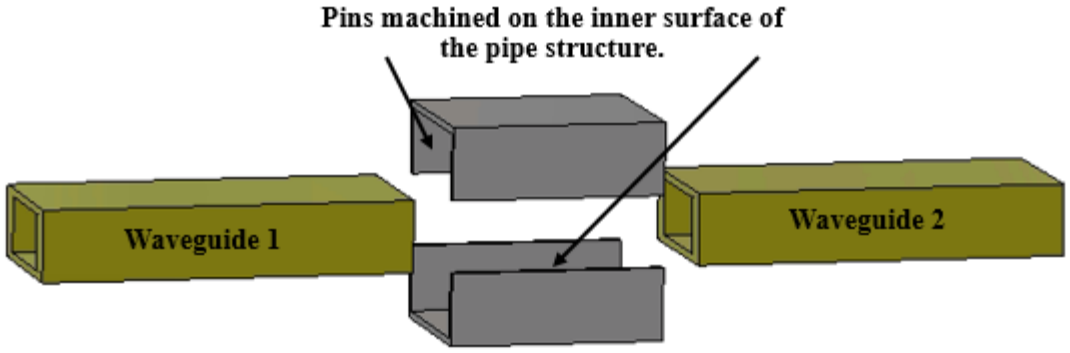

Fig.-6.1: Future possibility of the pipe contact structure keeping the waveguide structure smooth

- Considering pins embedded conductor tape to wrap around the pipe's structure for a novel, simple, and more practical solution, as illustrated in Figure 6.2. The AMC's width must equal to the outer wide wall width (ae) of the waveguide, and the distance between two AMCs must be equal to the outer narrow wall width + two pen heights i.e., (be + 2h). Here, *a* and *b* are the wide inner wall and the rectangular waveguide's narrow inner wall, respectively, and h is the pin height.

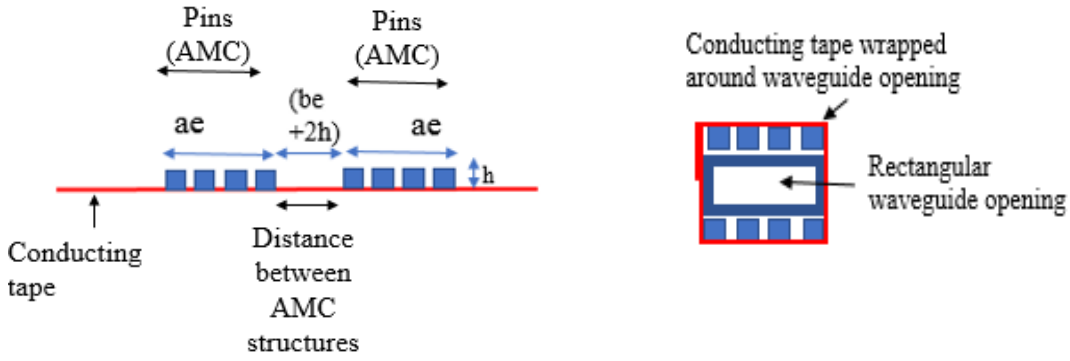

(a) (b)

Fig.-6.2: Introducing pin-embedded conductor tape to the rectangular waveguide pipe contact structure (a) Conductor tape with pins implanted and (b) Conductor tape wrapped around the waveguide opening

- If the pipe contact's circular junction is metalized rubber with pins around, then the flexible structure can be wrapped around the circular waveguide without any difficulty.
- For the circular waveguide pipe contact, the pins embedded conducting tape can be longer than the outside perimeter of the circular waveguide with trapezoidal-shaped pins to allow it for the wrapping, as shown in Figure 6.3.

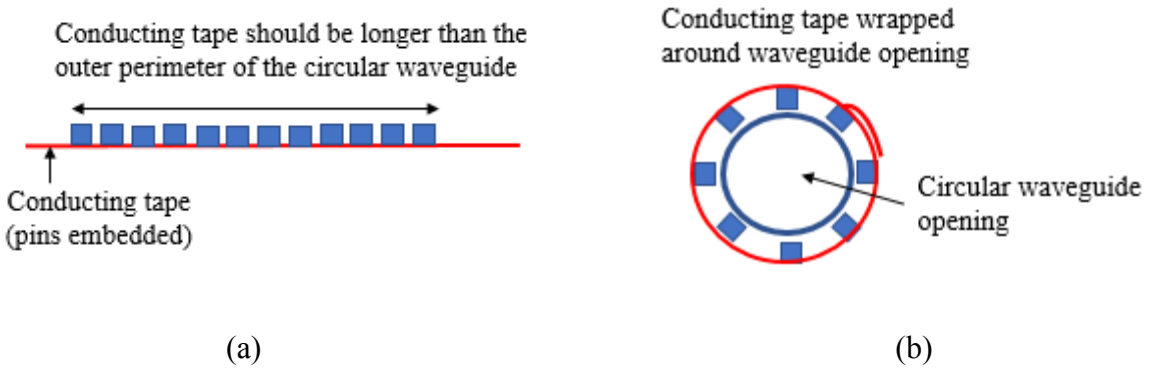

(a) (b)

Fig.-6.3: Pin-embedded conductor tape to the circular waveguide pipe contact structure (a) Conductor tape with pins embedded and (b) Conductor tape wrapped around the circular waveguide opening

- Familiarizing low-profile OMTs, i.e., with lesser components.
- As all the structures are made of conductors, scaling of the present dimensions to other frequency bands is a straight forward matter. Only dealing with even higher frequencies reaching the THz could be a matter of tuning based on the available tolerance.
- A patch with periodic pins that is suitable for the operating band could be used for a quick fix of any mm-wave waveguide cracks or any mm-wave damaged devices due to cracks that leak the signal.

Bibliography

[1] T. Halonen, J. Romero, and J. Melero, *GSM, GPRS and EDGE Performance: Evolution Towards 3G/UMTS*, John Wiley & Sons, 2004

[2] B. Furht and S. A. Ahson, *Long Term Evolution: 3GPP LTE Radio and Cellular Technology*, CRC Press, 2016.

[3] K. R. Santhi, V. K. Srivastava, G. S. Kumaran, and A. Butare, "Goals of true broad band's wireless next wave (4G-5G)", *2003 IEEE 58th Vehicular Technology Conference*, vol. 4, pp. 2317- 2321, Oct 2003.

[4] P. Zhouyue and F. Khan, "An introduction to millimeter-wave mobile broadband systems," *IEEE Communications Magazine*, vol. 49, no. 6, pp. 101–107, June 2011.

[5] E. Dahlman, S. Parkvall, and J. Sk¨old, *4G LTE/LTE-Advanced for Mobile Broadband*, Academic Press, 2011.

[6] C. X. Wang, F. Haider, X. Gao, X. H. You, Y. Yang, D. Yuan, H. M. Aggoune, H. Haas, S. Fletcher, and E. Hepsaydir, "Cellular architecture and key technologies for 5G wireless communication networks", *IEEE Communications Magazine*, vol. 52, no. 2, pp. 122- 130, February 2014.

[7] M. Fallgren, B. Timus, et al., "Scenarios, Requirements and KPIs for 5G Mobile and Wireless System", *METIS deliverable D*, vol. 1, p. 1, 2013.

[8] Huang, K.C., and D.J. Edwards, *Millimeter Wave Antennas for Gigabit Wireless Communications*, New York: John Wiley & Sons, 2008.

[9] T. K. Sarkar, M. C. Wicks, M. Salazar-Palma, and R. J. Bonneau, *Smart Antennas*. John Wiley & Sons, 2005, vol. 170.

[10] T. K. Sarkar, R. Mailloux, A. A. Oliner, M. Salazar-Palma, and D. L. Sengupta, *History of Wireless.* John Wiley & Sons, 2006, vol. 177.

[11] D. Pozar, *Microwave Engineering, 4th Edition,* John Wiley & Sons, 2011.

[12] J. Hirokawa and M. Ando, "Single-layer feed waveguide consisting of posts for Plane TEM wave excitation in parallel plates," *IEEE Transactions on Antennas and Propag*., vol. 46, no. 5, pp. 625–630, May 1998.

[13] P. S. Kildal, E. Alfonso, A. Valero-Nogueira, and E. Rajo-Iglesias, "Local Meta-material Based Waveguides in Gaps between Parallel Metal Plates," *IEEE Antennas and Wireless Propag. Letters*, vol. 8, pp. 84-87, Jan. 2009.

[14] T. S. Rappaport, J. N. Murdock, F. Gutierrez, "State of the art in 60-GHz integrated circuits and systems for wireless communications," *IEEE Proceedings*, vol. 99, no. 8, pp. 1390–1436, 2011.

[15] E. Rajo-Iglesias, M. Ferrando-Rocher, A.U. Zaman, "Gap Waveguide Technology for Millimeter-Wave Antenna Systems," *IEEE Commun. Mag.*, vol. 56, pp. 14–20, 2018.

[16] E. Rajo-Iglesias, P.S. Kildal, "Numerical studies of bandwidth of parallel-plate cut-off realised by a bed of nails, corrugations and mushroom-type electromagnetic bandgap for use in gap waveguides," *IET Microw. Antennas Propag.*, vol. 5, pp. 282–289, 2011.

[17] E. Rajo-Iglesias, A.U. Zaman, P.S. Kildal, "Parallel plate cavity mode suppression in microstrip circuit packages using a lid of nails," *IEEE Microw. Wirel. Compon. Lett.*, vol. 20, pp. 31–33, 2010.

[18] E. Rajo-Iglesias, E. Pucci, A.A. Kishk, P.S. Kildal, "Suppression of parallel plate modes in low frequency microstrip circuit packages using lid of printed zigzag wires," *IEEE Microw. Wirel. Compon. Lett.,* vol. 23, pp. 359–361, 2013.
[19] P.-S. Kildal, "Definition of artificially soft and hard surfaces for electromagnetic waves," *Electronics Letters*, vol. 24, no. 3, pp. 168- 170, Feb 1988.
[20] Y. Rahmat-Samii and H. Mosallaei, "Electromagnetic band-gap structures: classification, characterization, and applications," *11th International Conference on Antennas and Propagation*, vol. 2, pp. 560- 564, 2001.
[21] A. A. Kishk and P. S. Kildal, "Modelling of soft and hard surfaces using ideal perfect electric conducting/perfect magnetic conducting strip- grids," *IET Microwaves, Antennas & Propagation*, vol. 3, no. 2, pp. 296- 302, 2009.
[22] A. Valero-Nogueira, E. Alfonso, J. I. Herranz, and P. S. Kildal, "Experimental demonstration of local quasi-TEM gap modes in single-hardwall waveguides," *IEEE Microwave and Wireless Components Letters*, vol. 19, no. 9, pp. 536- 538, 2009.
[23] S. I. Shams, A. A. Kishk, "Printed texture with triangle flat pins for bandwidth enhancement of the ridge gap waveguide*," IEEE Trans. Microw. Theory Techn.*, vol. 7, pp. 2093- 2100, Jan. 2017.
[24] A. U. Zaman, V. Vassilev, P. S. Kildal, and A. Kishk, "Increasing parallel plate stop- band in gap waveguides using inverted pyramid-shaped nails for slot array application above 60GHz", *Proceedings of the 5th European Conference on Antennas and Propagation (EUCAP),* pp. 2254- 2257, April 2011,
[25] S. I. Shams and A. A. Kishk, "Double cone ultra wide band unit cell in ridge gap waveguides," *2014 IEEE Antennas and Propagation Society International Symposium (APSURSI),* pp. 1768- 1769, July 2014.
[26] Constantine A. Balanis, "Antenna Theory: Analysis and Design," 3rd Edition, NJ, USA: Wiley, 2005.
[27] M. Bosiljevac, A. Polemi, S. Maci, Z. Sipus, "Analytic approach to the analysis of ridge and groove gap waveguides- comparison of two methods," *Proceedings of the Fifth European Conference on Antennas and Propagation, EuCAP*, pp. 1886–1889, 2011.
[28] E. Rajo-Iglesias, P.-S. Kildal, "Groove gap waveguide: A rectangular waveguide between contactless metal plates enabled by parallel-plate cut-off," *Proceedings of the Fourth European Conference on Antennas and Propagation, EuCAP*, 2010.
[29] C. Oleson and A. Denning, "Millimeter wave vector analysis calibration and measurement problems caused by common waveguide irregularities," *56th ARFTG Conference Digest-Fall*, Boulder, AZ, USA, pp. 1- 9, 2000.
[30] P.-S. Kildal, "Waveguides and transmission lines in gaps between parallel conducting surfaces," Patent no. EP20080159791, 2009.
[31] E. Pucci and P.-S. Kildal, "Contactless non-leaking waveguide flange realized by bed of nails for millimeter wave applications," *6th European Conf. on Antennas and Propag*., Prague, pp. 3533- 3536, 2012.
[32] M. Ebrahimpouri, E. Rajo-Iglesias, Z. Sipus, O. Quevedo-Teruel, "Low-cost metasurface using glide symmetry for integrated waveguides," *Proc. 10th Eur. Conf. Antennas Propag. (EuCAP)*, pp. 1- 2, Apr. 2016.
[33] M. Ebrahimpouri, O. Quevedo-Teruel, and E. Rajo-Iglesias, "Design guidelines for gap waveguide technology based on glide-symmetric holey structures," *IEEE Microw. Wireless Compon. Lett.,* vol. 27, no. 6, pp. 542- 544, Jun. 2017.

[34] M. Ebrahimpouri, E. Rajo-Iglesias, and O. Quevedo-Teruel, "Wideband glide-symmetric holey structures for gap-waveguide technology," *Proc. 11th Eur. Conf. Antennas Propag. (EUCAP)*, pp. 1658- 1660, Mar. 2017.

[35] M. Ebrahimpouri, E. Rajo-Iglesias, Z. Sipus, O. Quevedo-Teruel, "Cost-effective gap waveguide technology based on glide-symmetric holey EBG structures," *IEEE Trans. Microw. Theory Techn.*, vol. 66, no. 2, pp. 927- 934, Feb. 2018.

[36] M. Ebrahimpouri, O. Quevedo-Teruel, and E. Rajo-Iglesias, "Design of microwave components in groove gap waveguide technology implemented by holey EBG," *Proc. 11th Eur. Conf. Antennas Propag. (EUCAP)*, pp. 746- 748, Mar. 2017.

[37] M. Ebrahimpouri, O. Quevedo-Teruel, A. A. Brazalez, and L. Manholm, "Using Glide-Symmetric Holes to Reduce Leakage Between Waveguide Flanges," *IEEE Microwave and Wireless Components Letters*, vol. 28, no. 6, Jun. 2018.

[38] S. H. V. Wambeck and A. H. Ross, "Performance of diversity receiving systems," *Proceedings of the IRE*, vol. 39, no. 3, pp. 256- 264, Mar. 1951.

[39] R. D. Tompkins, "A broad-band dual-mode circular waveguide transducer," *IRE Transactions on Microwave Theory and Techniques,* vol. 4, no. 3, pp. 181- 183, July 1956.

[40] R. W. Jackson, "A planar orthomode transducer," *IEEE Microwave and Wireless Components Letters*, vol. 11, no. 12, pp. 483- 485, Dec. 2001.

[41] J. M. Rebollar, J. Esteban, J. D. Frutos, "A dual frequency OMT in the Ku-band for TT&C applications," *IEEE Antennas and Propagation Society International Symposium.*, vol. 4, pp. 2258- 2261, vol.4, Jun. 1998.

[42] S. J. Skinner and G. L. James, "Wide-band orthomode transducers," *IEEE Transactions on Microwave Theory and Techniques,* vol. 39, no. 2, pp. 294- 300, Feb. 1991.

[43] Jens Bornemann Jarosla Uher, "Waveguide components for antenna feed systems: Theory and Cad.," Addison Wesley, 1976.

[44] J. Lahtinen, J. Pihlyckt, I. Mononen, S. J. Tauriainen, M. Kemppinen, M. T. Hallikainen, "Fully polarimetric microwave radiometer for remote sensing," *IEEE Transactions on Geoscience and Remote Sensing*, vol. 41, no. 8, pp. 1869-1878, Aug. 2003.

[45] G. L. James, "Wideband feed systems for radio telescopes," *IEEE MTT-S Microwave Symposium Digest*, pp. 1361- 1363, vol. 3, Jun. 1992.

[46] I. Dilworth, "A microwave receiver and transmitter system for a propagation experiment," *Proc. Radio receivers and associated systems*, pp. 319- 323, 1981.

[47] J. Brain, "The design and evaluation of a high performance 3m antenna for satellite communication", *Marconi Review*, vol. 41, pp. 218- 236, 1978.

[48] C. G. Montgomery, R. H. Dicke, E. M. Purcell, "Principles of microwave circuits," *IET*, no. 25, 1948.

[49] A. M. Boifot, E. Lier, T. Schaug-Pettersen, "Simple and broadband orthomode transducer (antenna feed)," *IEEE Proceedings H - Microwaves, Antennas and Propagation*, vol. 137, no. 6, pp. 396- 400, Dec 1990.

[50] A. Navarrini and R. Nesti, "Symmetric reverse-coupling waveguide orthomode transducer for the 3-mm band," *IEEE Trans. Microw. Theory Techn*., vol. 57, no. 1, pp. 80-88, Jan 2009.

[51] P. Sarasa, A. Baussois, and P. Regnier, "A compact single-horn c/x dual band and circular polarized Tx Rx antenna system," *IEEE Antennas and Propagation Society Symposium*, vol. 3, pp. 3039- 3042, Jun. 2004.

[52] J. A. Ruiz-Cruz, J. R. Montejo-Garai, J. M. Rebollar, "Optimal configurations for integrated antenna feeders with linear dual-polarization and multiple frequency bands," *IET Microwaves, Antennas Propagation*, vol. 5, no. 8, pp. 1016- 1022, Jun. 2011.
[53] A. Dunning, S. Srikanth, A. Kerr, "A simple orthomode transducer for centimeter to sub millimeter wavelengths," *Proc. Int. Symp. Space Terahertz Technol*., pp. 191-194, 2009.
[54] O. A. Peverini, R. Tascone, G. Virone, A. Olivieri, R. Orta, "Orthomode transducer for millimeter-wave correlation receivers*," IEEE Transactions on Microwave Theory and Techniques*, vol. 54, no. 5, pp. 2042- 2049, May 2006.
[55] A. Navarrini, R. L. Plambeck, "A turnstile junction waveguide orthomode transducer," *IEEE Transactions on Microwave Theory and Techniques*, vol. 54, no. 1, pp. 272- 277, Jan. 2006.
[56] G. Pisano, L. Pietranera, K. Isaak, L. Piccirillo, B. Johnson, B. Maffei, and S. Melhuish, "A broadband wr10 turnstile junction orthomode transducer", *IEEE Microwave and Wireless Components Letters,* vol. 17, no. 4, pp. 286- 288, April 2007.
[57] J. L. Cano, A. Tribak, R. Hoyland, A. Mediavilla, E. Artal, "Full band waveguide turnstile junction orthomode transducer with phase matched outputs," *International Journal of RF and Microwave Computer-Aided Engineering,* vol. 20, no. 3, pp. 333- 341, 2010.
[58] A. Tribak, J. L. Cano, A. Mediavilla, M. Boussouis, "Octave bandwidth compact turnstile-based orthomode transducer," *IEEE Microwave and Wireless Components Letters*, vol. 20, no. 10, pp. 539- 541, Oct. 2010.
[59] M. A. Meyer and H. B. Goldberg, "Applications of the turnstile junction," *IRE Transactions on Microwave Theory and Techniques*, vol. 3, no. 6, pp. 40- 45, December 1955.
[60] J. Uher, J. Bornemann, U. Rosenberg, "Waveguide components for antenna feed systems: Theory and CAD," Artech House Publishers, 1993.
[61] D. Henke and S. Claude, "Minimizing RF performance spikes in a cryogenic orthomode transducer (OMT)," *IEEE Transactions on Microwave Theory and Techniques*, vol. 62, no. 4, pp. 840- 850, Apr. 2014.
[62] G. Chattopadhyay and J. E. Carlstrom, "Fineline ortho-mode transducer for millimeter waves," *IEEE Microwave and Guided Wave Letters*, vol. 9, no. 9, pp. 339- 341, Sep 1999.
[63] A. Dunning, "Double ridged orthogonal mode transducer for the 16-26 GHz microwave band", *Proceedings of the Workshop on the Applications of Radio Science*, 2002.
[64] C. A. Leal-Sevillano, Y. Tian, M. J. Lancaster, J. A. Ruiz-Cruz, J. R. Montejo- Garai, J. M. Rebollar, "A micromachined dual-band orthomode transducer," *IEEE Transactions on Microwave Theory and Techniques,* vol. 62, no. 1, pp. 55- 63, Jan. 2014.
[65] E. Pucci and P.-S. Kildal, "Contactless non-leaking waveguide flange realized by bed of nails for millimeter wave applications," *6th European Conf. on Antennas and Propag*., Prague, Czech Republic, pp. 3533-3536, 2012.
[66] E. Alfonso, S. Carlred, S. Carlsson, L.-I. Sjöqvist, "Contactless flange adapters for mm-wave measurements," *11th European Conference on Antennas and Propagation*, Paris, France, 2017.
[67] E. Rajo-Iglesias and P.-S. Kildal, "Numerical studies of bandwidth of parallel-plate cut-off realised by a bed of nails, corrugations and mushroom-type electromagnetic bandgap for use in gap waveguides," *IET Microwaves, Antennas & Propag*., Prague, vol. 5, pp. 282-289, 2011.
[68] S. Rahiminejad, E. Pucci, V. Vassilev, P.-S. Kildal, S. Haasl, P. Enoksson, "Polymer gap adapter for contactless, robust, and fast measurements at 220–325 GHz," *J. Microelectromech. Syst*., vol. 25, no. 1, pp. 160–169, Feb 2016.

[69] D. Sun, Z. Chen, and J. Xu. “Flexible rectangular waveguide based on cylindrical contactless flange,” *Electron Lett*., vol. 52, no. 25, pp. 2042-2044, Dec 2016.
[70] X. Chen, W. Cui, Y. He, D. Sun, “Low Passive-Intermodulation Contactless Waveguide Adapter Based on Gap Waveguide Technology,” *11th European Conf. on Antennas and Propag.,* Krakow, Poland, 2019.
[71] P.-S. Kildal, “Three metamaterial-based gap waveguides between parallel metal plates for mm/submm waves,” *3rd Eur. Antennas Propag. Conf*., pp. 28–32, 2009.
[72] C. A. Balanis, “Antenna Theory: Analysis and Design,” 3rd Edition, NJ, USA: Wiley, 2005.
[73] W. L. Stutzman, G. A. Thiele, “Antenna Theory and Design,” 3rd Edition, USA, Wiley, May 2012.
[74] A.V. Nogueira, M. Baquero, J. I. Herranz, J. Domenech, E. Alfonso, A.Vila, “Gap Waveguides Using a Suspended Strip on a Bed of Nails,” *IEEE Antennas and Wireless Propag. Letters*, vol. 10, pp. 1006–1009, 2011.
[75] X. Ma, J. S. Ochoa, A. C. Cangellaris, “A Method for Modeling the Impact of Conductor Surface Roughness on Waveguiding Properties of Interconnects,” *IEEE 22nd Conference on Electrical Performance of Electronic Packaging and Systems*, San Jose, CA, USA, Oct. 2013.
[76] L. Tsang, X. Gu, H. Braunisch, “Effects of random rough surface on absorption by conductors at microwave frequencies,” *IEEE Microwave and Wireless Components Letters*, vol. 16, no. 4, pp. 221-223, 2006.
[77] L. Proekt and A. Cangellaris, “Investigation of the impact of conductor surface roughness on interconnect frequency-dependent ohmic loss,” *53rd Electronic Components and Technology Conference*, pp. 1004-1010, 2003.
[78] L. Tsang, H. Braunisch, R. Ding, X. Gu, “Random rough surface effects on wave propagation in interconnects,” *IEEE Transactions on Advanced Packaging*, vol. 33, no. 4, pp. 839-856, 2010.
[79] R. Ding, L. Tsang, H. Braunisch, W. Chang, “Wave propagation in parallel plate metallic waveguide with finite conductivity and three dimensional roughness,” *IEEE Transactions on Antennas and Propag*., vol. 60, no. 12, pp. 5867-5880, 2012.
[80] C. Warren, L. Pajewski, A. Ventura, A. Giannopoulos, “An evaluation of Finite-Difference and Finite-Integration Time-Domain modelling tools for Ground Penetrating Radar antennas,” *2016 10th European Conference on Antennas and Propagation (EuCAP),* Davos, Switzerland, Apr. 2016.
[81] S. Rahiminejad, E. Pucci, V. Vassilev, P.-S. Kildal, S. Haasl, P. Enoksson, “Polymer gap adapter for contactless, robust, and fast measurements at 220–325 GHz,” *J. Microelectromech. Syst*., vol. 25, no. 1, pp. 160–169, Feb 2016.
[82] W. Cui, X. Chen, Y. He, D. Sun, “Compact Waveguide Connection for Space Applications Using Gap Waveguide Technology,” *13th European Conf. on Antennas and Propag*., Krakow, Poland, 2019.
[83] D. Sun and J. Xu. “Real Time Rotatable Waveguide Twist Using Contactless Stacked Air-Gapped Waveguides,” *Microw. Wirel. Compon. Lett.,* vol. 27, no. 3, pp. 215-217, March 2017.
[84] Dongquan Sun, Zhenhua Chen, and Jinping Xu, “Flexible rectangular waveguide based on cylindrical contactless flange,” *Electron Lett*., vol. 52, no. 25, pp. 2042-2044, Dec 2016.

[85] Xiang Chen, Dongquan Sun, Wanzhao Cui, and Yongning He, "A Folded Contactless Waveguide Flange for Low Passive Intermodulation Applications," *IEEE Microw. Wirel. Compon. Lett.*, vol. 28, no. 10, pp. 864-866, October 2018.
[86] M. A. Abdelaal, and A. A. Kishk, "Ka-band 3D-Printed Wideband Groove Gap Waveguide Orthomode Transducer," *Transactions on Microwave Theory and Techniques*, vol. 67, no. 8, pp. 3361- 3369, June 2019.
[87] M. A. Abdelaal, S. I. Shams, and A. A. Kishk, "Asymmetric Compact OMT for X-Band SAR Applications," *Transactions on Microwave Theory and Techniques*, vol. 66, no. 4, pp. 1856-1863, April 2018.
[88] M. A. Abdelaal, S. I. Shams, M. A. Moharram, M. Elsaadany, and A. A. Kishk, "Compact Full band Based on Dual Mode Double Ridge Waveguide," *Transactions on Microwave Theory and Techniques*, vol. 66, no. 6, pp. 2767-2774, June 2018.
[89] D. Dousset, S. Claude, and K. Wu, "A compact high-performance orthomode transducer for the atacama large millimeter array (ALMA) band 1 (31-45 GHz)," *IEEE Access*, vol. 1, pp. 480-487, 2013.
[90] G. Engargiola and A. Navarrini, "K-band orthomode transducer with waveguide ports and balanced coaxial probes," *IEEE Trans. Microw. Theory Techn*., vol. 53, no. 5, pp. 1792-1801, May 2005.
[91] J. A. Ruiz-Cruz, J. R. Montejo-Gara, C. A. Leal-Sevillano, and J. M. Rebollar, "Orthomode Transducers With Folded Double-Symmetry Junctions for Broadband and Compact Antenna Feeds," *IEEE Transactions on Antennas and Propag*., vol. 66, no. 3, pp. 1160-1168, Mar. 2018.
[92] A. Gomez-Torrent, U. Shah, and J. Oberhammer, "Compact Silicon-Micromachined Wideband 220–330-GHz Turnstile Orthomode Transducer," *IEEE Transactions on Terahertz Science and Tech*., vol. 9, no. 1, pp. 38-46, Jan. 2019.
[93] R. Nesti, E. Orsi, G. Pelosi, and S. Selleri, "Design of Two Ku-Band Orthomode Transducers for Radio Astronomy Applications," *Progress In Electromagnetics Research*., vol. 163, no. 3, pp. 79-87, 2018.
[94] X. Chen, W. Cui, D. Sun, and Y. He, "Novel Compact Waveguide Flange Adapter for Passive Intermodulation Measurement Systems*," 2020 14th European Conference on Antennas and Propagation (EuCAP)*, Copenhagen, Denmark, Mar. 2020.
[95] C. Vicente, D. Wolk, H. L. Hartnagel, B. Gimeno, V. E. Boria, and D. Raboso, "Experimental Analysis of Passive Intermodulation at Waveguide Flange Bolted Connections*," 2020 14th European Conference on Antennas and Propagation (EuCAP)*, Copenhagen, Denmark, Mar. 2020.
[96] X. Zhao, Y. He, M. Ye, F. Gao, W. Peng, Y. Li, C. Bai, and W. Cui, "Analytic Passive Intermodulation Model for Flange Connection Based on Metallic Contact Nonlinearity Approximation*," IEEE Trans. Microw. Theory Techn.,* vol. 65, no. 7, pp. 2279- 2287, Jul. 2017.

List of the Author's Publications

[1] T. S. Amin and A. A. Kishk, "Contactless Waveguide Adapter for Multiple Frequency Bands," *2020 IEEE International Symposium on Antennas and Propagation and North American Radio Science Meeting*, Canada, 2020. (Presented)

[2] T. S. Amin and A. A. Kishk, "Contactless and Flangeless Pipe Contact for Standard Waveguides," *2020 IEEE International Symposium on Antennas and Propagation and North American Radio Science Meeting*, Canada, 2020. (Presented)